UNIVERSITY OF CALIFORNIA

Santa Barbara

Improved drug delivery technologies and real-time protein monitoring through advancements in directed evolution techniques and biosensor optimization

A dissertation submitted in partial satisfaction of the

requirements for the degree Doctor of Philosophy

in Materials

by

Faye Yi Fong

Committee in charge:

Professor H. Tom Soh, Chair

Professor Craig J. Hawker

Professor Cyrus Safinya

Professor Irene Chen

September 2017

The dissertation of Faye Yi Fong is approved.

_____

Professor Craig J. Hawker

_____

Professor Cyrus Safinya

_____

Professor Irene Chen

_____

Professor H. Tom Soh, Committee Chair

June 2017

Improved drug delivery technologies and real-time protein monitoring through advancements in directed evolution techniques and biosensor optimization

by

Faye Yi Fong

Acknowledgements

First and foremost, I would like to thank my advisor, Prof. H. Tom Soh for being my mentor and guide through the challenging and exciting journey of my graduate work. Without Tom's invaluable mentorship and encouragement, I would not have been able to finish my doctoral degree. I am thankful for the opportunity I had to be an active member of the Soh Laboratory.

I would also like to express my deep gratitude to my defense committee: Prof. Craig J. Hawker, Prof. Cyrus Safinya, and Prof. Irene Chen. Thank you for supporting my research and helping me to develop my dissertation.

This achievement would not have been possible without the help of my colleagues in the Soh Lab. I would like to express my special gratitude towards Prof. Seung Soo Oh, who served as a postdoctoral scholar during my graduate studies and advised me on matters great and small for most of the projects that I have described in this dissertation.

Thank you also to my labmates – we labored together and we laughed together.

Finally, I would like to thank my family and my "special friend" Amit for their unwavering support of my studies.

Curriculum Vitae

Faye Yi Fong

Education

Ph.D., Materials Engineering: June 2017

University of California, Santa Barbara, Santa Barbara, CA

Advisor: H. Tom Soh (now at Stanford)

B.A., Chemistry, June 2010

B.A., Biology, June 2010

Dartmouth College, Hanover, NH

Professional Employment

2010-2017: Graduate Student Researcher, Materials Department, University of California, Santa Barbara

2007-2010: Research Assistant, Dartmouth Medical School, Bursztajn group, Dartmouth College

2006-2007: Research Assistant, Chemistry Department, BelBruno group, Dartmouth College

Publications

1. F. Y. Fong, S.S. Oh, C.J. Hawker, H. T. Soh, “In vitro selection of pH-activated DNA nanostructures”, *Ange. Chem. Int. Ed.*, **128**, 15484 (2016).

2. A. J. Simon, L. T. Walls-Smith, M. J. Freddi, F. Y. Fong, V. Gubala, K. W. Plaxco, “Simultaneous measurement of the dissolution kinetics of responsive DNA hydrogels at multiple length scales”, *ACS Nano*., **11**, 461 (2017).

Conference Presentations

1. F. Y. Fong, S.S. Oh, C.J. Hawker, H. T. Soh, “In vitro selection of pH-activated DNA nanostructures”, *Materials Research Society (*2016)

Awards

2012-2015: California Institute of Regenerative Medicine Predoctoral Fellowship

2011: Xerox Technical Minority Scholarship

2010: Merck Index Award for top graduating seniors in undergraduate chemistry

2009: NIH Summer Internship Program (SIP) Exceptional Summer Student Award

2007-2008: Howard Hughes Medical Institute Biomedical Research Fellow

Abstract

Improved drug delivery technologies and real-time protein monitoring through advancements in directed evolution techniques and biosensor optimization

by

Faye Yi Fong

Whereas twentieth century medical research sought treatments to benefit as many individuals as possible, perhaps the watchword of the next century is “precision medicine”, which seeks to maximize the benefit of treatment for each individual. Every patient has a unique physiological and pathological profile. The effective dosage of a drug, the rate of disease progression, and even the risk of complications are determined by genetic and lifestyle factors specific to the individual. The next generation of medical innovation aims to customize healthcare to the unique needs of each patient.

One area of research in precision medicine is controlled drug delivery, which aims to precisely supply therapeutic molecules to the correct tissue and organ locations at the correct times. There is a universal general strategy: an engineered protective vehicle which reacts specifically to biological or physical triggers to release an encapsulated drug payload. Controlled drug delivery reduces toxic side effects, improves efficacy, and customizes therapy to the individual. Recently,

there has been heightened interest in the development of pH-controlled drug delivery. A clinically significant pH gradient exists across the endocytosis pathway where the pH changes from 7.4 at the plasma membrane to 5.2 in the late endosome. Endocytosis is responsible for trafficking and modifying many important proteins and as such, triggered activation of drugs at specific pH corresponding to specific modules of endocytosis is a rich area for therapeutic targeting.

Towards these applications, we have developed an *in vitro* selection process to generate nanocarriers which switch structure in response to shifting the pH in order to release a drug payload. We have also adapted our selection process to generate pH-controlled aptamers whose affinity for ligands can be turned on or off by changing the pH. The ultimate goal is the rapid generation of useful pH-controlled nanovehicles for customized delivery of any therapeutic payload.

But to fulfill the promise of precision medicine, there is also a great need for new diagnostics which can more quickly and cost-effectively return data about the patient. Currently, the standard of care for biomarker monitoring is the enzyme linked immunosorbent assay (ELISA). Although ELISAs are highly accurate, they are time- and labor-intensive, requiring the expertise of a qualified medical lab technician in a centralized facility. The best way to meet the diagnostics needs for precision medicine in the next century is to develop real-time sensors which are rapid, fully-automated, and function at the point-of-care.

To that end, we have built a real-time electrochemical aptasensor for monitoring α-thrombin protein directly in human plasma. In our devices, protein detection is achieved by the binding of the target protein with methylene blue-modified aptamers, which alters the measured output current. In parallel, the

incoming plasma sample stream is subjected to a pretreatment cocktail that blocks native inhibitors and prevents clot formation, thus amplifying the thrombin signal. Our platform could potentially be extended towards monitoring any protein of interest with results reported within minutes, directly at the patient's bedside.

Controlled drug delivery and real-time biomarker monitoring are powerful complementary technologies in precision medicine. We envision the possibility of maximum patient benefit from therapy, where controlled drug delivery is further finetuned by closely monitoring the individual's response to treatment.

Table of Contents

Chapter 1. Introduction

Since 1952, DNA has been confirmed as the genetic material[1]. The sequence information within it makes us what and perhaps, who we are as well. Since then, we have learned much about the chemical and physical properties of the DNA material. In contrast to the nucleic acid RNA, DNA lacks a 2' hydroxyl on its sugar group, affording it increased chemical stability as it is less susceptible to hydrolysis[2]. We also know that two complementary strands of DNA will hybridize into a double helix via Watson-Crick basepairing rules: { A-T, G-C }[3]. More recently, we have learned that DNA can exist in single-stranded form and can intramolecularly fold into interesting structures, not unlike RNA[4]. Notably, it is in single-stranded form that RNA has shown not only transcriptive functions, but recognition and catalytic functions[5]. Researchers have hypothesized and later confirmed that single-stranded DNA can also be designed to perform special functions.

To summarize: DNA is chemically stable, can be programmed to self-assemble, and folds into higher order structure when single-stranded. Researchers have thus recognized that synthesized DNA can be developed as a next generation material to perform many useful tasks. This is the story of several advancements in the field.

1.1 DNA: a next generation material for nano-engineering

The first explorations into DNA as a material for nanoscale engineering were purely structural. Researchers designed short DNA oligonucleotide sequences (oligos) which would self-assemble according to Watson-Crick basepairing rules

into sophisticated 2D and later, 3D structures[6]. For example, a fundamental structural motif is the immobile Holliday junction[7]. Four 16bp oligos were designed to hybridize unambiguously into a specified four-armed junction[7]. Importantly, the sequences were designed to minimize symmetry and therefore make strand migration negligible[7]. That is, the strands can only assemble in one conformation: the first 8 basepairs of Strand 1 will only hybridize with the last 8 basepairs of Strand 4, and the last 8 basepairs of Strand 1 will only hybridize with the first 8 basepairs of Strand 2[7]. It is easy to see that this DNA junction could be used to join larger modules for higher order structures. The advantages of being able to dictate complex structures at the nanoscale were recognized by many, and since then, researchers have made many elaborate and whimsical objects including smiley faces, tetrahedrons, and three-dimensional rastered-in pyramids[8]. The field has creatively been termed “DNA origami” and has demonstrated that DNA has a rich potential to be formed into sophisticated self-assembled nanostructures.

The next leap in DNA engineering came when it was discovered that single-stranded oligos could be programmed to fold into structures which could act as recognition elements for biological molecules, analogous to antibody-antigen binding[9]. These valuable oligo structures are known as “aptamers”, and they were the first demonstration that DNA could act as a functional material[9]. In the 1990s, several researchers developed “Systematic evolution of ligands by exponential enrichment” (SELEX) to discover aptamer sequences with binding affinity for a variety of protein and small molecule targets[9]. Perhaps the most canonically important early DNA aptamers were the two α-thrombin-binding aptamers independently discovered by Bock et al.[10] and Tasset et al[11]. Both aptamers are

G-rich sequences which fold into G-quadruplex chair structures[10],[11]. Each aptamer has high specificity and binding affinity for α-thrombin, but at different binding epitopes; the Bock aptamer binds at the fibrinogen-binding site[10] and the Tasset aptamer binds at the heparin site[11]. These aptamers are comparable to traditional antibodies in their affinity for thrombin and have also been shown to inhibit the binding of native ligands[10],[11]. There has been continued strong interest in finding aptamers against other biologically significant targets, owing to the advantageous properties of DNA-based affinity reagents: they possess greater thermal stability than protein antibodies, are cheaply chemically synthesized, and can be readily modified with side chains and substitutions via well-established DNA modification chemistry[9].

Recently, researchers have combined structural and functional DNA engineering to create multifunctional nanomachines. For example, one group designed a collection of oligos and fuel strands which together form a “DNA walker”, demonstrating the generation of precise mechanical force at the nanoscale[12]. Researchers have also developed nanomachines which react to specific stimuli to perform a prescribed function. For example, in reaction to UV irradiation, an azobenzene-modified DNA nanopore opens to release a drug payload from a mesoporous nanocontainer[13]. A DNA hydrogel has also been developed where the phase transition of the hydrogel material is controlled by the concentration of a specific analyte[14]. The hydrogel consisted of polymers modified with rationally designed DNA linkers which crosslink via hybridization but which also contain the sequence for the ATP-binding aptamer[14]. In the presence of an activating concentration of ATP, hybridization is disrupted and the hydrogel

dissolves[14]. There are countless other varieties of DNA machines including self-reporting sensors (molecular beacons)[15] and even catalysts (DNAzymes)[16]. Altogether, DNA possesses incredible potential as a next generation nanoscale engineering material and in this thesis, we will describe our efforts to develop it into useful nanocarriers and biosensors.

1.2 Precision medicine 1: Controlled drug delivery

The next century in medical research will be defined by the paradigm of "precision medicine". The mission of precision medicine is to develop technologies which more precisely diagnose and treat patients, customizing treatment to each individual, and thus maximizing patient benefit from therapy[17]. One of the main arms of this research philosophy has been the development of controlled drug delivery technologies. There are several drugs currently on the market which represent the classical methods of controlled release. For example, extended time release versions of established pharmaceuticals such as Zolpidem (sleep aid)[18] and Adderall (ADHD, narcolepsy treatment)[19] help patients achieve a more regular dosage over a longer period of time. Other well-established forms of controlled delivery are prodrugs such as 5-fluorouracil (chemotherapeutic) where the therapeutic molecule is administered as an inactive precursor that accumulates in the target tissue, and is then metabolized by the body into an active form[20]. The purpose of these multivarious technologies for controlled release is clear: to specify the location and times at which active molecules are administered, thereby reducing side effects and improving therapeutic outcomes[21].

However, new and unorthodox methods for controlled drug delivery are urgently needed because next generation pharmaceuticals no longer fit the traditional pharmacokinetic profile. Conventional medicines are small molecule drugs that are water soluble, pass with relative ease through the cell membrane, and a single therapeutic dose can be packaged into ~1 mL volume[22]. Next generation drugs include macromolecular assemblies such as fusion antibodies, nanoparticles, and gene therapy[22]. The new challenges for controlled drug delivery will be to package these drugs for improved bioavailability and to increase cellular internalization of the payload[22].

Perhaps the most exciting and difficult challenge for controlled drug delivery is the realization of the promise of gene therapy. Nucleic acid drugs for gene therapy face enormous transport challenges[23]. First, nucleic acids are vulnerable to attack by native nucleases in the blood[23]. Second, the payload must be targeted to the correct tissue or organ to reduce off-target toxicity[23]. Third, the delivery method must facilitate cellular and/or nuclear internalization of the nucleic acid payload, bypassing the natural size and charge exclusion of these membranes[23]. Currently, liposome- and nanoparticle-based schemes are being developed which access the cellular internalization pathway known as endocytosis in order to achieve drug uptake[23].

1.3 Targeting the endosome: pH-triggered drug delivery

In the first half of this thesis, we will discuss advancements we have made to develop endosome-targeting DNA machines for delivering a therapeutic payload.

Endocytosis is the process by which cells internalize materials. Although there are different subtypes of endocytosis (clathrin-mediated, caveolae, macropinocytosis, and phagocytosis), the general process involves deformation of the plasma membrane for engulfment of an external object, pinching off into an endosome, and then transport and maturation of the endosome along various pathways[24]. Early endosomes receive engulfed materials from the cell surface including nutrients which are carried in by transport proteins[24]. Typically, the transport proteins will release the nutrients before being returned to the plasma membrane via recycling endosomes[24]. Importantly, early endosomes are responsible for sorting the useful engulfed materials and transporting them to other cellular destinations such as the Golgi body[24]. For example, the early endosome may traffick proteins to the Golgi for important post-translational modifications[24]. When an early endosome has finished sorting out useful materials, they are left primarily with waste materials[24]. Early endosomes will mature into late endosomes, and finally, lysosomes, which will degrade the waste[24]. Furthermore, the endocytosis pathway is a highly attractive target for controlled drug delivery. Currently, there is great interest in developing drug delivery vehicles which selectively release their payload after engulfment in order to concentrate the dose inside the target tissue and reduce off-target side effects[25]. Additionally, due to the role of the endosomal network in protein trafficking, targeting therapeutics to specific endosomes in order to manipulate protein expression is a rich therapeutic opportunity[24].

At the start of internalization, the endosome pinches off from the cell membrane (pH 7.4) and then matures from early endosome (pH 5.5-6.0) to late

endosome (pH 5.2), and finally into the lysosome (pH 4.5)[26]. Importantly, in Nature, the characteristic pH gradient of the endocytosis pathway is used by the cell to control selective transport and delivery of engulfed molecules. The classsical example of this phenomenon is transferrin, a transport protein which carries Fe(III) into the cell[27]. At pH 7.4, transferrin strongly binds 2 molecules of Fe(III), but after internalization when the endosomal pH drops, transferrin's binding affinity for Fe(III) is greatly decreased and the ligand is released into the cell[27]. As such, it is of great interest to the research community to create analogous pH-triggered drug delivery systems which sequester a drug payload until endosomal uptake and acidification activates release.

We note that historically research in this area has focused on the development of polycationic polymers and nanoparticles for the delivery of therapeutic nucleic acids[28]. Typically, the system contains a positively charged component to shield the strongly negative phosphate backbone of the nucleic acid payload, enhancing absorption through the phospholipid membrane[28]. Furthermore, these systems are also coupled with a mechanism for pH-triggered cleavage in order to release the drug payload into the acidified endosome. For example, a polymeric micelle was developed where adriamycin was conjugated to the block copolymer via an acid-labile hydrazone linker, thus providing a mechanism for intracellular pH-dependent drug release[29]. Another well-established strategy is the synthesis of polymer micelles with reversibly protonated amine residues which swell or shrink in response to pH change in order to deliver encapsulated drugs[30].

Owing to the many useful material properties of DNA, in particular our ability to program it to execute complex functions, DNA machines have seen development as pH-triggered drug delivery vehicles[31]. Currently, such DNA machines are based on a handful of well-known pH-sensitive DNA motifs. Perhaps the most widely explored structure is the i-motif, a C-rich DNA sequence which contains no notable secondary structure at pH 7.4, but forms a stable C-quadruplex chair structure at pH 5.2[32]. The i-motif was first discovered as a recurring motif in telomeric DNA, but the role of its pH-dependent structure-switching in DNA expression is unknown[33]. The i-motif's pH-reactive behavior arises from its cytosine repeats[32]. At neutral pH, C•C mismatch basepairs are disfavored, but at low pH, protonated cytosines will form highly favored $C•C^+$ basepairs, creating a stable C-quadruplex structure[32]. The i-motif has been used creatively for many pH-dependent release applications[32]. For example, a drug delivery vehicle was developed where gold nanoparticles were decorated with an i-motif-containing DNA linker that could be loaded with siRNA via partial hybridization to a complementary region on the linker[34]. In the presence of acidic pH, the linker preferentially folded to form the C-quadruplex, thereby releasing the siRNA payload[34]. In another system, silica nanopores containing a small molecule payload were capped with i-motif DNA[35]. In its C-quadruplex form the i-motif closes the nanopore with high efficiency, but when the pH is raised, the i-motif unfolds and releases the payload[35]. There are also other well-known pH-responsive DNA motifs such as the triplex switch[36] and long A•G runs[37] which have been likewise incorporated into analagous systems for drug delivery.

Our work focuses on high-throughput methods to generate novel pH-reactive DNA motifs using a technique known as *in vitro* selection.

1.4 How selection works

Systematic evolution of ligands by exponential enrichment (SELEX), also termed selection, is an *in vitro* technique to generate molecules with specific properties by using selective pressure and amplification to identify best performers from an initially diverse combinatorial library[10]. In our subfield, we focus on DNA-based selections to find pH-controlled nanomachines.

Traditionally, selections are performed as follows: we start with a diverse combinatorial library of oligonucleotide sequences typically of length 100 bp where a subset of the basepairs are randomized. The library is challenged with a surface-bound target (typically on a nitrocellulose membrane or magnetic bead)[10], [38]. The sequences with some affinity will associate with the surface-bound target and be separated out from solution[10], [38]. These partitioned sequences are then amplified and subjected to further rounds of selection with increasing selection stringency[10], [38]. The sequence pool eventually converges to a subset of high-affinity winners[10], [38].

Briefly, we would like to sketch out mathematically how partitioning and amplification of a combinatorial pool leads to sequence convergence. Suppose you start with 100 unique sequences in your combinatorial library. Of the total 100 sequences, let's say that 10 of these sequences have 2X greater affinity for the target compared to the other 90. If 10% of sequences are collected in a round of selection, you will isolate 10 sequences. If all sequences in the starting library had

the same affinity for the target, the probability of being collected would be equal for all 100. However, since 10 of the sequences have 2X the probability of being picked, this means that 2 out of the 10 isolated sequences will be good binders. The 10 isolated sequences are amplified ten-fold to return the pool size to 100 sequences, where now there are 20 good binders and 80 poor binders. If the rate of enrichment remains constant, the next round will contain 40% good binders, the round after that 80% good binders, and by the fourth round, the pool will have converged to 100% good binders.

In our work, we have modified traditional selection into a “Falling-Off” SELEX scheme[39]. Instead of being in solution, our library is initially bound non-covalently to the target. We then subject the library-target complex to pH change which will stimulate a conformation switch in a subset of the sequences, releasing the best performing pH-reactive sequences into solution. We collect the eluent, amplify it and subject it to further rounds of selection. We will show that this powerful combinatorial technique allows us to generate pH-active drug delivery vehicles and pH-controlled aptamers in high-throughput.

1.5 Precision medicine 2: Real-time biomarker monitoring

Another important arm of research in precision medicine is improving diagnostics. In this area, our goals have been to increase the speed of returning measurements results and to reduce human labor expended when performing diagnostic assays. Currently, the only FDA-approved system for rapid continuous molecular monitoring is glucose monitoring for diabetics[40]. Importantly, this technology allows diabetic patients to rapidly respond to spikes in blood glucose

with insulin, thus allowing more effective regulation of blood sugar and improved patient outcomes[40]. While nearly every aspect of medicine could be improved by better biosensors, there is an especially great need for better, faster biosensors in the emergency room. Emergency room illnesses like traumatic injury and acute infection progress so quickly that regular biomarker assays (turnaround time ≥ 1 hour) may return information which no longer accurately describes the patient's condition[41]. As such, emergency room medicine until this point has depended mostly on symptomology and qualitative tests that do not provide molecular information[41].

Coagulopathy is a common complication encountered in the emergency room which may benefit greatly from faster reporting diagnostics[42]. Coagulation is a complex process by which tissue injury stimulates a network of coagulation proteins producing controlled enzymatic cleavage of soluble fibrinogen into insoluble fibrin, which combines with platelets to form clots to close a wound[42]. There are over twenty known procoagulation and anticoagulation factors which regulate this process as well as chemical crosstalk with immune system proteins[42]. Trauma-induced coagulopathy is where traumatic injury has caused huge blood volume loss, changes to the blood chemistry, and inflammation, resulting in massive dysregulation of typical blood concentrations of coagulation factors[42]. Traumatic injury victims are vulnerable to abnormal coagulation responses such as embolism (hypercoagulability) and hemmorhage (hypocoagulability) [42].

Current diagnostics for coagulopathy rely on symptomology and qualitative tests because these assays can be performed relatively quickly (<1 hour). For example, it is common to measure the prothrombin time (PT), where blood is drawn

from the patient, purified into plasma, activated by tissue factor, and the time for the plasma to clot is measured optically[43]. Thromboelastography (TEG) is another typical clinical assay where whole blood is permitted to clot around a rotating wire probe and the mechanical strength of the clot is measured as a function how strongly the clot retards rotation of the wire probe[43]. Unfortunately, these methods do not offer molecular information about protein and small molecule concentrations in the blood. In order to obtain molecular information, clinicians currently rely on the enzyme-linked immunosorbent assay (ELISA) which requires an expert technician to perform and for which the turnaround time ranges from hours to days[44], [45]. As such, although biomarker tests are highly valuable, emergency room physicians cannot rely on current technologies because they are too slow to report the current concentration of the biomarker of interest. Therefore, the future of precision medicine calls for biomarker tests that are quantitative, rapid, and automated. These next-generation diagnostics will enable us to closely monitor and treat fast moving illnesses in the emergency room and in the field.

1.6 Electrochemical aptamer sensors

There is a new approach to biosensors which has shown great potential for reporting changes in protein concentration rapidly and in an automated fashion. Aptamers have been modified into electrochemical aptasensors by labeling the oligo with a redox reporter, typically methylene blue, and anchoring them to a gold electrode surface inside a microfluidic device via gold-thiol covalent chemistry[46]. When the electrode is interrogated by a voltage, the redox tag may oxidize or reduce, and the transfer of electrons to or from the electrode gives rise to the

signaling current[46]. When the target protein in solution binds the aptasensor, it dramatically changes the conformation of the aptamer and accordingly, the electron transfer efficiency of the redox reporter[47]. The redox signaling current is linearly correlated with the protein concentration in solution[47]. Since aptamers are equilibrium binding affinity reagents, when the solution concentration drops, the aptamer releases the target and folds back into the unbound state, returning the current to its initial value[47]. These electrochemical aptamer binding (EAB) sensors are driven by miniature potentiostats that can be programmed to take current readings as often as every 10 seconds[47].

Whereas previously published examples of EAB sensors were single use[47], our group was the first to develop the continuous EAB sensor which could monitor a fluctuating molecular concentration in solution over time[48]. Ferguson *et al.* developed a continuous small molecule detection system which they called Microfluidic Electrochemical Detector for *In vivo* Continuous monitoring (MEDIC) [48]. MEDIC was able to continuously report the changing blood concentration of cocaine, kanamycin, and doxorubicin in live rats over several hours[48]. Significantly, the MEDIC approach showed great potential to monitor drug dosing and drug metabolism in real-time.

While EAB sensors formed the sensing component of MEDIC, the platform also relied on a second major innovation which permitted molecular detection to be done directly in blood. The sensor electrode was protected from biofouling by a continuous diffusion filter (CDF) [48]. The CDF consisted of a stacked laminar flow where a buffer sheath separated the blood sample flow from direct contact with aptasensor-modified electrodes[48]. Only high-diffusivity small molecules were able

to cross this barrier for sensor detection, whereas low-diffusivity biological interferents such as red blood cells, platelets, and proteins remained in the sample stream[48]. Since the chips were protected from biofouling via the CDF, measurements could be taken continuously over the course of hours, a clinically useful timescale.

In the second half of this thesis, we describe adapting the MEDIC system from measuring small molecules continuously to measuring proteins, which we call Protein MEDIC (PMEDIC). Specifically, we adapted MEDIC to continuously monitor the coagulation factor α-thrombin. To do this, we addressed a number of challenges, namely, how to monitor clot formation in blood without disrupting microfluidic flow, how to optimize the CDF to allow for protein detection, and how to rapidly regenerate the aptasensors for new measurements.

1.7 Objectives and Outline

Our goal is to develop new precision medicine technologies to improve the efficacy of medical treatment. We utilize next generation materials engineering of DNA machines towards achieving this goal. We have developed several interrelated technologies for controlled drug delivery as well as real-time molecular diagnostics.

Chapter 2: In this section, we describe the development of pH-controlled DNA nanostructures which deliver an antisense DNA drug payload. We set specific selection pressures to generate drug delivery vehicles which would encapsulate the drug payload at pH 7.5 and release at pH 5.2 within a 30 minute period. We found 10 sequences which would do this function with excellent pH-selectivity. Our best performer released 714-fold more payload at low pH than high pH, demonstrating the potential of our approach for generating customized pH-controlled drug delivery vehicles.

Chapter 3: In this section, we describe an extension of the selection technique developed in Chapter 2, used now to generate customized pH-controlled aptamers. In this work, we set selection conditions to generate aptamers which would turn on their affinity for Streptavidin at pH 7.5 and turn it off at pH 5.2. Thus, by simply changing the solution pH, we can now modulate the binding affinity of our aptamers for their targets. In the future, pH control over aptamers may enable us to selectively activate aptamer therapeutics during endocytosis and reset aptamer-based diagnostics with ease.

Chapter 4: In this section, we describe the PMEDIC platform, a system for continuous monitoring of coagulation factor α-thrombin. We show that by

combining the continuous reporting properties of electrochemical aptasensors, the biofouling protection of the CDF, and a pretreatment cocktail to prevent the action of native inhibitors in plasma, we could observe thrombin generation *in situ* from human plasma in real-time.

Chapter 5: In this section, we describe development of a new module for the PMEDIC system, where we thermally regenerate the electrochemical aptasensors. By rapidly displacing the bound protein via thermal melting of the aptamer structure, we have reset the sensor to take a new measurement. Thermal regeneration of PMEDIC can increase the rate of reporting up to 12-fold compared to waiting for sensor re-equilibration. We achieved this effect by putting the PMEDIC chip into thermal contact with a programmable mini-thermoelectric heater/cooler and optimized the system to reset PMEDIC as rapidly as possible.

Chapter 6: We conclude by discussing outlook and future directions for ongoing research.

Chapter 2. *In vitro* selection of pH-activated DNA nanostructures

2.1 Introduction

Cells often utilize changes in local pH to achieve molecular transport and processing. For example, ligands internalized by the cell are processed by the endosome for trafficking to specific cell compartments or further transported to the lysosome for degradation[26]. The pH of the late endosome (pH ~5.2) and lysosome (pH ~4.5) are significantly more acidic than the extracellular environment (pH ~7.4),[26] and there has been great interest in exploiting this pH difference to achieve controlled delivery of drugs into the cell.[28], [49] In particular, there is growing interest in pH-sensitive DNA nanostructures, because they are stable, programmable, and are readily integrated with other functional nucleic acids such as antisense DNA and siRNA.[50] To date, most pH-sensitive DNA nanostructures have been constructed based on motifs that are already known to be pH-responsive. For example, a number of investigators have incorporated the "i-motif" to achieve pH-triggered structure switching.[51-54] At neutral pH, the i-motif possesses negligible secondary structure, but in acidic conditions, non-canonical base-pairs form a C-quadruplex.[32] The i-motif has been used to demonstrate rapid pH-controlled loading and release of a complementary DNA strand.[55,56] More recently, a pH-controlled "triplex switch" has been described, which switches between duplex and triplex forms.[36]

This chapter is adapted with permission from Fong, Faye Y.; Oh, Seung S.; Hawker, Craig J.; Soh H. Tom. *Angewandte Chemie Int. Ed.* **2016**, 128, 15484-15488.

Ricci and co-workers incorporated a triplex motif distal to the ligand binding site for pH-dependent allosteric control over DNA loading/release.[57] Their strategy increased the variety of DNA ligands which could be delivered by placing the pH-sensitive motif distal to the DNA binding site and the pH-sensitivity could be tuned by varying the CGC content of the triplex.[57] While demonstrably powerful, the design of nanomachines incorporating the i-motif and triplex switch is restricted by pre-determined geometry and orientation requirements.[32,36,57] Furthermore, while the triplex switch is more facilely tuned, the i-motif requires significant rational optimization to customize range of pH-sensitivity.[32, 58, 59] Moreover, strategies to tune the efficiency/rate of ligand release have not been investigated.

Here we describe a selection-based approach for the de novo generation of pH-activated DNA nanostructures (PADNAs) with optimized pH-response properties. We present a new strategy where we set selection conditions to tune the pH-sensitivity and efficiency/rate of release. Using our strategy, we discovered PADNAs that selectively release Mipomersen, an FDA-approved antisense DNA drug for the treatment of hypercholesterolemia,[60] with exceptional pH sensitivity—achieving up to a ~714-fold increase in payload release at pH 5.2 compared to 7.5.

2.2 Results and Discussion

2.2.1 Library Design

Our starting library comprises three domains (Scheme 2.1A). The 17-nucleotide (nt) central domain is designed to hybridize with Mipomersen (20-nt) and thereby sequester it in an inactive state at pH 7.5. The central domain is flanked by two randomized release domains (22- and 21-nt), which are subject to selection. Finally, each PADNA molecule contains forward and reverse PCR primer-binding sites at the distal ends of the sequence (20-nt). All sequences are provided in the Supplementary Section (see 2.4.1, Table 2.S1).

2.2.2 Selection of pH-activated DNA nanostructures

We hybridized our starting PADNA library (initially comprising 100 picomoles or 6×10^{13} molecules) with 150 pmol of biotinylated Mipomersen, and then immobilized the assembly onto streptavidin (SA)-coated magnetic beads (Scheme 2.1B). We incubated overnight in pH 7.5 buffer, and then discarded PADNAs that were not immobilized on the beads. Next, we challenged the assemblies with pH 5.2 buffer and collected the PADNAs that released from the beads. We PCR amplified and generated single-stranded products for the next round of selection or for high-throughput sequencing. We performed 12 rounds of selection, increasing stringency in each round by decreasing the PADNA:Mipomersen ratio (for details, see 2.5.2.)

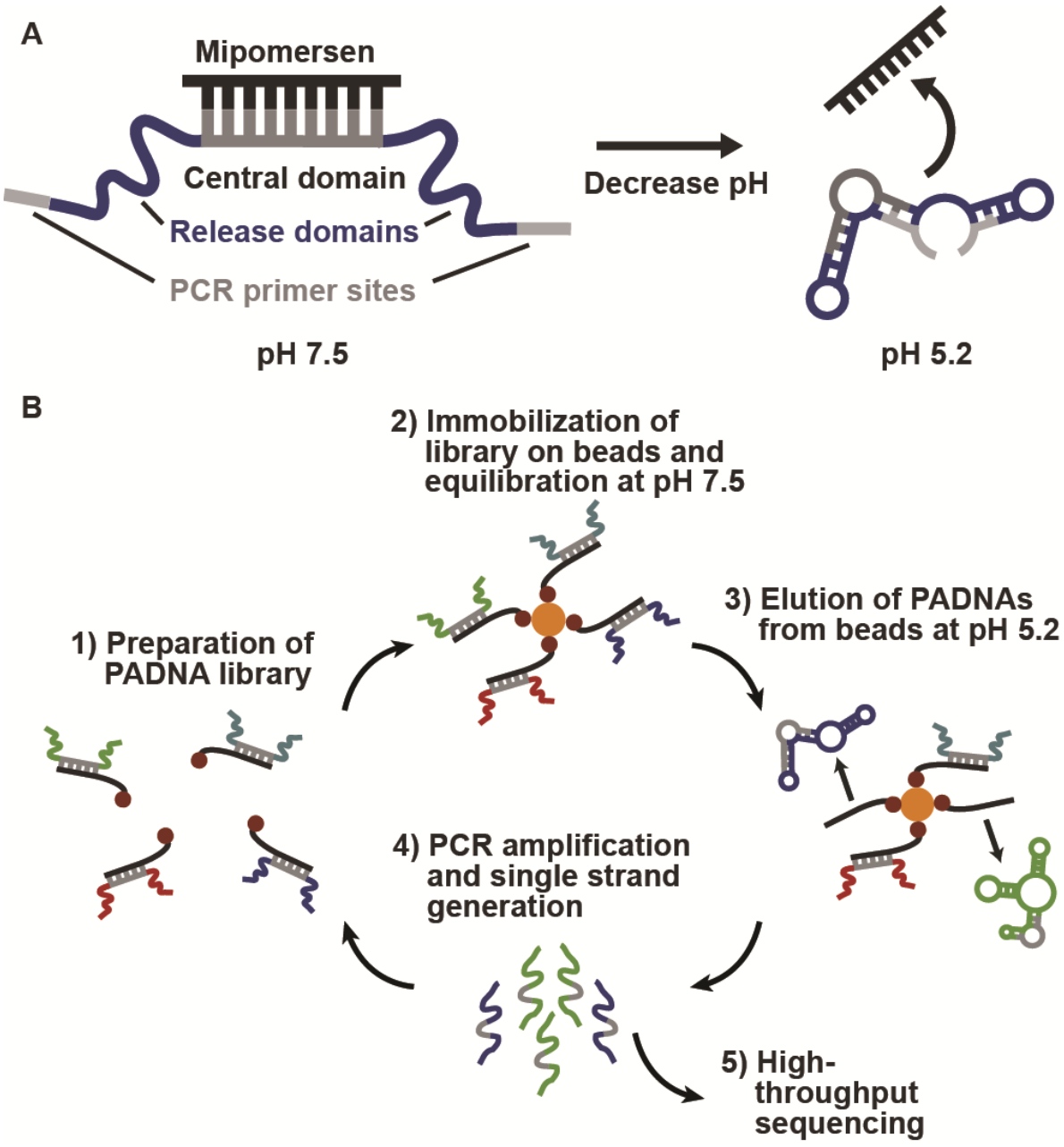

Scheme 2.1. Library design and selection of pH-responsive PADNAs.

At the end of each round, we performed PCR amplification of samples taken from the eluents, loaded them onto a polyacrylamide gel and determined the “release ratio”—the amount of PADNAs released at pH 5.2 in comparison to pH 7.5 (Figure 2.1). This ratio increased over the course of selection, as seen by the differences in band intensities, reaching ~27 by R12. PADNAs showed minimal release in the presence of excess SA, confirming that they do not bind to the SA that was used during selection to conjugate Mipomersen to the beads.

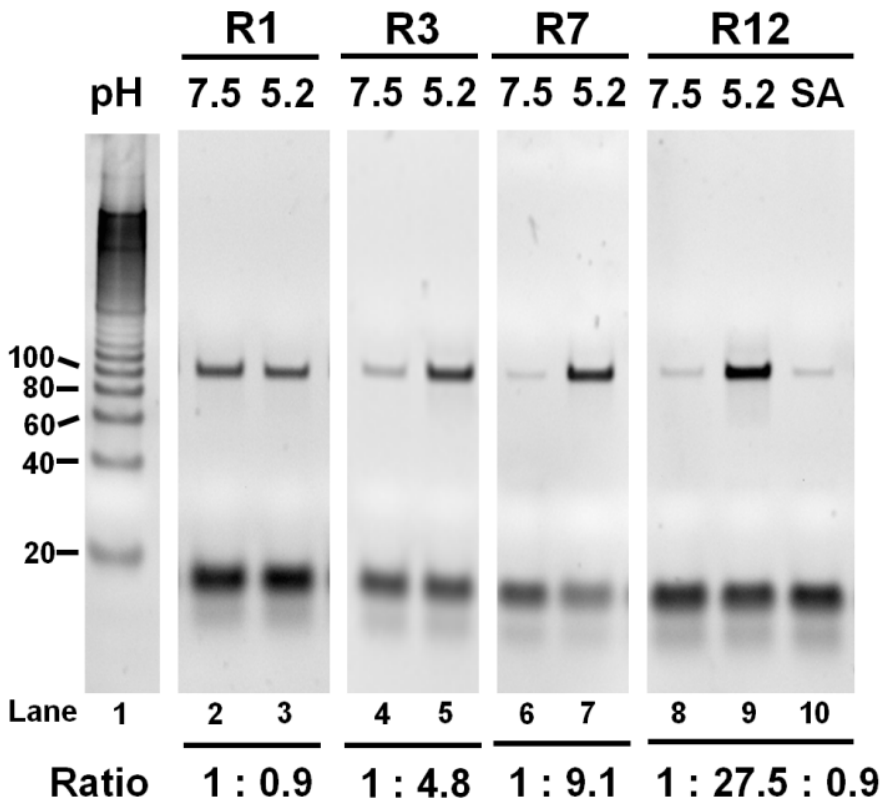

Figure 2.1. Gel images comparing the DNA eluted after 30 minutes in pH 7.5 or pH 5.2 PBSMT over multiple rounds of selection (lanes 2-9). Lane 1 contains the 20-bp ruler. Lane 10 shows elution of the R12 pool for 30 minutes in pH 7.5 buffer with 1 uM Streptavidin.

2.2.3 High-throughput sequencing analysis of the R12 pool

We analyzed the R12 pool with high-throughput sequencing, obtaining more than 2 million sequences. Surprisingly, the R12 pool maintained a high level of diversity, where the highest copy number of any single sequence did not exceed 91. We found that none of the 100 most abundant PADNAs contained known pH-responsive elements such as the i-motif, poly-dA repeats,[61] or the long homopyrimidine/homopurine runs that are signatures of DNA triplexes.[62] These results suggest that PADNAs are novel pH-sensitive structures that are mechanistically distinct from previously reported motifs.

2.2.4 qPCR characterization of individual sequences

We used qPCR to obtain the release ratio for the ten most abundant PADNAs. The release ratio of the top ten PADNAs ranged from 93–714 (see 2.4.2, Table 2.S2). We focused our analysis on PADNA-1 because it was the most highly represented in the R12 pool. PADNA-1 exhibits an excellent release ratio of 145, as quantified by qPCR (Figure 2.2A). We confirmed that the structure-switching function of PADNA-1 arises from the selected release domains by comparing our results with negative controls (Table 2.S2, bottom two rows). We also measured release across a range of pH gradients (Figure 2.2B). First, we challenged the PADNA-1/Mipomersen complex with pH 9.6, and found minimal release. This indicates PADNA-1 responds specifically to acidic pH. Second, we observed that PADNA-1 shows increasing release in proportion to decreasing pH, rather than a sudden release of all Mipomersen at pH 5.2 (Figure 2.2B). This property is advantageous for continuous distribution of Mipomersen throughout the endosomal

maturation process, rather than delivery restricted to the late endosome where the pH is ~5.2.

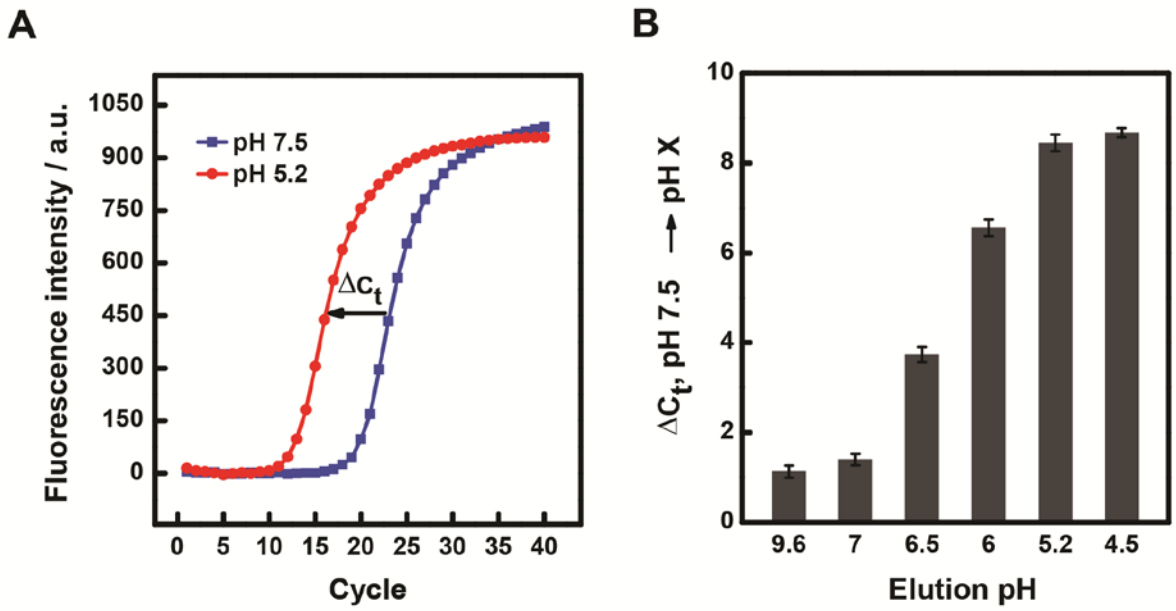

Figure 2.2. Efficiency and specificity of Mipomersen release by PADNA-1. (A) qPCR measurements show PADNA-1 release from magnetic beads in response to shifting the pH from 7.5 to 5.2. (B) qPCR measurements of PADNA-1 release across a range of pH from alkaline (9.6) to acidic (4.5).

2.2.5 Real-time fluorescence measurement of PADNA release

We monitored pH-dependent Mipomersen release via a real-time fluorescence assay. Specifically, we modified Mipomersen with 5-carboxytetramethyl-rhodamine (TAMRA) on T4 and PADNA-1 with Black Hole Quencher 2 (BHQ2) on T54 (see 2.4.1, Table 2.S1). We chose TAMRA for these experiments because its fluorescence is known to be stable in acidic pH.[63] When Mipomersen hybridizes to PADNA-1, TAMRA fluorescence is quenched. When Mipomersen is released by acidic pH, the fluorescence is restored (see 2.4.3, Scheme 2.S1).

First, we challenged the complex with pH 9.6 and observed no change in signal, confirming that PADNA-1 does not release in response to basic pH shift (Figure 2.3A).

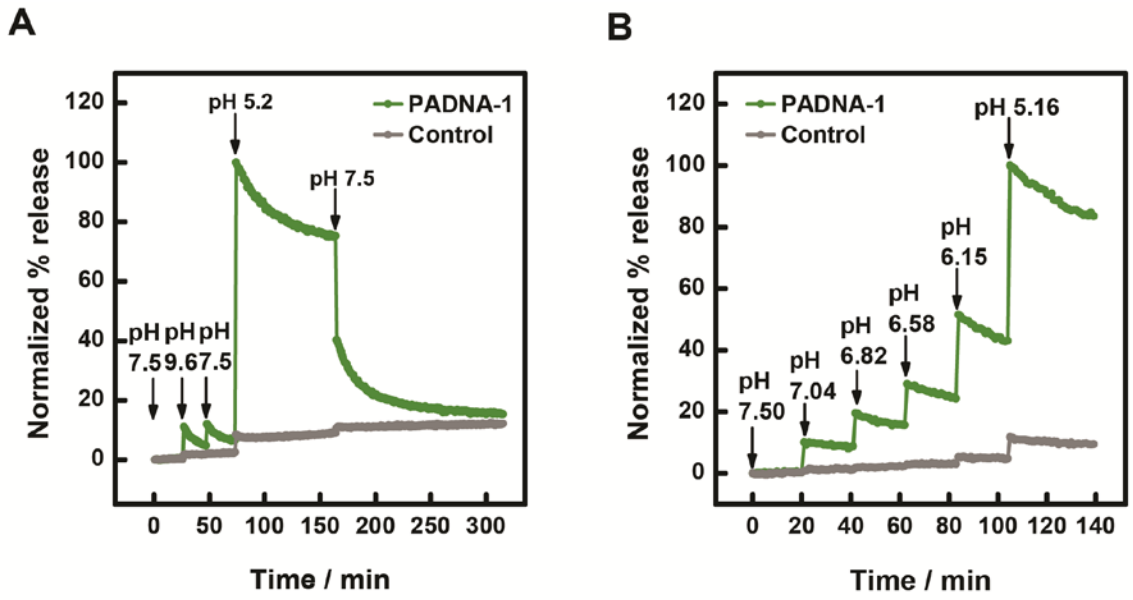

Figure 2.3. (A) Real-time measurement of fluorophore-labeled Mipomersen release from quencher-labeled PADNA-1. (B) Real-time titration experiments showed that the fraction of released Mipomersen increases monotonically with decreasing pH. The poly-T control (gray), is a negative control sequence where the release domains of PADNA-1 are replaced with polyT (see 2.4.1, Table 2.S1). As expected, the polyT control showed minimal response under identical conditions. Data were normalized to the maximum value of release at pH 5.2. Details for this calculation are described in Figure 2.S1. We note that the fluorescence signal measured in these experiments appears to decay due to photobleaching of TAMRA (see 2.4.3, Figure 2.S1).

This result is consistent with our qPCR measurements (Figure 2.2B). When we decreased the pH to 5.2, however, we observed rapid Mipomersen release (<1 min response time). We note that the maximum release at pH 5.2 observed in this assay was 50.5% of total Mipomersen. We attribute this to the TAMRA and BHQ2 modifications, which may impede release by stabilizing the duplex.[64] Finally, we cycled the pH back to 7.5 and found that Mipomersen re-loaded onto PADNA-1,

with free Mipomersen decreasing to ~15% of its maximum signal over the course of 120 minutes. Re-association appears to be a slow reaction whereas release is a fast process. This property is advantageous for drug delivery because it ensures a high rate of delivery with low rates of reabsorption during endosomal uptake. We further confirmed the reversibility of PADNA-1 loading and release by performing repeated cycling between pH 7.5 and 5.2 (see 2.4.4, Figure 2.S2). Next, we used our fluorophore-quencher assay to monitor continuous stepwise pH titration between 7.5 and 5.2, and found that the release of Mipomersen increased proportionally with the gradual lowering of pH (Figure 2.3B). These results agree with pH titration experiments performed via qPCR (Figure 2.2B).

2.2.6 Unpacking the structure-switching mechanism of PADNA-1

M-fold software predicted highly-ordered secondary structure for PADNA-1,[65] where the release domains and primer regions hybridize extensively with the central domain (Scheme 2.2). We hypothesize that part of the structure-switching mechanism arises from the reversible pH-dependent stabilization of mismatch base-pairs, including two C-A pairs at sites (1) and (2). Protonation of the adenosine N1 moiety reorganizes a C-A mismatch into a C•A^+ wobble pair which has been reported to contribute up to -10 kcal/mol to the free energy.[66] We predict that at pH 5.2, PADNA-1 adopts a low-pH conformation in which the primer and release domains hybridize with the central domain, thereby displacing Mipomersen. Interestingly, the pKa of these C-A mismatches can be estimated from Figure 2.3B to be ~5.5, which differs from previously reported values (~7.5) measured under similar conditions.[66, 67] We believe that secondary/tertiary interactions with C-A

mismatches may shift the pKa. For example, it has been shown that multiple C-A mismatches in the same duplex can lower the pKa.[68] In Nature, a lead-dependent ribozyme has been shown to contain multiple adenine bases with perturbed pKa values thought to be supported by tertiary interactions.[69]

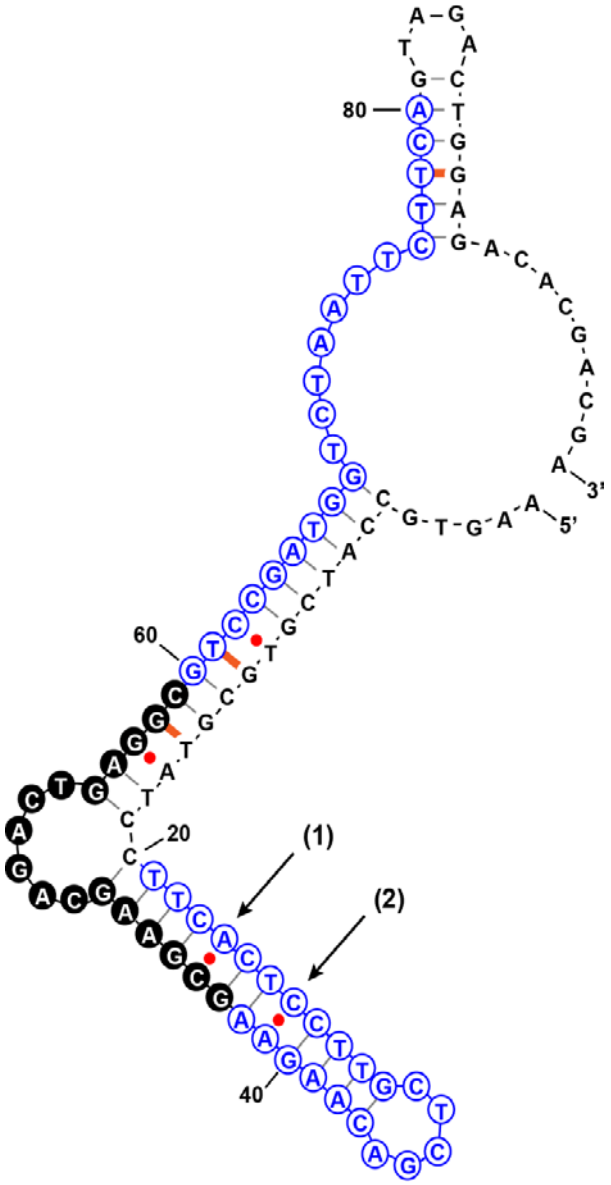

Scheme 2.2. Predicted secondary structure of PADNA-1. Red dots are high-free-energy mismatched base-pairs, orange dashes are low-free-energy mismatches, black dashes are canonical base-pairs. The central domain consists of 17 bases marked by filled black circles.

To test our model, we substituted C-T for the C-A mismatches at either or both sites (1) and (2) in PADNA-1, and then used qPCR to measure the resulting change in release ratio (Figure 2.4A). The C-T basepair is a pH-insensitive analog to C-A, and would thus be expected to impede pH-triggered function. C-T substitution at site (1) reduced the release ratio to 6, and substitution at both sites knocked out the release function completely. Our results suggested that C•A^+ wobble pairs play a major role in stabilizing the low pH conformation of PADNA-1 that displaces Mipomersen from the central domain.

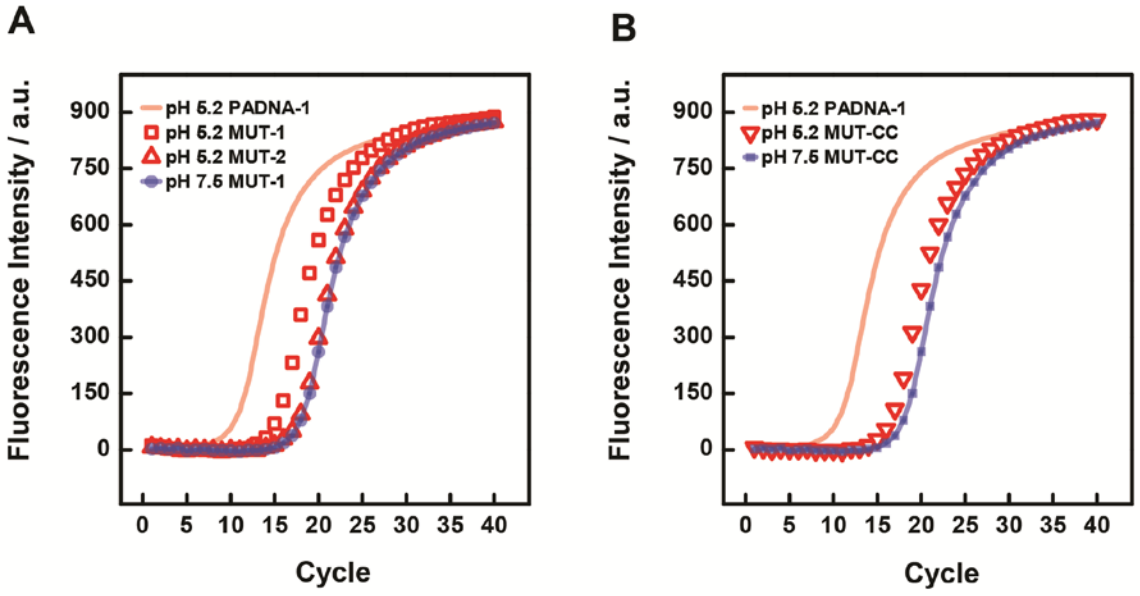

Figure 2.4. (A) MUT-1 showed decreased release at pH 5.2, yielding a reduced ΔCt value of 2.76 +/- 0.03. MUT-2 showed almost complete loss of function, yielding a ΔCt of 0.71 +/- 0.03. Data are also shown for MUT-1 release at pH 7.5 (essentially identical to data for MUT-2 and PADNA-1). Release from PADNA-1 at pH 5.2 is also shown, with the fit line reproduced from Figure 2.2A for comparison. (B) MUT-CC yielded a ΔCt of 1.71 +/- 0.07.

Interestingly, we also examined mutants where we replaced the C-A mismatches with G-C or A-T Watson Crick base-pairs. We found that these mutants released ~80% of loaded Mipomersen at pH 7.5 according to fluorescence

monitoring (see 2.4.5, Figure 2.S3). Since G-C/A-T basepairs would be expected to promote intramolecular folding of PADNA-1 at pH 7.5, these results support the hypothesis that stabilization of basepairs at sites (1) and (2) makes a large contribution to the structure-switching release mechanism.

Since C-C mismatches are also known to form protonated wobble pairs (C^+•C),[33] we tested whether mutants with C-C substitutions at sites (1) and (2) could rescue structure-switching function (Figure 2.4B). However, such mutants only exhibited a release ratio of 3. Based on these observations, we believe that the structure-switching mechanism relies on specific tertiary interactions with protonated adenine residues, and this is a subject of future investigations.

2.3 Conclusions

In this work, we report a discovery-driven approach to identify pH-activated, structure-switching DNA nanostructures. PADNAs respond specifically to a shift from neutral to acidic pH, undergoing a conformational change that results in highly selective release of the antisense drug Mipomersen. For example, PADNA-1 releases Mipomersen with 145-fold selectivity at pH 5.2 versus 7.5. None of the pH-dependent structure-switching sequences we generated were related to known motifs, suggesting that they may operate via novel structure-switching mechanisms. We found strong evidence that the reversible formation of C•A^+ wobble pairs contributes to the pH-responsive function of PADNA-1. Although our results are preliminary, PADNAs demonstrate excellent potential for tightly regulated drug delivery. *In vitro* selection offers exciting opportunities to discover new functional DNA motifs and we anticipate that it could be adapted to identify other sequences

with distinct pH response characteristics and drug release profiles.

2.4 Supplementary section

2.4.1 Oligos used for selection and characterization

Table 2.S1. All sequences written 5' to 3'.

Forward primer	FAM-AAGTGCCATCGTGCGTATCC
Reverse primer	Phos-TCGTCGTGTCTCCAGTCTAC
Biotin-Mipomersen	Biotin-T_{20}-GCCTCAGTCTGCTTCGCACC
Lib17	AAGTGCCATCGTGCGTATCC-N_{22}-GCGAAGCAGACTGAGGC-N_{21}-GTAGACTGGAGACACGACGA
PolyT control	AAGTGCCATCGTGCGTATCC-T_{22}-GCGAAGCAGACTGAGGC-T_{21}-GTAGACTGGAGACACGACGA
TAMRA-Mipomersen	GCC(T-TAMRA)CAGTCTGCTTCGCACC
BHQ2-PADNA-1	AAGTGCCATCGTGCGTATCCTTCACTCCTTGCTCGACAAGAAGCGAAGCAGAC(T-BHQ2)GAGGCGTCCGATGGTCTAATTCTTCAGTAGACTGGAGACACGACGA
BHQ2-polyT control	AAGTGCCATCGTGCGTATCC-T_{22}-GCGAAGCAGAC(T-BHQ2)GAGGC-T_{21}-GTAGACTGGAGACACGACGA
GC-Q	AAGTGCCATCGTGCGTATCCTTC(G)CTCCTTGCTCGACAAG(G)AGCGAAGCAGAC(T-BHQ2)GAGGCGTCCGATGGTCTAATTCTTCAGTAGACTGGAGACACGACGA
AT-Q	AAGTGCCATCGTGCGTATCCTTCACT(T)CTTGCTCGACAAGAAG(T)GAAGCAGAC(T-BHQ2)GAGGCGTCCGATGGTCTAATTCTTCAGTAGACTGGAGACACGACGA
MUT-1	AAGTGCCATCGTGCGTATCCTTC(T)CTCCTTGCTCGACAAGAAGCGAAGCAGAC TGAGGCGTCCGATGGTCTAATTCTTCAGTAGACTGGAGACACGACGA
MUT-2	AAGTGCCATCGTGCGTATCCTTC(T)CTCCTTGCTCGACAAG(T)AGCGAAGCAGA CTGAGGCGTCCGATGGTCTAATTCTTCAGTAGACTGGAGACACGACGA
MUT-CC	AAGTGCCATCGTGCGTATCCTTC(C)CTCCTTGCTCGACAAG(C)AGCGAAGCAG ACTGAGGCGTCCGATGGTCTAATTCTTCAGTAGACTGGAGACACGACGA

2.4.2 Release ratios of PADNAs identified by HTS and negative controls

Table 2.S2

Sequence ID	Copy number	Sequences without primer sites (5' --> 3')	Release ratio
PADNA-1	91	TTCACTCCTTGCTCGACAAGAAGCGAAGCAGACTGAG GCGTCCGATGGTCTAATTCTTCA	145
PADNA-2	86	TTCACGTTTGTTCTACAAAAGCGAAGCAGACTGAGGC GCGTGCCCTGTCGTGCACCACGG	714
PADNA-3	83	TGAACATTGACGTGTAGTCAATGCGAAGCAGACTGAG GCGCCTCTCTAGTTTGACCTTGG	108
PADNA-4	80	CGCTCCGCTAATATCTATGTTAGCGAAGCAGACTGAG GCGCGATGATGTCTACACTGACG	93
PADNA-6	71	TCCGCTAACTCCGAAAGAGGTAGCGAAGCAGACTGAG GCGCGCCTCCGGCTCGTGTATCG	180
PADNA-7	69	TTCGCAAATTTGGTTACAAATCGCGAAGCAGACTGAGG CGCGCCTTTATGTCTATTCGTT	121
PADNA-9	65	AACTTCACGTCTTCTTGAAAACGCGAAGCAGACTGAG GCGCGTCGAATGGCCTAAACACA	231
PADNA-13	57	TAGCTTCACGATATTTAATACCGCGAAGCAGACTGAGG CGCGTTACCTCCACAGCTTGCT	161
PADNA-18	55	GCTTCACGTTAATTTATTACACGCGAAGCAGACTGAGG CATGCCTCCTGACGTGATCCAC	205
PADNA-20	54	TTCATGCGGAACTTTTTCCACACGAAGCAGACTGAGG CGCGCCTTTGAGTCGATTTGTAG	201
Lib17	-	N_{22}-GCGAAGCAGACTGAGGC-N_{21}	<1
PolyT	-	T_{22}-GCGAAGCAGACTGAGGC-T_{21}	1

2.4.3 Calculations for real time fluorescence monitoring assay

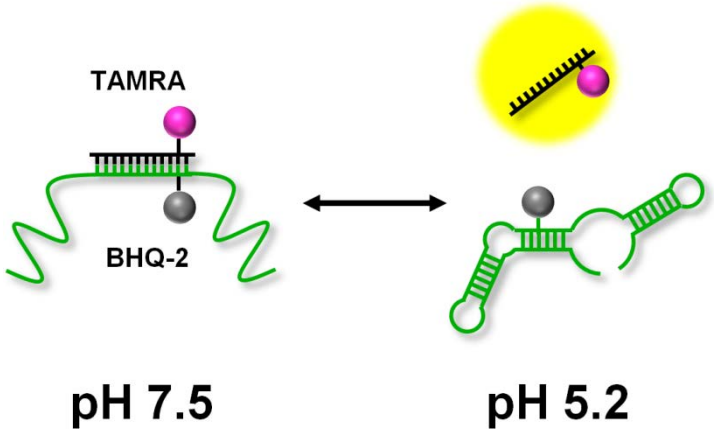

Scheme 2.S1. At pH 7.5, TAMRA-labeled Mipomersen hybridizes with a BHQ2-labeled PADNA molecule, which quenches its fluorescence. When the pH is shifted to 5.2, Mipomersen is released and TAMRA fluorescence is restored.

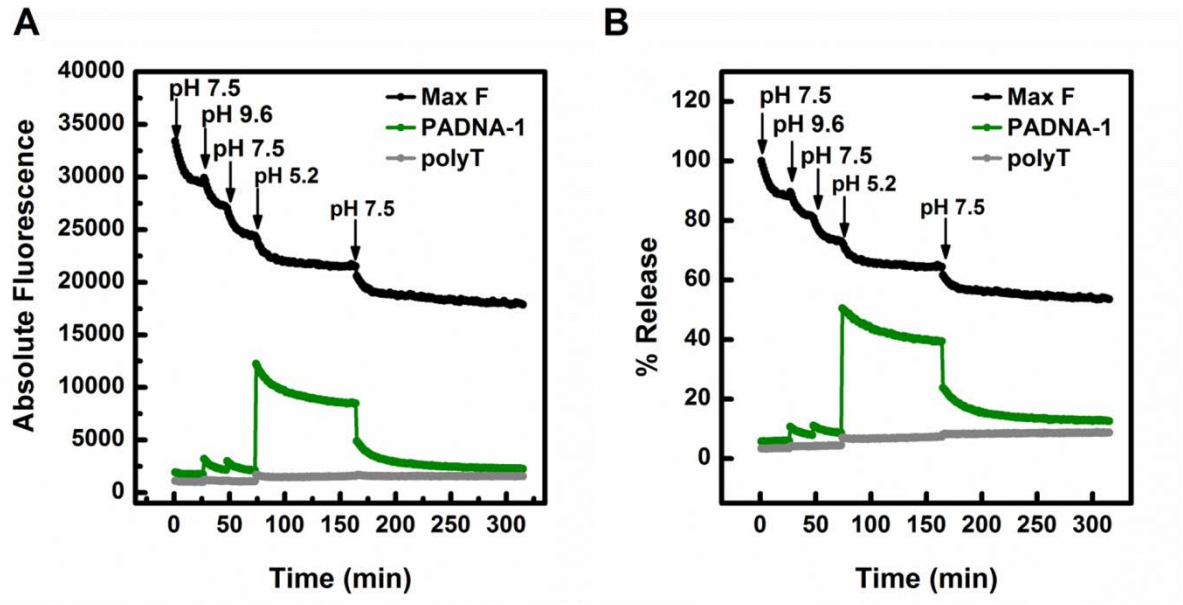

Figure 2.S1. (A) Raw fluorescence data used to produce Figure 3A. Max F represents the signal corresponding to TAMRA-labeled Mipomersen in the absence of BHQ2-labeled PADNA-1. Max F decreases throughout the experiment due to photobleaching of TAMRA. (B) In order to normalize our results relative to TAMRA photobleaching, we calculated the % Release using Equation 1 (below). However, the rate of photobleaching decay for the TAMRA-Mipomersen sample differed slightly from the TAMRA-Mipomersen + BHQ2-PADNA-1 sample and as such, a small photobleaching artifact is visible.

From the absolute fluorescence values, we calculated "% Release" as follows:

% Release = Absolute fluorescence of sample / Max fluorescence x 100% (1)

However, as we noted in the manuscript, the maximum % release at pH 5.2 was capped at 50.5%, perhaps due to the influence of TAMRA and BHQ2 modifications. Therefore, we calculated "Normalized % Release", which results in the plot Figure 3A.

Normalized % Release = % Release / 50.5% x 100% (2)

2.4.4 Reversible loading and release of PADNA-1

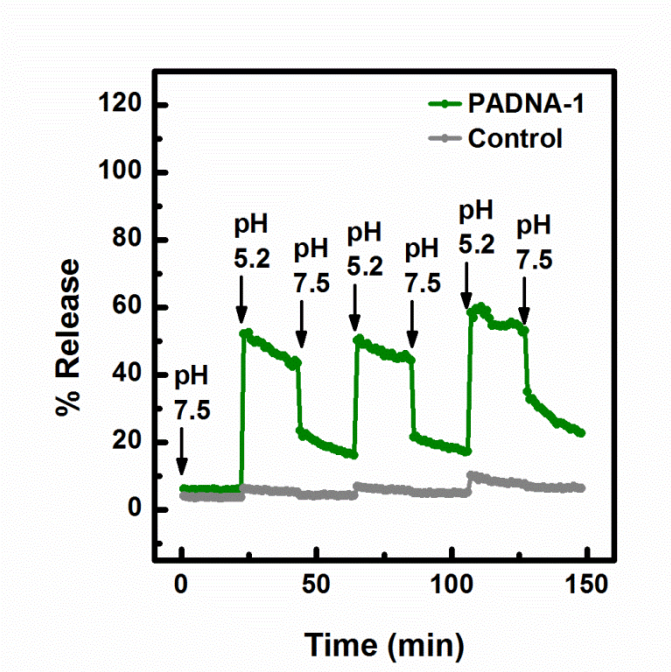

Figure 2.S2. PADNA-1/Mipomersen loading and release is reversible.

2.4.5 Real-time fluorescence monitoring of PADNA-1 mutants

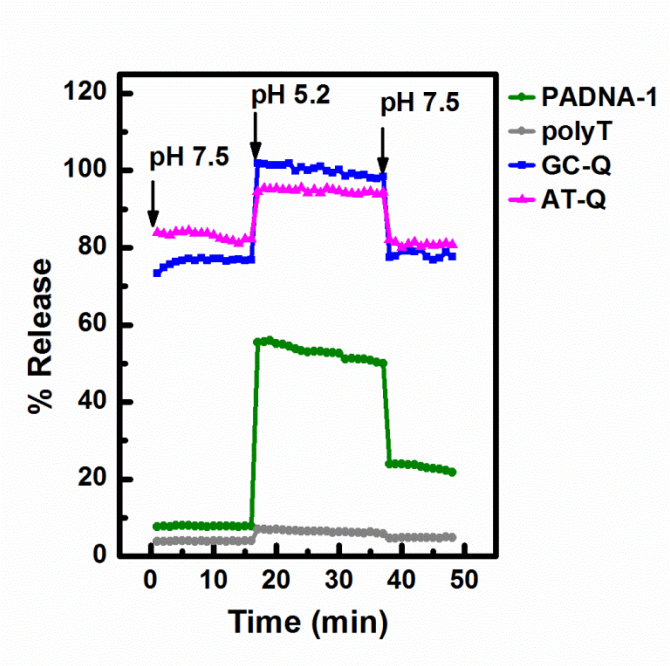

Figure 2.S3. Real-time measurement of fluorophore-labeled Mipomersen release from quencher-labeled mutants of PADNA-1 where C-A mismatches at sites (1) and (2) have been replaced G-C or A-T Watson Crick basepairs. We found that at pH 7.5, the GC mutant (GC-Q) released 76.8% of the loaded Mipomersen. Similarly, the AT mutant (AT-Q) released 82.2% of Mipomersen. This is consistent with our hypothesis for the structure-switching mechanism because G-C or A-T basepairs would stabilize intramolecular folding of PADNA-1 and promote strong release of Mipomersen at pH 7.5. Interestingly, when the GC and AT mutants are challenged with pH 5.2, we observe further Mipomersen release reaching 100%. We believe this effect is likely due to the formation of additional favorable tertiary contacts at low pH.

2.5 Experimental section

2.5.1 Reagents.

The random ssDNA library (Lib17), Mipomersen strand, FAM-labeled forward primer and phosphorylated reverse primer were synthesized and purified by Integrated DNA Technologies (Coralville, IA). Each single-stranded DNA (ssDNA) library component consists of a central 60-mer region flanked by two 20-mer PCR primer sequences. The central region includes a 17-nt Mipomersen-binding sequence flanked by two randomized sequences (22- and 21-nt). GoTaq Master Mix and MyOne streptavidin C1 Dynabeads were purchased from Life Technologies (Carlsbad, CA). Unmodified PADNA clones, TAMRA-labeled Mipomersen strand, and BHQ2-labeled clones were synthesized and purified by Biosearch Technologies (San Diego, CA). SA was purchased from Roche Technologies (Germany). iQ SYBR Green Supermix was purchased from Bio-Rad Laboratories (Hercules, CA) for qPCR experiments. λ-exonuclease for single strand generation was purchased from New England BioLabs.

2.5.2 Library Preparation and Immobilization

Lib17 (see 2.4.1, Table 2.S1) was reconstituted as a 500 μM solution in 1X TE, with concentration confirmed via UV-vis measurement. We mixed 100 pmol of Lib17, or 6.02 x 1013 unique sequences, with 150 pmol of biotinylated Mipomersen and hybridized in 200 μL of pH 7.5 1X PBSMT by heating at 95 °C for 5 min, and then slowly cooling down to room temperature (RT) over 20 min. This mixture was then incubated for 20 minutes at RT with 100 μL of SA-coated magnetic beads in

pH 7.5 1X PBSMT. Nonspecifically bound DNA molecules were removed by washing library-bead assemblies with PBST buffer in which the ionic strength was gradually decreased (R1: no wash; R2: x2 in 1X; R3: x1 in 1X, x1 in 1/2 X, x1 in 1/4 X; R4: do R3 wash sequence, then x1 in 1/8 X, x1 in 1/16 X, x1 in 1/32 X; R5-R12: same as R4). The beads were then resuspended in pH 7.5 1X PBSMT overnight. Afterwards, the supernatant was discarded to remove nonspecifically releasing sequences prior to selection.

2.5.3 *In vitro* PADNA selection

In R1, the library-bead assemblies were challenged with 200 µL pH 5.2 1X PBSMT for 30 minutes at RT. PADNA molecules that underwent acid-induced structure-switching were separated from Mipomersen-coated beads using a magnetic particle concentrator (Life Technologies). The resulting supernatant was PCR amplified in 100 µL PCR reactions containing 50 µL GoTaq Master Mix, 0.50 µL 100 µM FAM-labeled forward primer and phosphorylated reverse primer, 10 µL PADNA molecules, and 39 µL nuclease-free water. GoTaq polymerase was activated prior to PCR by heating reactions to 95 °C for 15 min, followed by 25 cycles of a three-step PCR reaction (30-s denaturation at 95 °C, 30-s annealing at 56 °C, 30-s extension at 72 °C). 8 µL of PCR mixture was collected and resolved on a 10% PAGE-TBE gel to determine the optimal PCR amplification cycle number with minimal byproducts. Collected PADNA pools from each round were PCR amplified at the optimized cycle number.

After full PCR amplification, phosphorylated double-stranded DNA (dsDNA) was purified using the MinElute PCR Purification Kit (Qiagen). Purified dsDNA was

enzymatically digested with 36 µL λ-exonuclease in 21.8 µL 10X lambda exonuclease buffer for 90 minutes at 37C. The resulting ssDNA product was purified using phenol-chloroform extraction/ethanol precipitation overnight at -80 °C. The resulting ssDNA pool was quantified via UV-vis at 260 nm and then prepared for the next round of selection.

Over 12 rounds of selection, we systematically decreased the amount (in pmol) of ssDNA library to apply higher selection stringency (R1-R6: 100, R7: 10, R8: 2, R9-R10: 1, R11-12: 0.1). From R3 onward, we also performed negative selections using 1 µM SA. The negative selections were performed in 200 uL of pH 7.5 1X PBSMT for 30 min at RT.

2.5.4 High-Throughput Sequencing of Isolated PADNAs

After 12 rounds of selection, the enriched pool was PCR amplified with unmodified forward and reverse primers under the reaction conditions described above at an optimized PCR cycle number determined by pilot PCR. These PCR products were then purified by the MinElute PCR Purification Kit (Qiagen) and sequenced with Illumina MiSeq Next Generation Sequencing at the GENEWIZ San Diego Laboratory using a 30% PhiX control.

2.5.5 PADNA Characterization via qPCR

100 pmol of each individual PADNA ssDNA sequence was mixed with 150 pmol of biotinylated Mipomersen and hybridized in 200 µL of pH 7.5 1X PBSMT by heating at 95 °C for 5 min, and then slowly cooling down to room temperature (RT) over 20 min. This mixture was then incubated for 20 minutes at RT with 100 µL of SA-coated magnetic beads in pH 7.5 1X PBSMT. Our qPCR measurement confirmed that 60% of our PADNAs was immobilized after the preparation step. The PADNA/bead assemblies were challenged with 1X PBSMT (pH 4.5 – pH 9.6) for 30 min at RT and the eluents collected. The quantities of PADNAs released as a result of pH-induced structure-switching were subsequently determined by qPCR. Each PCR reaction contained 10 µL iQ SYBR Green Supermix, 8.8 µL PCR water, 0.1 µL each of 0.1 mM forward and reverse primers and 1 µL DNA template. Fluorescence signals were monitored using the iQ 5 multicolor qPCR Detection System (Bio-Rad) and a ΔCt value was determined for each pH shift. All samples were tested in triplicate. Release ratio was calculated from the following formula: $2^{\Delta Ct}$.

2.5.6 PADNA Characterization via Real-Time Fluorescence Measurements

We mixed 0.5 µM BHQ2-modified PADNA-1 or control sequence with 0.5 uM TAMRA-labeled Mipomersen and hybridized in 200 µL of pH 7.5 1X PBSMT by heating at 95 °C for 5 min, and then slowly cooling down to room temperature (RT) over 20 min. The mixtures were transferred to a black 96-well microplate (Microfluor 2, Thermo Scientific; Waltham MA) and equilibrated for 30 minutes at RT. The pH was cycled between 5.2 and 7.5 using small volumes of 1 M HCl or NaOH and the

fluorescence emission was measured at 579 nm using a TECAN microplate reader (San Jose, CA) with the following settings: excitation wavelength = 525 nm, excitation bandwidth = 5 nm, and emission bandwidth = 5 nm.

Chapter 3. *In vitro* selection of a pH-gated structure-switching aptamer

3.1 Introduction

Aptamers are affinity reagents composed of nucleic acids which are generated by an *in vitro* process known as Systematic Evolution of Ligands by Exponential Enrichment (SELEX)[70]. Aptamers have been found which can bind with high affinity and specificity to a broad range of target molecules including proteins[10], small molecules[71], and whole cells[72]. The ease of chemical synthesis and modification of aptamers as well as their high thermal stability arises from the material properties of being composed of nucleic acids (DNA, RNA, modified oligonucleotides)[70], [73]. As such, aptamers are emergent competitors to traditional protein-based antibodies. Aptamers have found applications as biosensors[73] and as therapeutic molecules[74]. Most notably, the FDA-approved medicine, Macugen, is an aptamer inhibitor of vasoendothelial growth facor (VEGF) used for the treatment of wet age-related macular degeneration (AMD)[74].

Recently, there has been growing interest in developing pH-reactive aptamers where 'catch-and-release' of the ligand is controlled by changes in pH. Potential applications have been proposed for pH-controlled drug delivery[57], [75], sensors[76] , and biological separation[77]. Shastri and co-workers made use of the inherent pH-sensitivity of the thrombin binding aptamer (TBA) to reversibly catch and release its ligand[77].

At the date of compiling this thesis, June 2017, this work is still in progress. The contents are thus presented as preliminary results.

However, this approach has two notable disadvantages: first, many aptamers are not innately pH-reactive and second, there is no method to tune the pH-switching behavior. As such, several groups have designed allosteric methods to impart pH-control by incorporating known pH-sensitive modules. Ricci and co-workers created a pH-dependent cocaine-binding aptamer (CBA) by appending a pH-sensitive triplex motif distal to the ligand binding site[57]. The range of pH-sensitivity of their modified aptamer was demonstrated to be tunable by varying the %GC content of the triplex module[57]. Other groups have found success using the i-motif[76] and polyA sequence[75] to impart pH control over aptamer affinity. Notably, strategies based on the i-motif are constrained by the difficulty in tuning its pH-responsive properties[58], [59] and applications of the polyA sequence are limited to aptamer sequences which are specifically G-rich in nature[75].

Although these strategies are reasonably effective, the design of pH-controlled aptamers is constrained by the geometry and orientation requirements of known pH-active motifs[32],[36]. For example, it would be extremely challenging to attempt to minimize the size of the pH-reactive module. Moreover, determining the optimal location for insertion is not trivial, since incorporating a foreign nucleotide sequence could interfere with normal folding of the aptamer. Previously, our group described an *in vitro* selection to generate novel pH-activated DNA nanostructures (PADNAs)[78]. We set selection conditions to tune structure-switching behavior over a custom pH range[78]. Here we describe a selection-based approach to generate pH-gated structure-switching aptamers (PGSAs) where the binding affinity is directly modulated by changing the pH. As a model, we selected for PGSAs that selectively switch off affinity for Streptavidin at pH 5.2 and switch on affinity at pH

7.5 (Scheme 3.1A). Our selection technique generated an enriched pool of PGSA molecules which showed a 6-fold decrease in affinity at pH 5.2 compared to 7.5. We obtained 82 unique sequences from the enriched pool which we are currently assaying for individual pH-reactivity performance. On the basis of these results, we conclude that it should be feasible to adapt our selection process to generate aptamers with pH-controlled affinity over any desired pH range for diagnostic or therapeutic applications.

3.2 Results and Discussion

3.2.1 Library design

Our starting library (Lib_Min) comprises three domains (Scheme 3.1B). The 29-nucleotide (nt) central domain is a well known Streptavidin binding aptamer (SBA29) with a Kd of ~100 nM as previously reported by several groups[79-82]. SBA29 is thought to form a stem-bulge-loop structure[19] with moderate affinity for the biotin binding sites of Streptavidin[79],. The central domain is appended to a 16-nt randomized release domain which is subject to the forces of selection. In this arrangement, the release domain may fold with the central domain to disrupt the functional structure of SBA29 and turn off affinity for Streptavidin at low pH. Finally, each PGSA molecule contains forward and reverse PCR primer-binding sites at the distal ends of the sequence (20-nt).

3.2.2 Selection of pH-gated structure-switching aptamers

We selected PGSA molecules capable of pH-controlled structure-switching by incubating the library with Streptavidin (SA)-coated magnetic beads at pH 7.5, and later isolating the molecules that selectively release from the beads when challenged with pH 5.2 (Scheme 3.1C, see 3.4 for details). Specifically, we applied 10 pmols of our starting library to SA-coated magnetic beads, allowing the library to become immobilized by binding via the SBA29 central domain. We equilibrated overnight in pH 7.5 buffer, and then discarded molecules which were not immobilized on the beads. Next, we challenged the assemblies with pH 5.2 buffer and collected PGSAs which released from the beads. We PCR amplified and generated single-stranded products for the next round of selection or for bacterial cloning and sequencing. We performed 6 rounds of selection, systematically increasing selection stringency by applying additional SA-coated magnetic beads to the sample during the pH 5.2 elution steps. This technique increased the number of available SA binding sites to make PGSA re-binding more favorable, thus increasing the stringency of selection for structure-switching release.

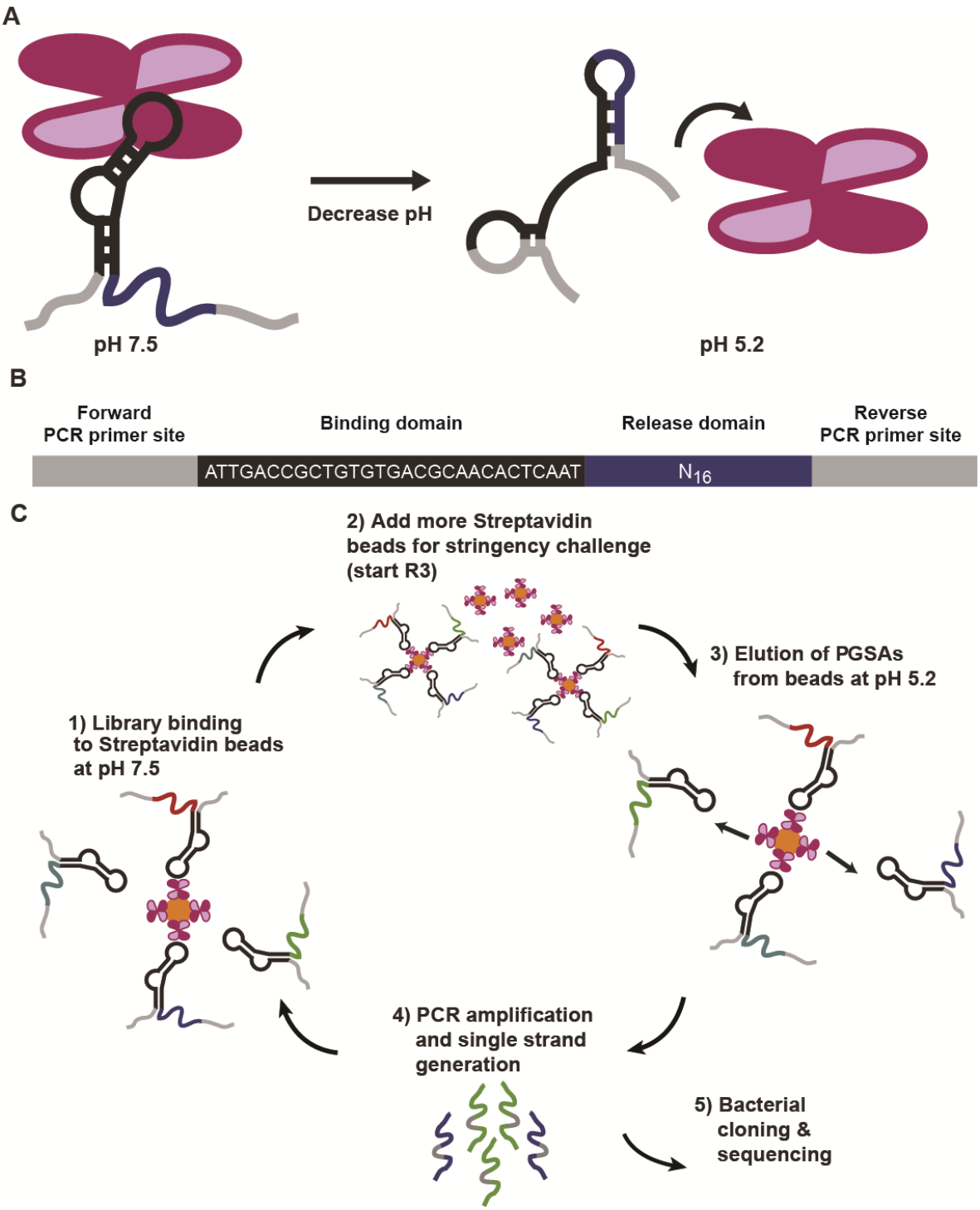

Scheme 3.1. Design and selection of Streptavidin PGSAs. (A) Our PGSA was designed to switch structure in response to decreased pH, disrupt normal folding of the aptamer and switch off its affinity for Streptavidin. This liberates Streptavidin and restores its biological functions. (B) We *in vitro* selected our PGSA from a library of DNA molecules comprised of a 29-nt binding domain (black) appended to a randomized 16-nt release domain (blue), and flanked by two 20-nt PCR primer sites (grey). The binding domain consists of the Streptavidin binding aptamer SBA29 previously described

by Bing and co-workers, which is known to have bind Streptavidin with a Kd ~100 nM[79]. (C) Overview of the selection process. First, we incubated 10 pmol of PGSA library with SA-coated magnetic beads in pH 7.5 selection buffer and allowed the reaction to reach binding equilibrium overnight. Next, we challenged the PGSA-bead assemblies with pH 5.2 selection buffer and eluted PGSA molecules capable of structure-switching. The eluent was PCR-amplified and purified single-stranded DNAs were generated. This enriched pool was then prepared for the next round of selection. Over the course of the selection, we tuned selection stringency by applying additional SA-coated magnetic beads to the sample before the pH 5.2 buffer challenge. Excess SA binding sites makes re-binding more favorable, and thus, only the most efficient structure-switchers will release from the beads and be collected for further enrichment. At the end of the selection, the enriched pool was cloned via bacteria and sequenced.

3.2.3 Enriched PGSA pool shows pH-controlled structure-switching

At the end of each round, we PCR-amplified samples taken from the eluents and ran gel electrophoresis to determine the "release ratio" – the amount of PGSAs released at pH 5.2 compared to pH 7.5 (Figure 3.1). This ratio increased over the course of the selection, as seen by the differences in band intensities, reaching ~6-fold by R6. As such, the enriched pool exhibited clear structure-switching functionality in response to pH change. We also examined the amount of DNA eluted in the absence of excess SA stringency challenge and found that ~9-fold more DNA is eluted at pH 7.5, demonstrating that this is an effective method to increase selection stringency for structure-switching release.

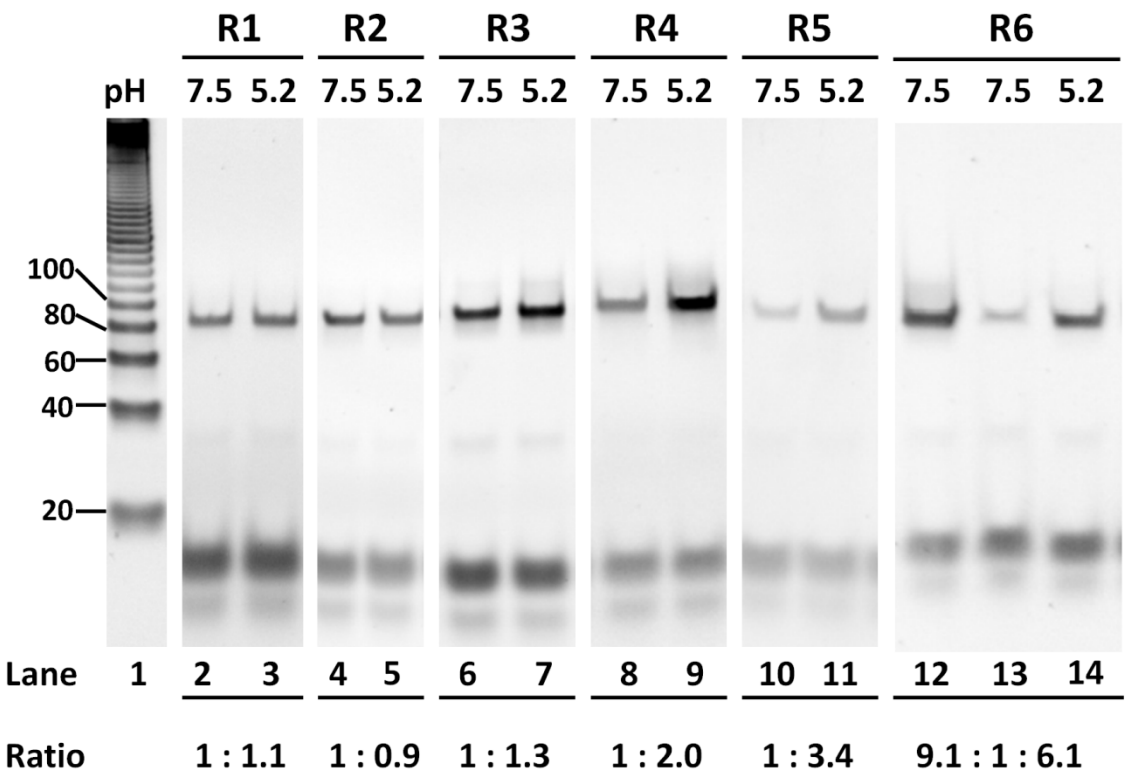

Figure 3.1. Gel images comparing the DNA eluted after 30 minutes in pH 7.4 or pH 5.2 selection buffer over multiple rounds of selection (lanes 2-11 and 13-14). Lane 1 contains the 20-bp molecular ruler. Lane 12 shows elution of the R6 pool for 30 minutes in pH 7.5 buffer without excess SA stringency challenge.

3.2.4 Identification of individual PGSA sequences

We analyzed the R6 pool with bacterial cloning and sequencing, obtaining 82 unique sequences (Table 3.1). In our sequence alignment, we found that our PGSAs did not contain known pH-responsive modules such as the i-motif[58], the triplex switch[57], or poly-dA repeats[61]. These results suggest that PGSAs inhibit SBA29 binding affinity through novel pH-controlled mechanisms.

Table 3.1. PGSAs identified by Sanger sequencing

Sequence ID	Sequences without primer sites (5' --> 3')	Copy number
PGSA-1	GGAGCGTGCGAAACG	2
PGSA-2	ATTACGCTGCCGACG	1
PGSA-3	GGCTTGAGCATAACG	1
PGSA-5	GGAGCCCTGACGGAG	2
PGSA-6	TGTTACGCCCGAACG	1
PGSA-7	GGATATGCTTTGCCG	1
PGSA-8	GATACTCTGAAGGGG	1
PGSA-9	GGGCCCAACGCGTTC	1
PGSA-10	GGTGTAAATACGACG	1
PGSA-11	GGAAATCAATAGGGA	1
PGSA-12	AATCTAAAGTAGGGT	1
PGSA-13	GGGCTACGCCACTAG	1
PGSA-14	GGATGAGATGCGTAG	1
PGSA-15	GGAAATTAACTAGCG	1
PGSA-16	AGGATCGCCGTGGAG	1
PGSA-17	GGTGAGCGATAGTTG	1
PGSA-18	CGATTCGCACGACCGT	3
PGSA-19	GAGAGCATCAAGGAGG	1
PGSA-20	TTGATCCGTGAGGGGT	1
PGSA-21	GGAGACTCTCGGAGTA	1
PGSA-22	TGTATCGCCTTTACGT	1
PGSA-23	GAATCGCGCCTCTAGT	1
PGSA-24	GGACTCATAAACGCGT	1
PGSA-25	GAGTATTGCACGACGN	1
PGSA-27	GTTATTACGTGTACGT	1
PGSA-28	GTGCTACGCCTCTTGT	1
PGSA-29	AAGATCGTACTGTTGT	2
PGSA-30	GGAAAAGGCCGCTCGT	1
PGSA-32	GTGCAGATGGGTCAGT	1
PGSA-33	GAACGCCCCAAGTGGT	1
PGSA-34	CGGAGCCNCCCGGAAG	1
PGSA-35	GGACTAGGAGTAACGT	1
PGSA-36	AGGGGACGCGCCCCGT	1
PGSA-37	GGGAGCGCTGGGTCGG	1
PGSA-38	TGTATACGAGTGGCGT	1
PGSA-39	GGACTCCCAGAGTTGG	1
PGSA-40	GGATAGAGGCGATCGG	1
PGSA-41	GGGGAGCCTTAACCGT	2

PGSA-42	GCCAGATATCCGTGGT	1
PGSA-43	GGGTACTTTCGTACGG	1
PGSA-44	GGAATTAGTGCGTTGT	1
PGSA-45	TTATCGCTACTGTTGT	2
PGSA-46	GGAGATCTTAGGGTGT	1
PGSA-48	TGATCGCTTGCGTAGT	1
PGSA-50	TTACGCCGGCTGTGGT	1
PGSA-51	GGATGCCTCACTGAGT	1
PGSA-52	GGTACGCAGGCCGTGT	1
PGSA-53	ACAAACGCATAGTCGA	1
PGSA-54	GGTTCCCGCCTNACGG	1
PGSA-56	GGATAGAGTACAGAGT	2
PGSA-58	GTTATCGCCCGTTCGG	1
PGSA-59	GTACGCCGCAGGTTGT	1
PGSA-60	GTAGGATATCGCAAGT	1
PGSA-62	AGGGTACGCCCAAAGT	1
PGSA-63	GGTTCGGGCCCGAAGT	1
PGSA-64	GGATTGTGATAGCCGT	1
PGSA-65	CAGCACGTAATCTAGT	1
PGSA-66	AGGAACGCTAAGACGT	1
PGSA-67	GATACTATAAACAAGT	1
PGSA-68	GTATTACGACGTCGGT	1
PGSA-69	GATCGCCGCATTCCGT	1
PGSA-70	GTATCGCCGCCTGAGT	2
PGSA-71	GGAGCGAACAGGGAGT	1
PGSA-72	GGATCGGCAGCGTTGG	1
PGSA-74	GAGTACGGGAAGGGGT	1
PGSA-75	GATGCCGCGTTGTTGT	1
PGSA-76	GAGTAAGCATCGTCTT	1
PGSA-77	GGACCGGTAGCGTCGA	1
PGSA-78	GATGCACGATAGTGGT	1
PGSA-79	GGGTGCATTATGTAGT	1
PGSA-80	GGACATCCTTAGACGG	1
PGSA-81	GGAGGCCTCGCGTAGT	1
PGSA-82	GTTATATCGCATTCGT	1
PGSA-83	GATCGCCATTTGGAGG	1
PGSA-84	GACTACGGCCGTCCGG	1
PGSA-86	TATACGCCGGACTCGG	1
PGSA-88	GGAAAGAGGGTCGCGT	1
PGSA-89	GAGCAGCCAATCTAGT	1
PGSA-90	GGGGAGCCCGCGACGG	1

PGSA-92	CGGAGCCGCCCCCCGT	1
PGSA-93	GGGTTAGCCGCGTAGT	1
PGSA-94	CGTAATACGCCGACGT	1

3.2.5 Structure-function relationship of PGSAs

M-fold software was used to predict the secondary structure of the 8 PGSAs with copy number >1 when sequenced[65]. In particular, PGSA-45 is of interest because the predicted secondary structure in solution does not form the expected stem-bulge-loop of SBA29 (Figure 3.2A). Instead, the release domain is predicted to partially fold with the binding domain forming a stem loop (Figure 3.2B). The loop is relatively large, comprising 16 basepairs, which offers a significant energetic penalty at pH 7.5. However, we hypothesize that at pH 5.2 several low-pH stabilized wobble pairs ($C{\bullet}A^+$, $C^+{\bullet}C$, $A^+{\bullet}G$)[33],[61],[66] may facilitate the formation of a stable low-pH conformation that outcompetes the functional SBA29 structure and collapses binding affinity for Streptavidin (Figure 3.2C). These simulations suggest that PGSA-45 may be induced to form functional SBA29 in the presence of Streptavidin at pH 7.5 (Figure 3.2A). As the pH decreases, it may pass through intermediate states (Figure 3.2B) and then achieve a stable conformation at pH 5.2 which releases Streptavidin (Figure 3.2C). As this work is still in progress, we require additional data to comment further on the mechanism. We plan to examine variants of PGSA-45 where the putative low-pH-stabilized basepairs have been replaced with pH-insensitive analogs in order to establish which sites are most critical for pH-gated structure-switching.

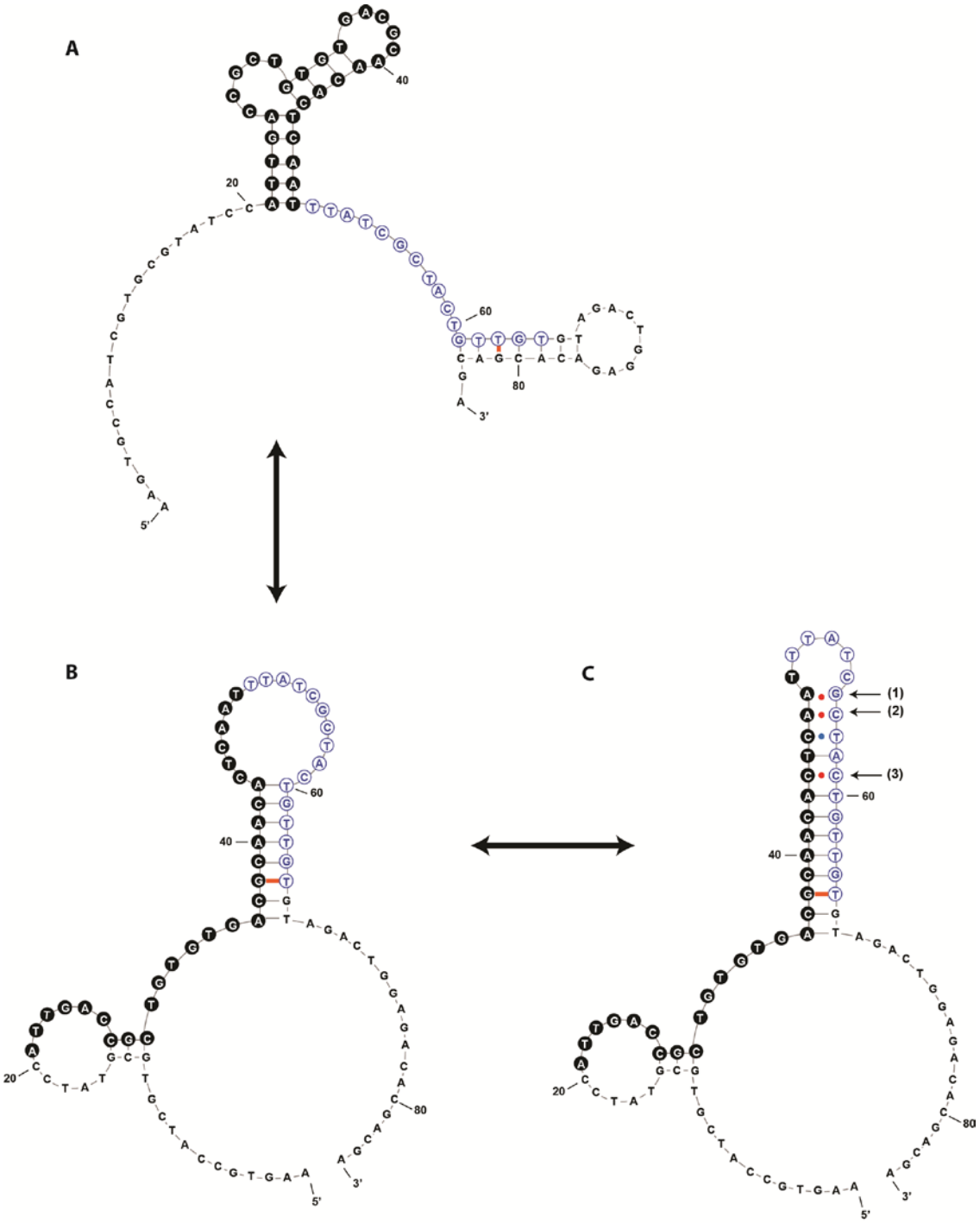

Figure 3.2. Predicted secondary structures of PGSA-45. (A) Structure predicted when constrained to form stem-bulge-loop of functional SBA29. (B) The lowest energy competing structure formed at pH 7.5, which may be an intermediate between (A) and (C). (C) Hypothetical low-pH-stabilized structure at pH 5.2. Acid-stabilized wobble pairs (red dots) at sites (1), (2), and (3) may promote formation of a strongly stabilized duplex at pH 5.2, thus outcompeting the functional binding form of SBA29. Low energy mismatches (orange dashes) and high energy mismatches (blue dots) are also noted.

3.3 Conclusions

In this work, we have demonstrated that PGSA SELEX is an efficient and highly tunable platform for the generation of pH-gated structure-switching aptamers. Using this method, we performed a selection against Streptavidin protein and selected for high affinity binding at pH 7.5, which is turned off by a structure change induced by decreasing the pH to 5.2. Within six rounds of selection, we obtained an enriched pool which showed high affinity binding at pH 7.5, and a 6-fold decrease in affinity at pH 5.2. We obtained 82 unique sequences from bacterial cloning and sequencing which we are currently testing via qPCR assay for individual pH-reactive structure-switching performance. We also plan to measure mutants of these sequences in order to definitively describe the pH-induced mechanism of structure-switching.

We designed this selection to demonstrate that a very small (16-nt) randomized region can be effectively selected to exert pH-control over aptamer affinity. Minimizing the size of the DNA construct is useful because it enables potential applications such as endocytic drug delivery, where charge and size exclusion are important factors[26]. We believe that future experiments should entail selections with varying sizes of randomized regions to balance size with performance.

3.4 Experimental section

3.4.1 Reagents

The random ssDNA library (Lib_Min), FAM-labeled forward primer and phospohrylated reverse primer were syntheiszed and purified by Integrated DNA Technologies (Coralville, IA). Each single-stranded DNA (ssDNA) library consists of a central 45-mer region flanked by two 20-mer PCR primer sequences. The central region includes a 29-nt Streptavidin-binding sequenced adjacent to a randomized sequence (16-nt). GoTaq Master Mix and MyOne Streptavidin C1 Dynabeads were purchased from Life Technologies (Carlsbad, CA). Minelute PCR clean-up kit from Qiagen was used to recover purified amplicons after PCR amplification (Hilden, Germany). λ-exonuclease for single strand generation was purchased from New England Biolabs (Ipswich, MA). All other reagents were purchased from Fisher Scientific. The selection buffer (SB) is prepared from 20 mM Tris-HCl, 100 mM NaCl, 2 mM $MgCl_2$, 5 mM KCl, 1 mM $CaCl_2$, and then the pH is adjusted to either pH 7.5 or pH 5.2 via 1M HCl.

3.4.2 Library Preparation and Immobilization

Lib_Min was reconstituted as a 500 uM solution in 1X TE, and the concentration was confirmed via UV-Vis measurement. We measured out 10 pmol, or 6.02×10^{12} sequences into 100 ul SB, heated at 95°C for 10 min, snap cooled the solution to 4°C for 10 min, and then equilibrated to RT for 10 min to promote intramolecular DNA folding. We applied this heat-treated solution to 8 ul of MyOne C1 SA-coated magnetic beads plus 92 ul of SB for a total sample volume of 200 ul.

This mixture was incubated for 1 h at RT with rotation. Nonspecifically bound DNA molecules were removed by washing library-bead assembles with SB x3.

3.4.3 *In vitro* PGSA Selection

In R1, the library-bead assemblies were challenged with 200 ul pH 5.2 SB for 30 m at RT. PGSA molecules that switched structure and released from the beads at low pH were separated from SA-coated beads using a magnetic particle concentrator (Life Technologies). The resulting supernatant was PCR amplified in 100 uL PCR reactions containing 50 uL GoTaq Master Mix, 0.50 uL 100 uM FAM-labeled forward primer and phosphorylated reverse primer, 10 uL PGSA molecules, and 39 uL nuclease-free water. GoTaq polymerase was activate prior to PCR by heating reactions to 95°C for 15 min, followed by 25 cycles of a three-step PCR reaction (30-s denaturation at 95°C, 30-s annealing at 56°C, 30-s extension at 72°C). 8 uL of PCR mixture was collected resolved on a 10% PAGE-TBE gel to determine the optimal PCR amplification cycle number with minimal high molecular weight byproducts. Collected PGSA pools from each round were PCR amplified at the optimized cycle number.

After full PCR amplification of the supernatant, phosphorylated double-stranded DNA (dsDNA) was purified with the MinElute PCR Purification Kit (Qiagen). Purified dsDNA was enzymatically digested with 36 uL λ-exonuclease in 21.8 ul 10X exonuclease buffer for 90 m at 37C. The resulting ssDNA product was purified via phenol-chloroform extraction and ethanol precipitation overnight at -80°C. The concentration of the purified ssDNA product was quantified via UV-Vis at 260 nm and then prepared for the next round of selection.

Over 6 rounds of selection, we systematically increased the stringency of selection by applying additional SA-coated magnetic beads (in ul) during the pH 5.2 challenge step (R3: 100, R4: 150, R5: 180, R6: 400).

3.4.4 Bacterial cloning and sequencing

After 6 rounds of selection, the enriched pool was PCR amplified with unmodified forward and reverse primers under the PCR reaction conditions described above and purified with the MinElute PCR Purification Kit (Qiagen). We mixed 256 pg of the purified amplicons with 1 uL of TOPO vector, 1 ul of salt solution, and 3 ul nuclease-free water from the TOPO TA Cloning kit (Life Technologies) and incubated at RT for 5 m. We transferred this mixture to 1 vial of One Shot Mach1-T1^{R} competent E coli and heat shocked for 30 s in a 42°C heat block, and then immediately put the reaction on ice for 2 m. We added 250 ul SOC medium and shook at 37°C for 1 hour at 225 rpm. We spread this solution onto pre-warmed agar plates containing 50 ug/ml kanamycin and allowed the colonies to grow overnight. The next day, we picked 94 colonies and transferred them to a gridded agar plate and sent it to the GENEWIZ San Diego Laboratory for Sanger sequencing.

3.5. A pragmatic guide on how to tune up a selection

In this section, we would like to describe the crucial preparation we performed to bring up a novel selection platform, an aspect which is not typically described in published articles. We hope to communicate practical information that will help new researchers develop selection schemes that are more likely to work.

3.5.1 Preparing a target protein

In bead-based selection schemes, the first bottleneck encountered will be the variable yield when conjugating target proteins to magnetic beads. Simply speaking, if you cannot attach your protein of interest to magnetic beads, you have to try alternative selection schemes (nitrocellulose membrane binding[83], capillary electrophoresis[84], or particle display SELEX[85] are possibilities).

The most common method of conjugating proteins to beads is via EDC/NHS reaction. The EDC/NHS method activates primary amines in the protein to react with carboxylic acid groups on the bead surface, forming covalent amide bonds[86]. In general, we have found that <15% of input protein will be successfully attached to the beads. We believe this happens when few primary amines on the protein are available for conjugation, perhaps due to shielding by the protein's tertiary structure or steric hindrance from post-translational glycosylation.

Originally, our first choices for target proteins were IgE and VEGF because the aptamers for these proteins, D17.4[87] and SL2-B[88], are well-characterized, length-minimized, high affinity binders. However, both IgE and VEGF showed negligible conjugation to magnetic beads. The result was consistent with previous literature, where selections for IgE and VEGF aptamers used a capillary

electrophoresis or filter-binding setup and thus, did not require bead conjugation. Eventually, we chose Streptavidin to be our model system because Streptavidin-coated magnetic beads were available off-the-shelf (Thermo Fisher Scientific). To expand our PGSA selection technique to other proteins, we recommend adapting the process to non-bead-based selection methods.

3.5.2 Designing a selection library

A typical selection library is 100 bp or fewer in length and these are readily synthesized by commercial suppliers. Although currently some companies, such as Integrated DNA Technologies, offer synthesis of so-called 'Ultramers' which can be up to 200 bp in length, the pros and cons of selection with such a long library are not well understood.

We wanted to design a selection library that would minimize the size of our construct but still have sufficient diversity to evolve our desired function. As such, we limited ourselves to designs with a 100 bp maximum length. We considered three different strategies for library design (Scheme 3.2). Design 1 incorporated the full SBA29 sequence flanked by two randomized regions (15-nt and 16-nt) (Scheme 3.2A). Design 2 contained SBA29 adjacent to one randomized region (16-nt) (Scheme 3.2B). Design 3 contained an SBA29 truncate flanked by two randomized regions (18-nt and 19-nt) (Scheme 3.2C). In Design 3, the first and last three bases of the aptamer are truncated in order to re-select the properties of the stem in SBA29. Design 3 was informed by a Hg^{2+}-controlled Streptavidin binding aptamer reported by Mei and co-workers, where one or more basepairs in the stem of SBA29 were replaced with T•T mismatches[89]. In the absence of Hg^{2+}, the

sequence would unfold, but when Hg^{2+} intercalated with T•T mismatches, the stem was stabilized and SBA29 binding affinity is restored[89]. Thus in Design 3, we reasoned that we could truncate SBA29 and select for a stem with pH-responsive basepairs.

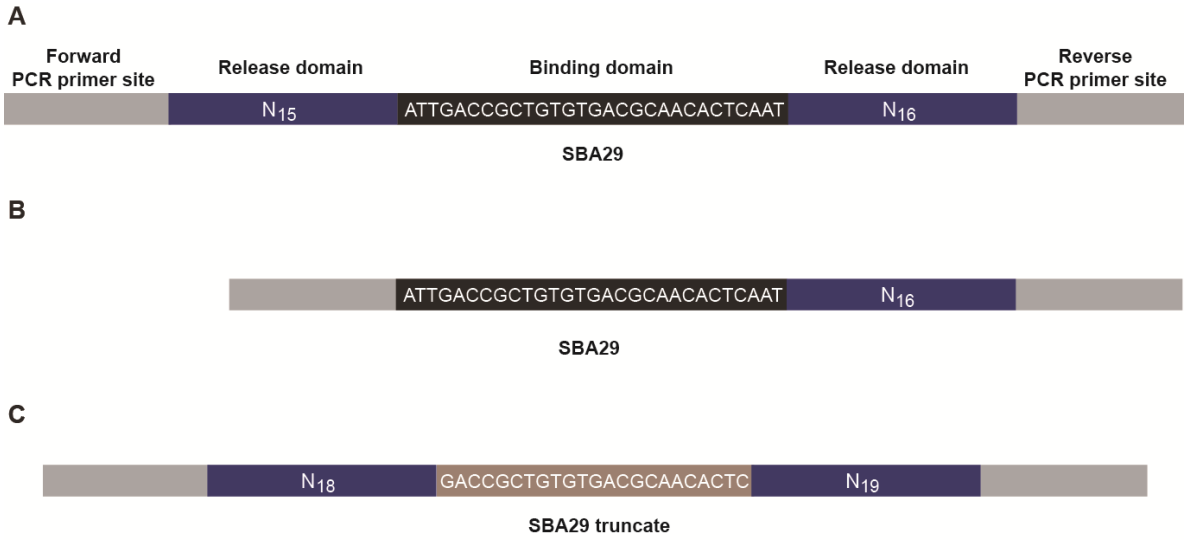

Scheme 3.2. The library designs considered for PGSA SELEX. (A) Design 1 contains the full SBA29 sequence and two randomized release domains to maximize sequence diversity. (B) Design 2 also contains the SBA29 binding domain, but has only one adjacent randomized domain, selecting for a size minimized construct. (C) Design 3 incorporates a SBA29 truncate, in order to re-select the SBA29 stem for pH-reactivity.

Chronologically, we attempted Design 3 first. However, after six rounds, there was no visible enrichment so we stopped (Figure 3.3). We do not definitively know why this design was unsuccessful, but we hypothesize that truncating SBA29 led to re-selection for binding affinity, rather than pH-sensitivity. We could confirm this hypothesis by sequencing the pool to see if the library re-selected for the original stem of SBA29.

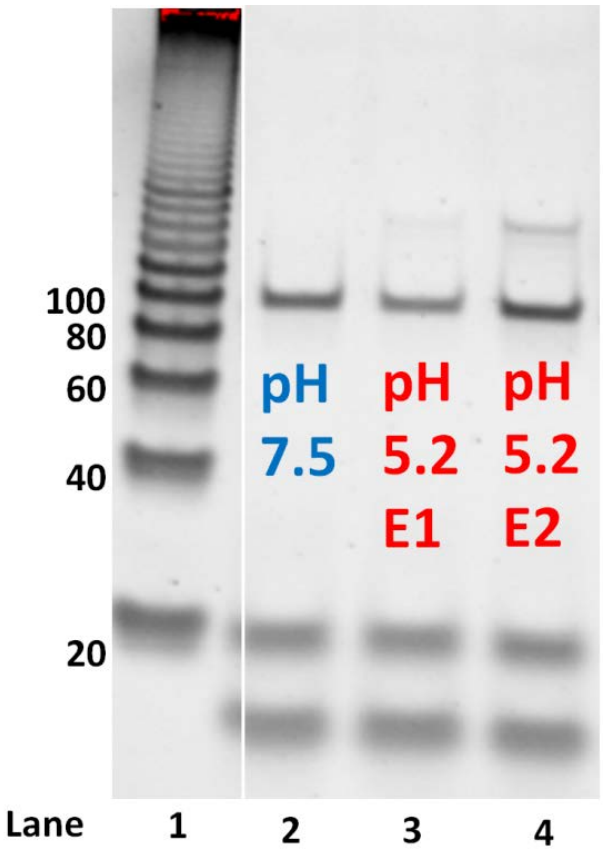

Figure 3.3. Gel image showing comparing the DNA eluted after 30 minutes in pH 7.5 or pH 5.2 SB after 6 rounds of selection using Library Design 3 (lanes 2-4). The amount of DNA eluted at pH 5.2 was virtually the same as at pH 7.5, suggesting that there was no enrichment for pH-reactive structure-switchers. While the bands corresponding to pH 5.2 eluents appear to have some additional mass compared to pH 7.5, it is a distinct high molecular weight byproduct of PCR amplification. Lane 1 contains the 20-bp ruler.

Next, we pursued Design 2 because we wanted to investigate whether a very small randomized region could be selected for pH-responsivity. Design 2 was a success and yielded an enriched pool as described earlier in this chapter (Design 2 is named Lib_Min, see 3.2.1). In the future, we would like to try Design 1 to see if randomized regions flanking both sides of SBA29 may yield even more effective pH-control over structure-switching.

We would also like to comment on the importance of designing unique primers for each selection library. Primer binding sequences (typically 20-nt) are built into all selection libraries for the purpose of specific PCR amplification of the oligo of interest. Re-using primer sequences can lead to cross-contamination, where other people's libraries become amplified in your pool and convolute your selection. There are excellent guides online for designing primers[90]. A shortcut is to use primers previously published in the literature, but if you do so, your laboratory group must maintain a master list so that individual researchers do not accidentally use the same set.

3.5.3 Measuring the loading efficiency of the library

PGSA selection is a sub-type of "Falling-off SELEX" [39],[91], where the library starts out "loaded" onto a bead or other surface, and when challenged with a stimulus, some sequences switch structure and release into the eluent, which is amplified and used for subsequent rounds of selection. It is important to load a sufficient amount of library molecules onto the beads to achieve satisfactory coverage of library diversity. For example, if you have 10^{12} unique sequences in your library, it would be ideal to have at least 10^{12} library molecules load onto the

beads for 1X coverage. If you have 10^{12} unique sequences, but you can load 10^{13} library molecules, you will achieve 10X coverage.

In our system, we incorporated the SBA29 sequence (Kd ~100 nM) into the PGSA library to give it inherent loading affinity for Streptavidin-coated magnetic beads. However, we were concerned that the PGSA library could have significantly reduced loading efficiency compared to SBA29 because it is known that unminimized aptamers have poor affinity for their targets. As such, we performed an experiment to measure the loading efficiency given our chosen selection conditions (Figure 3.4). We combined 10 pmol of PGSA library with 8 ul SA-coated beads (~100 pmol of SA) and equilibrated this loading reaction (Rxn) for 1 hour. Afterwards, we recovered the beads via MPC, washed 3 times with selection buffer, and then ran the sample on a polyacrylamide gel with a standard curve. We determined that that the amount of DNA loaded onto SA-coated beads, or loading fraction (LF), was ~12% of the input, or 1.2 pmols. Since the PGSA library has 16 randomized bases or 4^{16} unique sequences, 1.2 pmol provides 168X coverage.

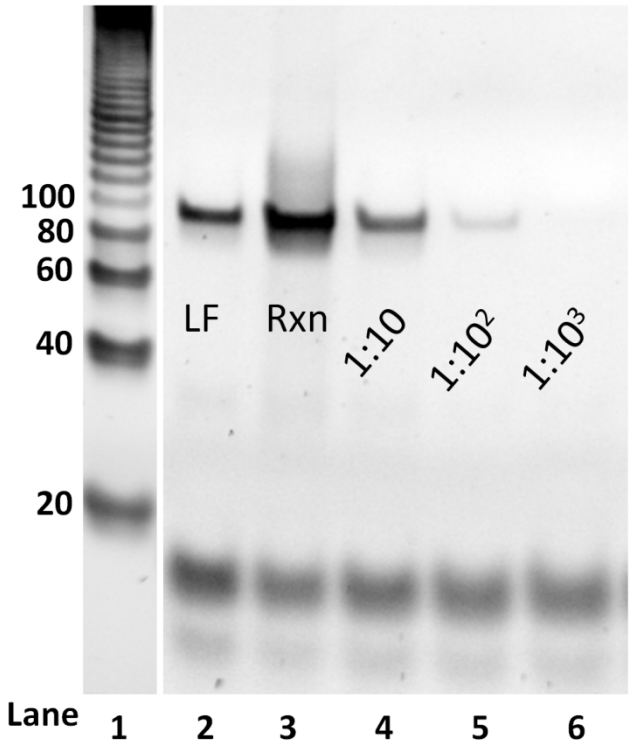

Figure 3.4. Measuring the loading efficiency of the starting PGSA library (Design 2, Scheme 3.2B). Lane 2 shows the amount of DNA bound to 8 ul of SA-coated magnetic beads, or loading fraction (LF). We compared this to a standard curve (lanes 3-6) derived from serial dilution of the loading reaction (Rxn). Comparing the density of the bands in lanes 2 and 4, we calculated that the loading efficiency was ~12%, or 1.2 pmol of PGSA library loaded onto the beads, offering suitable coverage of the library diversity.

We note that it is also important to confirm that the library is loading onto SA-coated beads via specific binding between SBA29 and the biotin site of Streptavidin. This is because in the elution step of PGSA selection, it is desirable to only collect sequences which have released by disrupting specific binding of SBA29 to the biotin site of Streptavidin. In the future, we plan to confirm the specificity of PGSA library loading by performing a competition assay with biotin.

3.5.4 Round-to-round monitoring via comparative elution assay

You should always have a method to assess at each round if your selection is progressing and whether enrichment is occuring at a suitably fast rate. To do this, we developed a “comparative elution assay”, where we take samples from 4 eluents during the selection, run these on a PAGE gel and compare the band densities of the eluted DNA (Figure 3.5). The four eluents represent: the first 30 m elution at pH 7.5, the second 30 m elution at pH 7.5 after stringency challenge has been applied, the first 30 m elution in pH 5.2, and the second 30 m elution in pH 5.2 as a replicate (lanes 9-12, Figure 3.5).

When we performed this comparative elution assay using the loaded beads from Figure 3.3, the results were close to ideal expected behavior. The amount of DNA eluted at pH 7.5 (lane 2) was about the same as the amounts eluted at pH 5.2 (lanes 3, 4). This result is expected in R1 where there has not yet been significant enrichment for structure-switchers. As you perform further rounds, and if the pool is enriching, you would expect the pH 5.2 elution bands (3, 4) to increase in density when compared to the pH 7.5 elution band (2) (see Figure 3.1, section 3.2.3), i.e. you would like to see your “release ratio” increase. We discuss an example of an undesirable result later in section 3.6.6 (Figure 3.7).

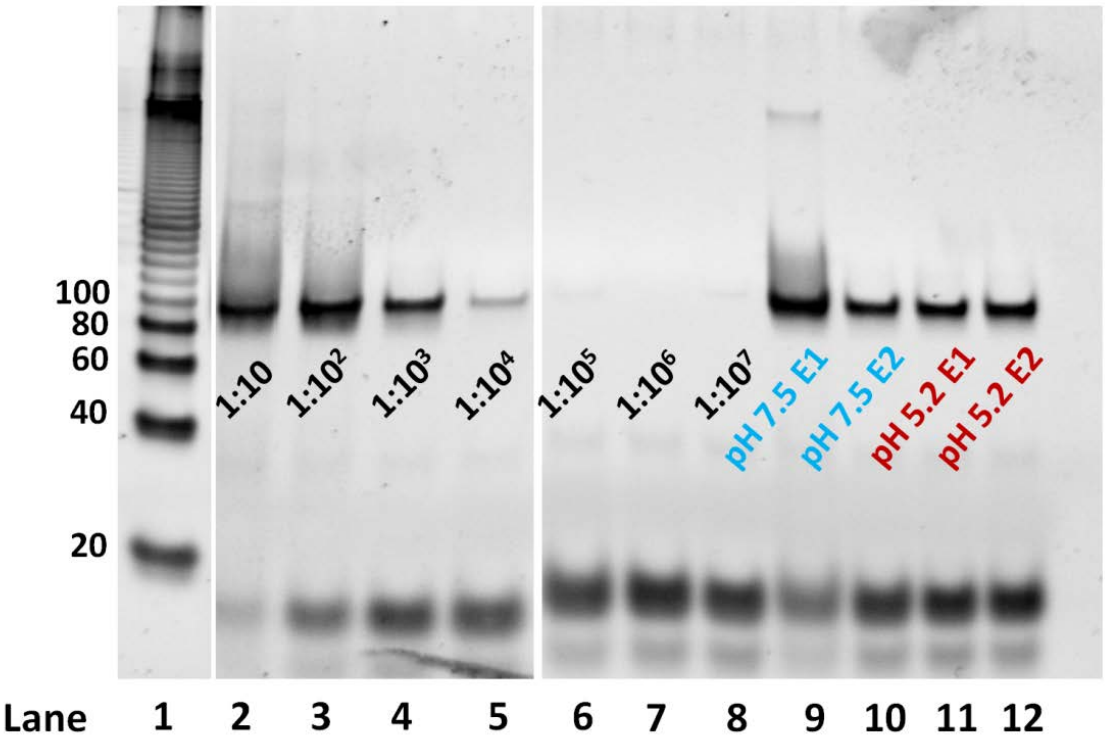

Figure 3.5. Comparative elution assay for R1 calibration experiment. Lane 9 shows the DNA eluted in pH 7.5 SB for 30 m. Lane 10 shows the DNA eluted in pH 7.5 SB after stringency challenge has been applied. The DNA eluted at pH 5.2 is shown in lanes 11 and 12. Lanes 2-7 represent a standard curve created by serial dilution of the initial loading reaction Rxn.

The second function of a comparative elution assay is to measure the enrichment rate of the selection pool. In general, it is desirable to collect 1% or less of the input DNA for every round of selection, or in other words, to reduce the diversity of sequences in your pool by 10^2. That way, if you start from a pool of ~10^{11} diversity as we did, you can estimate that the pool will converge in approximately ~6 rounds. We compared the elutions taken at pH 5.2 (lanes 11 and 12, Figure 3.5) with a standard curve (lanes 2-8, Figure 3.5) and found that ~0.8%, or 0.008 of the bead-bound library was eluted. Therefore, we estimated that enrichment is occuring at ~10^2-fold per round, as desired.

We note that we performed comprehensive comparative elution assays for every round of PGSA SELEX to monitor selection progress. However in Figure 3.1, for clarity's sake, we cropped the assay to just show increasing "release ratio", demonstrating pool enrichment.

3.5.5 Developing a stringency challenge method

In order to maintain a fast enrichment rate, it is necessary to have a straightforward and tunable strategy for increasing the stringency of selection. In the case of falling-off SELEX, the stringency strategy must increase favorability of the pool re-loading onto beads. As such, only the best structure-switchers can overcome the increased energy barrier for release into the collected eluent. For PGSA SELEX, we developed a stringency strategy where we added excess SA-coated beads to the sample after initial library loading had been performed. The increased number of SA binding sites favored re-loading of the library onto beads, raising the energy barrier for structure-switching release.

To measure the effect of our stringency challenge at each round, we compared the bands corresponding to the amount of DNA eluted at pH 7.5 before and after the stringency challenge (lane 9 vs 10) to determine the "stringency ratio" (Figure 3.5). In this example, ~10-fold less DNA eluted into solution when the stringency challenge was applied, indicating that our strategy is indeed creating a higher energy barrier for structure-switching release (1:10 stringency ratio) (Figure 3.5). As the pool becomes enriched over the course of selection, the average release efficiency also increases. Therefore, the stringency challenge must continuously be increased to pick out the best structure-switchers. The stringency

ratio measured in the previous round helps us to decide how much to increase the strength of the challenge in the next round.

We would like to make an important technical comment, which is that as you increase the amount of beads applied for stringency, it is important to wash your sample several times in the elution buffer of the next step and check the pH before submitting to a full 30 m elution. The reason for this is that a large bead pellet collected on the MPC is still hydrated by a significant amount of buffer from the previous elution, which can deleteriously alter the pH of the next elution. For example, we found that when transitioning from a pH 7.5 to 5.2 elution step, while using 400 ul of SA-coated beads, the nominally pH 5.2 elution was actually found to have a pH of ~6.6 (Table 3.2). This is undesirable because it means that you are selecting for structure-switchers activated by pH 6.6, not your target pH of 5.2.

Table 3.2. Buffering effect of increasing stringency challenge beads

	Stringency challenge beads (ul)			
	100	150	180	400
Nominal pH	5.2	5.2	5.2	5.2
Measured pH	5.2	5.5	6.0	6.6
Measured pH (3x wash)	5.2	5.2	5.2	5.5

There are other methods to apply a stringency challenge. Instead of increasing the amount of SA-coated beads, you can decrease the amount of input DNA, such that the ratio of Streptavidin:DNA is still increased. Decreasing the temperature of the system during the elution or lowering the ionic strength of the buffer will also increase stringency. These alternative techniques may be used to continue increasing stringency even after the practical handling volume of SA-coated beads (~1000 ul) has been reached.

3.5.6 Choosing a suitable selection buffer

Many different "biological" buffers (PBS, MES, Tris, other "Good's Buffers") have been used for aptamer selection. The most important consideration for PGSA SELEX was to choose a selection buffer which supported the correct folding of SBA29, and therefore, high loading efficiency of the PGSA library onto beads. In previous papers describing selection for Streptavidin aptamers, PBS + Tw-20 pH 7.4 was used, so we chose to try this buffer first[79-82]. We performed a comparative elution assay (using the same selection conditions as 3.6.3) and oddly, found that the amount of DNA steadily decreased in chronological order of elution, regardless of the buffer pH (Figure 3.6). This trend stands in contrast to the expected behavior discussed in Figure 3.5, where there should be uniform bands for both pH 7.5 and 5.2 elutions in R1. Based on this evidence, we believe that SBA29 actually has relatively poor affinity for Streptavidin in PBS + Tw-20 (we note that Bing and co-workers never reported the Kd of the enriched pool in PBS + Tw-20, only the Kd of the minimized aptamer in Tris buffer[79]). We hypothesized that each "elution" acted as a wash step; that is, the weakly associated library molecules were washed off

the beads with each “elution”. We concluded that PBS + Tw-20 was not a good buffer for PGSA SELEX.

We revisited the literature and found that while PBS + Tw-20 was used for aptamer selection, 20 mM Tris buffer was used universally among several follow-up papers for binding characterization of SBA29[79-82]. We surmised that proper folding of SBA29 is dependent on 20 mM Tris-HCl buffer, so that is what we used for all subsequent work (see Figs.3.1, 3.3-3.5, Experimental section for full recipe). We note that this result illustrates an important aspect of analyzing previous literature when designing your own experiments. Be suspicious of differences between selection conditions and characterization conditions. Pay attention to what protocols are preferred by follow-up papers. It is the unexplained changes which demand close inspection.

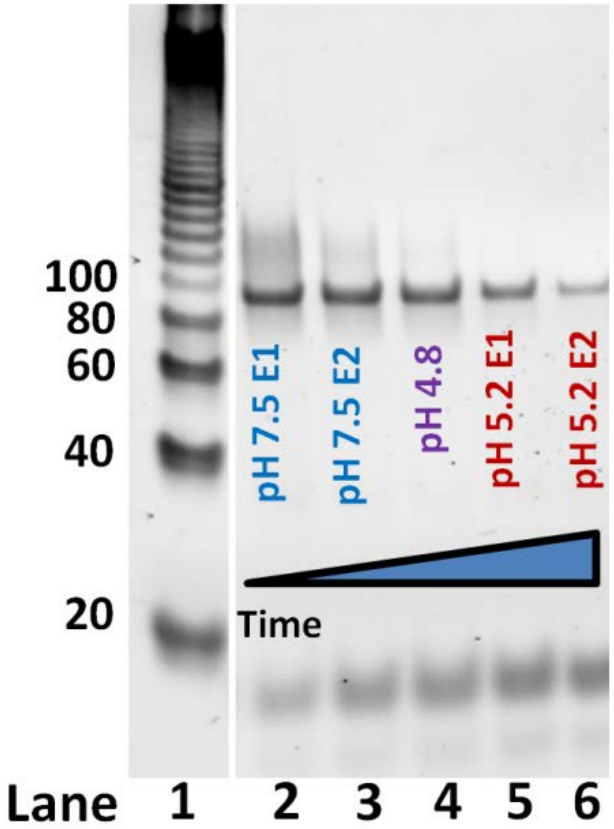

Fig 3.6. Comparative elution assay of Library Design 2 conducted in PBS + Tw-20 under standard selection conditions. The amount of DNA released into the eluent decreases in chronological order, and with no relation to buffer pH. The trend suggests that the library has poor affinity in PBS + Tw-20, and that each “elution” is washing off non-specific binding.

3.5.7 Final remarks on tuning up a selection

Performing a selection is extremely costly, both in time and money. A single round of selection requires 2-3 days on average to complete, and depending on the initial diversity of your library, may require ~8 rounds to see evidence of enrichment. The largest recurring monetary cost is PCR mix, where every round requires 4 mLs of reagent, and the cost for 25 mLs is ~$500. As such, it may take up to a month

and $1000+ to determine that your selection is not working. Multiple iterations of such selections can lead to years of opportunity cost for the researcher.

In our experience, success comes if more time is spent on design and preparation than the act of carrying out a selection. First and foremost, determine the simplest scheme to create selection pressure in your system to evolve your desired function. Second, design your selection libraries based on a reasonable hypothesis for how changes in DNA folding can carry out your desired function. Third, develop a method to estimate the rate of pool convergence (loss of diversity). Knowing the rate of convergence allows you to estimate when you can expect signs of enrichment for a successful effort and conversely, when to go back to the drawing board. When it comes to SELEX, it is great to succeed, but good to fail quickly.

Chapter 4. Continuous *in situ* generation and detection of α-thrombin protein via a real-time electrochemical aptasensor (PMEDIC)

4.1 Introduction

The measurement of *in vivo* protein biomarkers is fundamental to modern medicine because it enables clinicians to diagnose patients and monitor their response to treatment based on quantitative molecular information. In the emergency room where a patient's condition can devolve rapidly due to acute illness or trauma injuries, there is a great need for fast-reporting protein sensors.

Coagulopathy describes a class of medical conditions where the normal coagulation response has become dysfunctional, often arising as a complication to traumatic injury cases[42]. Due to significant blood volume loss as well as biochemical changes from distress (acidosis, hypothermia), the composition of a patient's blood can be greatly altered from equilibrium, leading in some cases to excess thrombogenic responses, and in other cases, uncontrolled bleeding[42],[92]. The standard methods for monitoring coagulopathy are prothrombin time (PT, time for a plasma sample to clot when activated by tissue factor) and thromboelastogram (TEG, viscoelastic measurement of clot strength)[92],[43]. Although these assays are relatively rapid, they require the labor of a skilled technician, which limits the frequency at which patients can be reassessed.

At the date of compiling this thesis, June 2017, this work is still in progress. The contents are thus presented as preliminary results.

Enzyme-linked immunosorbent assay (ELISA) for coagulation factors is practiced less commonly because the turnaround time averages ~2 hours[44], and thus cannot provide the temporal resolution (~15 m)[93] needed for emergency intervention procedures.

Previously in our group, aptamers have been developed into rapid-response electrochemical "aptasensors" which reported in real-time the *in vivo* concentrations of Doxorubicin injected into a live rat[48] (also see section 1.6). The microfluidic electrochemical detector for *in vivo* continuous monitoring (MEDIC) reports changes in small molecule target concentrations within minutes, requires no externally applied reagents or operator labor, and measures directly in whole blood for real-time reporting[48]. We sought to expand the platform for the detection of protein biomarkers, which we called Protein MEDIC (PMEDIC).

In this work, we built PMEDIC to continuously monitor α-thrombin, a key biomarker in the coagulation cascade which reacts with fibrinogen to produce clots[94]. We demonstrated continuous aptasensor measurement of arbitrarily fluctuating concentrations of thrombin under microfluidic flow. We optimized fluid flow conditions to show detection of purified α-thrombin spiked into pool normal plasma (PNP). Finally, we generated native, activated thrombin by introducing tissue factor into PNP, and successfully tracked its *in situ* generation in real-time. PMEDIC could enable direct monitoring of coagulopathy as well as patient response to therapy via quantitative measurement of native protein biomarkers. In combination with MEDIC, which monitors the body's metabolism of input medications, this creates the opportunity for closed loop personalized medicine.

4.2 Results and Discussion

4.2.1 Principle and Design of PMEDIC

The PMEDIC platform consists of three modules which enable real-time thrombin generation and measurement: an electrochemical aptasensor, a sample pre-treatment cocktail, and a selective sheath flow delivery system. These modules are housed within a chip device containing a single microfluidic chamber which serves as the electrochemical measurement readout cell. The chip is constructed from glass and PDMS layers using standard microfabrication techniques. The electrochemical cell within the chamber consists of Au counter, reference and working electrodes. Currently, there is a sample input and and a buffer input line, and in the future, we plan to install an additional mixer module to apply the pre-treatment cocktail to the sample before encountering the chip, so as to enable a continuous flow of pre-treated sample volume.

The electrochemical aptasensor probe is the central module of the PMEDIC platform (Scheme 4.1A). The probes are self-assembled onto the integrated electrodes where they undergo reversible structure-switching in response to binding thrombin. The probes are modified at the 3' end with a methylene blue (MB) redox reporter which produces a Faradaic current when interrogated by the potentiostat. The value of the output current is determined by the equilibrium probability of the aptamer-bound MB reporter striking the surface of the Au working electrode[95]. In our system, the thrombin binding aptamer (TBA), switches between a relatively unstructured DNA strand to a highly structured G-quadruplex when bound to target, thereby changing the electron transfer rate[47].

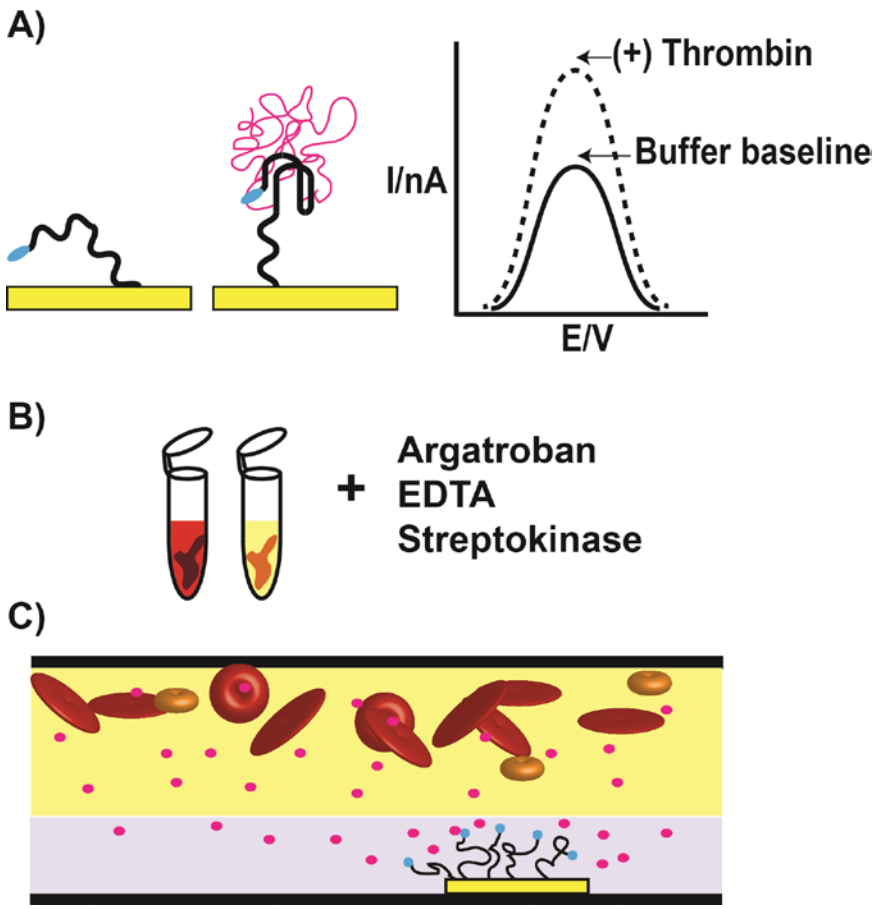

Scheme 4.1. Principle and design of PMEDIC platform. A) Electrochemical aptasensors provide reagentless, instantaneous readout of thrombin concentration change. B) Sample pretreatment cocktail prepares biological samples for long-term continuous monitoring. C) Optimized continuous diffusion filter prevents electrode fouling via a protective buffer sheath which screens out cells, platelets, and high molecular weight proteins.

Although single-use electrochemical TBA sensors have previously been demonstrated in serum[47], accurate continuous monitoring applications have not been possible due to several factors. First, the formation of physical clots disrupts microfluidic flow, making it impossible to accurately assign measurements of concentration to the correct point in time. Second, antithrombin III (ATIII), a native thrombin inhibitor present in uM concentrations in blood[96] rapidly binds free thrombin to produce thrombin-antithrombin III (TAT) complex[97] which is not

detectable by TBA, thereby reducing the magnitude of our target signal. We designed a novel pre-treatment cocktail consisting of Argatroban, EDTA, and Streptokinase to address these concerns (Scheme 4.1B).

Another challenge unique to continuous monitoring of unprocessed biological media is the phenomenon of "bio-fouling", where cell matter and proteins will irreversibly adsorb to the aptasensor probes over time and kill their functionality[98]. The MEDIC platform designed a continuous-flow diffusion filter (CDF) tuned to exclude large particles and proteins, but which permitted high diffusivity small molecule targets to reach the aptasensor[48]. For our new system, we took advantage of the fact that thrombin is a relatively spherical and small molecular weight protein with relatively high diffusivity[99]. We relaxed the selectivity of the CDF to permit a fraction of high diffusivity proteins to reach the aptasensor (Scheme 4.1C).

4.2.2 The electrochemical thrombin aptasensor

For the design of the electrochemical thrombin aptasensor, we chose the Bock-15 TBA because of its demonstrated high specificity compared to serum albumin and chymotrypsin[47] (see 4.4.1, Reagents). The Bock-15 TBA was modified at its 3' end with a MB redox reporter and at its 5' end with a thiol linker. The thiol linker provides for the formation of Au-thiol covalent bonds to functionalize the aptasensor to the Au electrode surface[47]. After we functionalized the Au electrodes with the TBA sensors, we passivated the surface with hexanethiol.

Via continuous microfluidic delivery, we pulsed increasing concentration steps of purifed α-thrombin in buffer and measured the electrochemical current

response (Figure 4.1). At 50, 100, and 500 nM thrombin, we obtained 300, 350, and 450% signal gain, respectively (Figure 4.1). Next, we pulsed decreasing concentration steps of thrombin and observed complementary decreases in signal (Figure 4.1). All samples were delivered continuously and measurements were taken in real-time. These results demonstrate that our system can monitor a dynamically fluctuating concentration of thrombin and that these changes can be resolved rapidly (~5-10 minutes). We note that the device equilibrates to decreases in concentration somewhat more slowly and this is thought to be due to multivalent binding effects[100] slowing the off-rate (see Chapter 5).

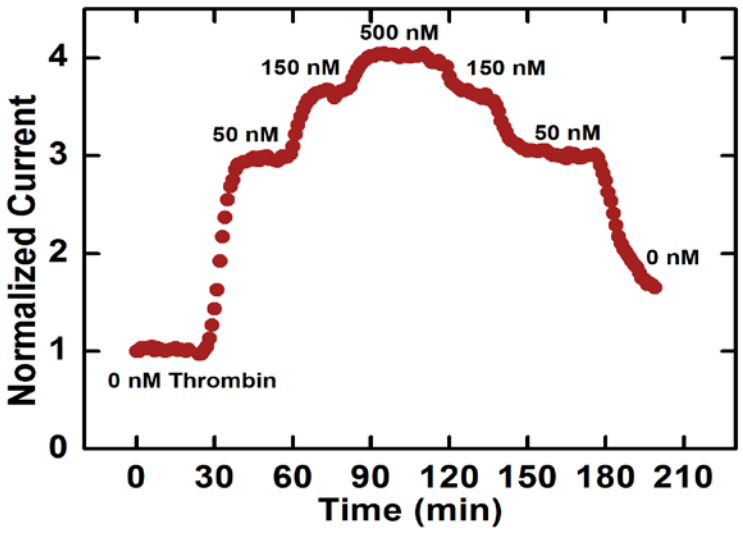

Figure 4.1. Continuous electrochemical measurement of purified α-thrombin dissolved in buffer. The device is able to rapidly report dynamically fluctuating thrombin concentrations.

From these curves, we were also able to estimate the approximate linear range to be 0-30 nM and the binding affinity (Kd) to be ~30 nM. Previously, we have measured the Kd of TBA in solution using a fluorescence bead binding assay to be ~0.7 nM (Figure 4.2), which agrees with literature values[101]. The decrease in affinity when functionalized onto the Au electrodes in our device was not unexpected since TBA was selected to perform its function in solution. By anchoring the 5' end to a surface, TBA has reduced degrees of conformational freedom and decreased affinity for thrombin. In the future, we believe that it would be beneficial to select for new thrombin binding probes whose affinity for thrombin will not be reduced by functionalization onto a surface. A promising possibility is the use of particle display SELEX, where the DNA selection library is already affixed to the surface of a bead and then subjected to selection pressure[85]. However, for the purpose of our current experiment, we decided that it would still be possible to demonstrate the advantages of the PMEDIC system with a thrombin aptasensor with Kd ~30 nM.

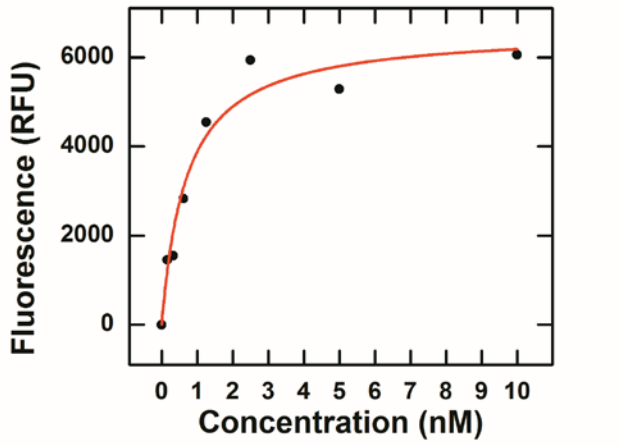

Figure 4.2. Fluorescence bead-based binding assay of TBA in solution. We measured the Kd to be 0.70 nM +/- 0.1, which agrees with typical literature values which report the Kd of TBA to be between 1-10 nM[85].

4.2.3 Specificity of PMEDIC sensor

The PMEDIC sensor is highly specific for free α-thrombin, which is hugely advantageous for direct detection in unmodified human plasma and/or blood. While human plasma and/or blood contains an immense variety of off-target molecules, we were specifically concerned about two thrombin-related species: prothrombin (PT) and thrombin-antithrombin III (TAT) complex. Prothrombin is a 72 kD[102] protein comprised of two units of α-thrombin bridged by covalent bonds[103]. In the uncleaved state, prothrombin is inactive and does not catalyze the formation of fibrin clots[103]. Cleavage of prothrombin yields two active units of α-thrombin[103]. Prothrombin exists constitutively as an inactive thrombin precursor at 1.41 uM physiologically[104], whereas active thrombin is produced in response to injury in pM concentrations[105]. Owing to the high level of similarity between thrombin and prothrombin (composition and structure), it was important to demonstrate that PMEDIC could discriminate between these two species. We challenged our system with 50 nM of thrombin in the absence or presence of 1.4 uM prothrombin and found that both resulted in ~30% signal change, indicating that our sensor was highly specific for thrombin recognition (Figure 4.3). Therefore, we reasoned that PMEDIC measurements of thrombin in clinical samples would not be obfuscated by the presence of prothrombin.

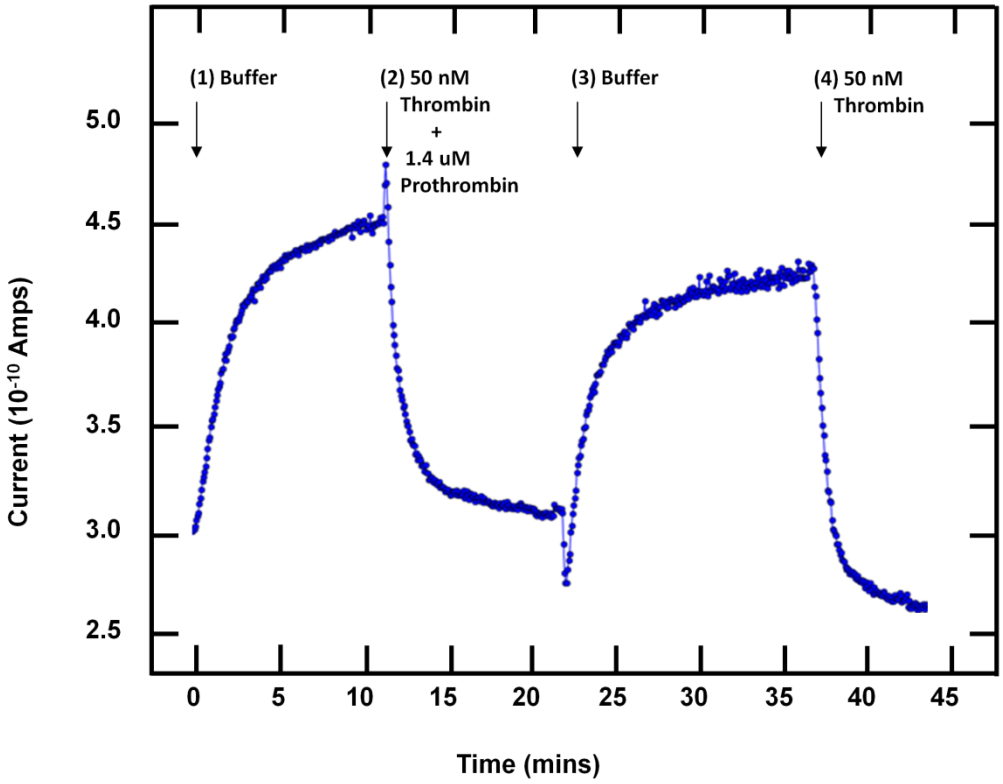

Figure 4.3. PMEDIC specifically binds to α-thrombin and is unaffected by the presence of physiological levels (uM) of the prothrombin precursor molecule. While the absolute current measurement showed a small amount of drift where the baseline signal in buffer drifted from ~45 nA to ~42 nA, the signal change in response to thrombin challenge relative to the baseline signal was ~30% in either the presence or absence of excess prothrombin.

We also challenged our system with 50 nM of purified thrombin, and then applied an equimolar amount of antithrombin III into the sample tube (Figure 4.4). We observed an ~46% signal decrease in response to the initial 50 nM pulse of thrombin which rapidly decayed to baseline signal after the introduction of antithrombin III (Figure 4.4). When we found that TBA could no longer detect thrombin when it was complexed to ATIII, we confirmed that ATIII must inhibit thrombin at the fibrinogen binding site (Exosite I)[10].

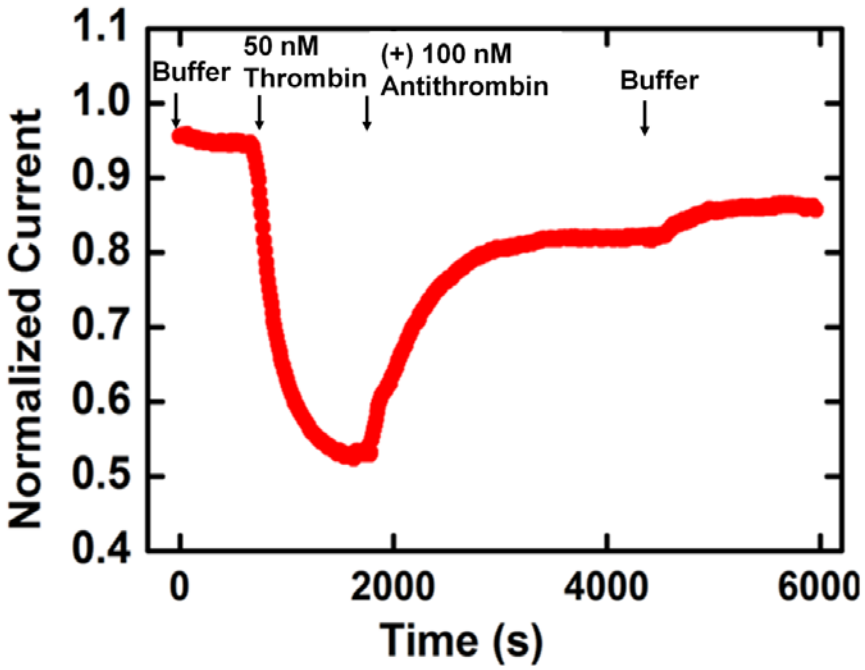

Figure 4.4. PMEDIC is unable to detect α-thrombin when it is in complex with its native inhibitor, antithrombin III. Initially, when we injected a 50 nM pulse of thrombin, we observed ~46% signal decrease relative to the baseline. Subsequently, we added an excess molar amount of antithrombin III to the source test tube containing thrombin and we observed a rapid return to baseline signal. We reasoned that when TAT complex is formed, antithrombin III blocks the aptasensor recognition site of TBA.

We reasoned that we could pursue two possible strategies: (1) develop an aptasensor probe against TAT or (2) develop a sample treatment which would block TAT complex formation. While it could be possible to make a TAT aptasensor by modifying the the Tasset-29 TBA (which binds Exosite II, the heparin binding site)[11], we felt that this strategy had a very long lead time. Moreover, measuring TAT is not as valuable as directly profiling active thrombin. Importantly, the half-life of active thrombin generated by injury is 10-20s before being complexed with ATIII (TAT half-life is 3 days)[105]. We realized that it was of

paramount importance to measure α-thrombin as it is generated in real-time in order to accurately interpret the progress of a patient's coagulopathy.

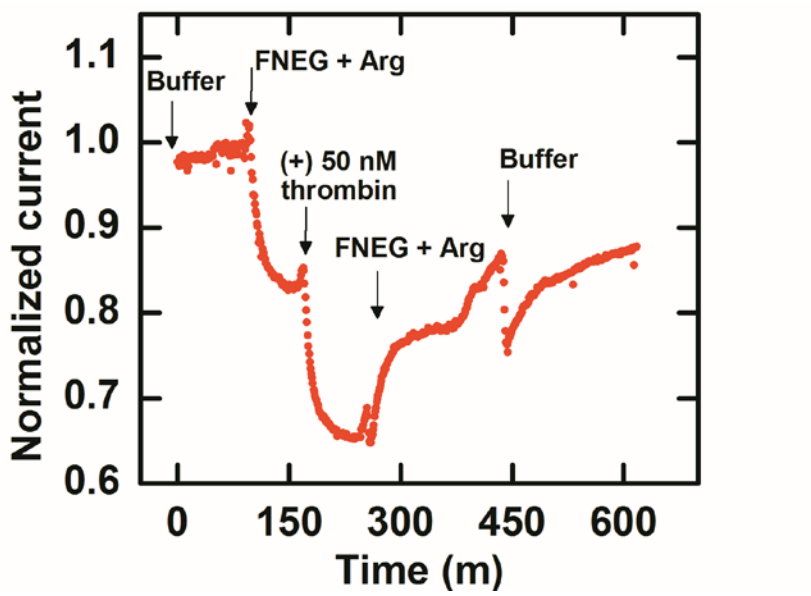

Figure 4.5. Argatroban (Arg), a commercially available small molecule thrombin inhibitor, outcompetes native antithrombin III binding, but still permits TBA to detect purified α-thrombin. In this experiment, we pre-treated human plasma (fibrinogen negative, FNEG) with Arg and established a baseline signal. Next, we spiked in 50 nM of purified thrombin into the source test tube and measured ~20% signal decrease. Since we were able to report a signal change in response to thrombin, we reasoned that native antithrombin III in plasma was suitably outcompeted by Arg. Finally, we switched the sample stream to plain buffer but we observed a disrupted electrochemical signal which we attribute to the formation of physical clots interrupting continuous microfluidic flow.

We investigated a number of commercially available thrombin inhibitors and identified Argatroban, a small molecule anti-thrombogenic drug as a potentially useful candidate[106]. We performed an experiment where we pretreated human plasma with 150 uM Argatroban and then spiked in 50 nM purified thrombin (Figure 4.5). We observed a signal decrease of ~20% corresponding to the thrombin challenge, suggesting that Argatroban was able to suitably outcompete native

antithrombin III present in real human plasma (Figure 4.5). Therefore, we reasoned that a pre-treatment with Argatroban is a simple, effective strategy to profile active thrombin directly in biological sample.

We note that we used fibrinogen-negative (FNEG) plasma to conduct this experiment. This is because we anticipated that spiking in a high concentration of purified α-thrombin would catalyze the formation of fibrin clots from the fibrinogen molecules present in complete human plasma. We have previously observed that fibrin clots will form throughout the tubing and also inside the microfluidic sample chamber and can dramatically disrupt microfluidic flow. FNEG plasma has been depleted of the majority of its native fibrinogen, and as such, we hoped that we could demonstrate the ability of our device to detect thrombin in plasma with minimal disruption of microfluidic flow. In the experiment above, microfluidic flow was steady until t = 450 m, when a clot is likely to have formed, causing the electrodes to run dry before buffer flow was restored (Figure 4.5). Even brief interruptions to microfluidic flow can shift the electrochemical signal baseline and make it difficult to interpret continuous measurements, so in later sections of this chapter, we continued to optimize a pretreatment cocktail which would more fully suppress errant formation of disruptive clots (see Section 4.2.5).

4.2.4 Detection of purified thrombin in pooled normal plasma

Previously, we showed that we could detect purified α-thrombin in FNEG plasma with reasonable reliability. But our next challenge was to detect α-thrombin in whole human plasma. We note that in our experiments with FNEG plasma we observed non-specific signal decrease due to the presence of plasma directly interacting with the aptasensor-modified electrodes. However, since we were still able to detect purified α-thrombin against this background, we decided to test whether we could detect it in Argatroban-treated pooled normal plasma (PNP) without further modifications or the CDF platform.

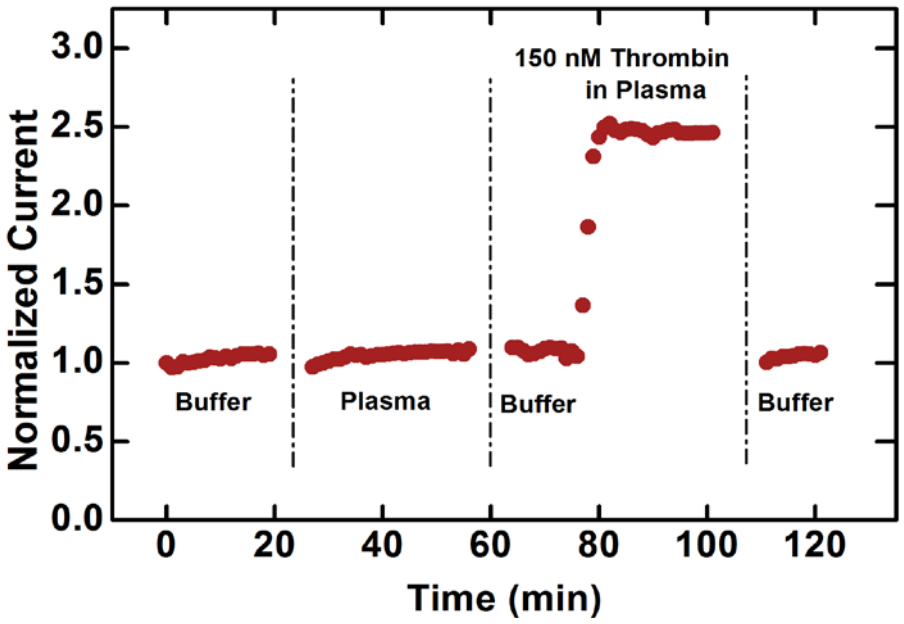

Figure 4.6. Detection of purified α-thrombin in PNP. PNP was first pretreated for 10 minutes with Argatroban to prevent the formation of fibrin clots and to prevent signal inhibition by native antithrombin III.

We observed that even without implementing the CDF, we were able to detect 150 nM of purified α-thrombin directly in PNP as a 250% increase in signal compared to buffer baseline (Figure 4.6). Notably, the PNP appeared not to create as significant of an electrochemical signal artifact and after a buffer wash, the device appeared to be able to recover its original baseline signal (Figure 4.6). We do not know why some devices are more robust against fouling but we attribute this variation to uncontrolled differences in aptasensor and passivation alkanethiol self-assembly. From these experiments, we confirmed that purified thrombin could be detected directly in biological sample.

4.2.5 Detection of *in situ* generated native thrombin in plasma

Whereas all of our previous experiments dealt with the detection of commercially obtained, purified, α-thrombin, our next challenge was to generate native thrombin directly from PNP and determine if our aptasensor devices could detect it. Tissue factor (TF) is a protein that is typically sequestered by the endothelial lining of blood vessels[94]. When injury occurs and damages the blood vessel, tissue factor is released into the bloodstream where it activates the coagulation cascade in order to close the wound[94]. Although there is not a consensus on what the physiological concentrations of TF are in the bloodstream during injury, typical laboratory tests and precedent in the literature suggest that 10 pM of TF is a suitable amount to initiate coagulation *in vitro* for study[107],[108].

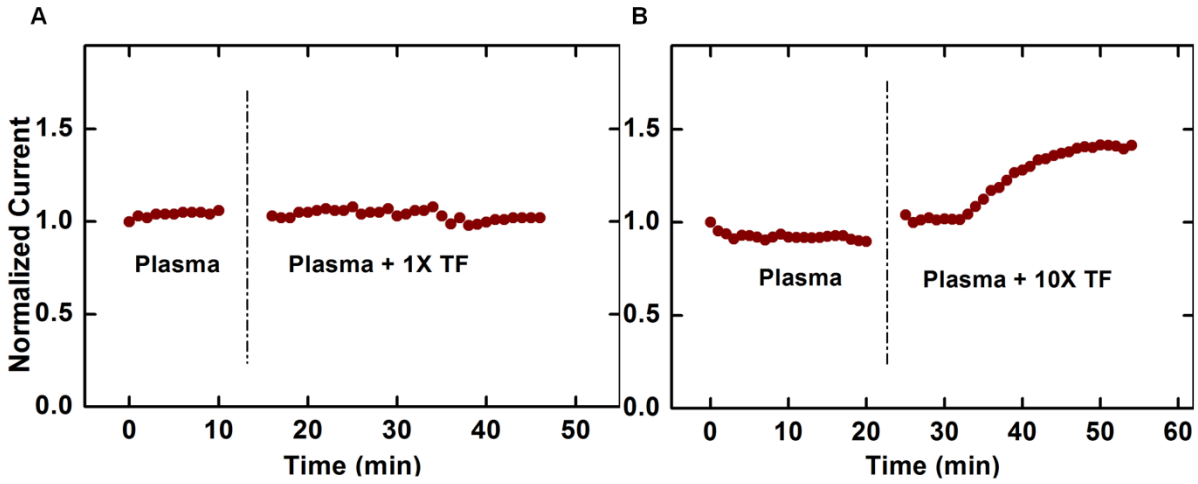

Figure 4.7. *In situ* generation of native thrombin from PNP. A) We initiated the coagulation cascade with 10 pM of TF, considered a 1X dose, but did not observe a significant signal change. B) We increased the amount of TF to 100 pM (10X) and we were then able to observe 150% signal increase, which we believe is due to native thrombin generation.

As such, we performed an experiment where we applied 10 pM (1X dose) or 100 pM (10X dose) of TF to 1 mL of Argatroban-treated PNP and measured the increase in thrombin concentration over time (Figure 4.7). Surprisingly, initiation with 1X TF did not generate a signficant signal change (Figure 4.7). We believe that this is due to the high signal background that arises when measuring directly in plasma (see Figure 4.5). Perhaps under 1X TF conditions, not enough thrombin was generated for us to detect a signal change over the plasma background. We increased the dose to 10X TF and then we were able to observe 150% signal increase occurring over 20 minutes (Figure 4.7). Due to batch-to-batch variation in self-assembly and the signal background caused by plasma, we are not able to calculate the concentration of thrombin generated in these two experiments. In the future, we could explicitly measure this value by performing ELISA measurements on this sample, post-experiment. The main takeaway from this experiment is that

we were fairly confident that not only could we generate thrombin from PNP, but that we could detect at least a fraction of natively generated α-thrombin with our devices.

However, we recognized that we needed to reduce the background due to PNP contact with the electrodes, so we implemented an optimized continuous diffusion filter (CDF). We note that in our experiment with fibrinogen depleted plasma, simply equilibrating the chip with plasma caused a ~20% signal decrease relative to the baseline in buffer (Figure 4.5). Since α-thrombin is not present in significant quantities in unactivated plasma[105], we surmised that this was a non-specific signal change in response to the significant protein content of human plasma which greatly decreases the dynamic range of detection of the aptasensor. Furthermore, the chip sensor never recovered to its initial current baseline even after washing in buffer, suggesting that bio-fouling of the sensor occurred (Figure 4.5). As we previously alluded to in 4.2.1, the MEDIC system addressed fouling by creating a continuous diffusion filter (CDF) where a protective sheath stream is stacked between the aptasensor-modified electrodes and the sample stream via laminar flow[48]. Ferguson and co-workers tuned the flowrate and the thickness of the protective sheath layer to permit only high-diffusivity small molecules to travel to the aptasensor-modified electrodes, whereas low-diffusivity interferents such as blood cells, platelets, and proteins were unable to diffuse into the detection area during the time in which the sample volume traveled through the chip[48]. In the PMEDIC system, we reduced the thickness of the protective sheath layer from 125 μm to 50 μm to permit a fraction of high-diffusivity small proteins to travel to the aptasensor-modified electrodes. We believe that the majority of fouling arises from

protein interferents that exist at high concentration in the plasma, namely immunoglobulin G (IgG) and human serum albumin (HSA)[109]. Therefore, we believed that relaxing the CDF to permit a fraction of small proteins would allow us to still detect our target, thrombin, but screen out the majority of fouling proteins. We took advantage of the fact that thrombin is a small (36 kD), relatively spherical protein, with a hydrodynamic radius of 2.4 nm[99]. The Stokes-Einstein equation, therefore, calculates its diffusitivity to be 41.8 $\mu m^2/s$[99]. In comparison, IgG and albumin are typically ~150 kD[27] and ~70 kD non-spherical proteins[111].

Furthermore, we note that in our experiments with FNEG plasma, microfluidic flow was not disrupted by clot formation for 450 minutes when the sample was pretreated with Argatroban (Figure 4.5). We identified that we needed to extend our ability to perform continuous monitoring by adding further components to the pretreatment cocktail to suppress fibrin clot formation. We added two more components: EDTA and Streptokinase. EDTA is a chelating agent which removes Ca^{2+} from solution, a divalent ion binding partner for many coagulation factors[94]. Streptokinase is a bacterially derived fibrinolytic – an enzyme which breaks down clots[112].

At this time, we had assembled a complete PMEDIC platform consisting of the aptasensor, the pretreatment cocktail, and optimized CDF. Under microfluidic sample flow with a protective CDF, we first equilibrated the sample in buffer, then in Argatroban-doped PNP (Figure 4.8). We paused microfluidic flow and applied 1X TF for 5 minutes. Next, we quickly mixed in EDTA and Streptokinase to halt the formation of large fibrin clots and re-started sample flow. We observed an excellent ~35% signal decrease over 3000 s (Figure 4.8).

The improved PMEDIC platform demonstrated several novel achievements. First, the optimized CDF permitted us to shield the aptasensor-modified electrodes from the majority of fouling effects, yet permitted the transport and detection of our protein target α-thrombin. This was evidenced by how the baseline signal in plasma was not substantially changed from the baseline signal in buffer. Second, the pretreatment cocktail prevented native inhibitors from diminishing the signal of generated thrombin. In combination with the background reducing effects of the CDF, these two innovations permitted us to see a large signal change (~35%) in response to 1X TF generated thrombin. Moreover, the pretreatment cocktail prevented the formation of fibrin clots which would have disrupted continuous measurement for nearly 2 hours, a time scale which would be relevant for clinical applications of this device.

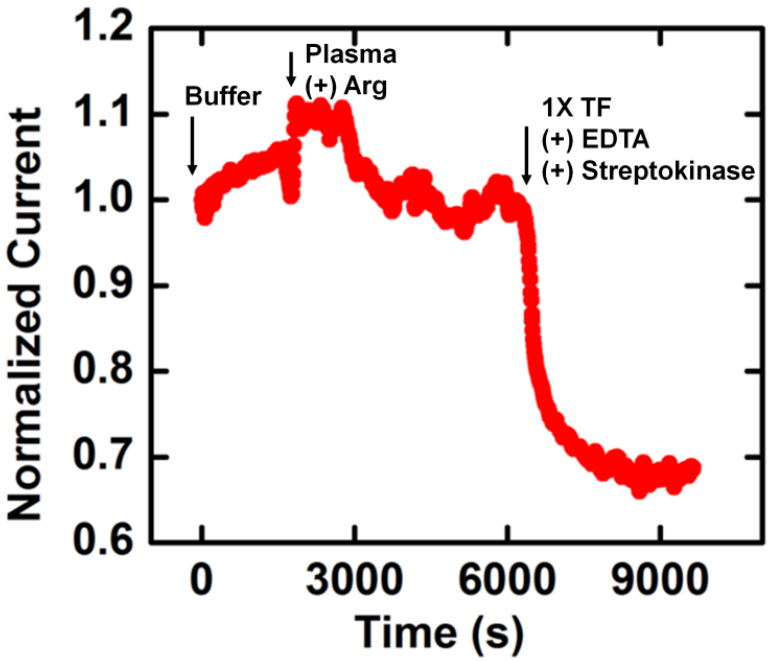

Figure 4.8. Demonstration of the complete PMEDIC platform. We equilibrated the device in PNP pretreated with Arg. Although we observed a momentary disturbance in the baseline signal this effect settled after 3000 s. At t = 6000 s, we paused sample flow, spiked in 1X TF for 5 minutes, then immediately mixed in the rest of the pretreatment cocktail. We observed ~35% signal decrease in response.

4.3 Conclusions

In summary, we have developed a new platform called PMEDIC which enables us to not only generate native thrombin from human plasma, but to continuously monitor it *in situ*. To the best of our knowledge, this is the first ever demonstration of generating and detecting native thrombin in a continuous monitoring device. Previous works in the literature have been limited to the detection of commercial, purified α-thrombin and to single-measurement sensors. In this work, we showed that the PMEDIC sensor was highly specific for α-thrombin and was not sensitive to either its precursor molecule, prothrombin, nor its downstream deactived product, TAT. We designed a novel pretreatment cocktail

which amplified our ability to detect thrombin by preventing signal loss due to complexation with native inhibitors. The cocktail was also highly effective in preventing the formation of fibrin clots which would have disrupted microfluidic flow and thus extended our ability to monitor thrombin continuously to over 100 minutes. Finally, we optimized the CDF to permit our target protein to be transported to the aptasensor-modified electrodes for detection, but to still screen out the majority of bio-fouling blood proteins. Altogether, PMEDIC has demonstrated potential for continuous monitoring of thrombin in the emergency room, which could enable closer tracking of coagulopathy and more rapid medical intervention.

Although PMEDIC has many advantageous attributes, there are remaining challenges to address. While TBA aptasensor has a Kd of ~30 nM, physiological levels of thrombin are in the fM – pM range[105]. We believe that it may be possible to achieve more relevant levels of sensitivity by re-designing the HD1-22 bivalent thrombin sensor into an electrochemical sensor, since it has a reported Kd of <1 pM[105]. Another issue of concern is that our optimization of CDF permissivity is a technique that is only suitable for the detection of high-diffusivity protein targets, which will not be applicable if the protein of interest is of medium to large size. It is of great importance to consider other strategies not based on a diffusion gradient to protect the electrodes from fouling.

In the future, it may be of interest to reconceive the fundamental premise of how to achieve continuous monitoring of biomolecules. In this work, we have developed many innovations to prolong the usable lifetime of a single device, which provides reporting of concentration change every ~5 minutes. But we reiterate that in consultation with Dr. Mitch Cohen, M.D. (UCSF), a world expert on coagulopathy

and emergency room medicine, measuring thrombin every 15-30 minutes would already be sufficiently fast to provide clinical benefit. In future works, we envision a platform based on an array of single-use aptasensor chips without complicated protective systems. Each single-use chip would be automated to run a self-calibration against a standard curve of concentrations and then take a single measurement of thrombin concentration and never be used again since subsequent measurements would be less accurate due to fouling. A timer system for the array would then wait for 15 minutes, and then activate the next chip in the array to repeat these actions. Given that our sensor devices can be made relatively inexpensively and in bulk (~100 chips in one batch), construction of an array of these chips is practical.

4.4 Experimental Section

4.4.1 Reagents

The probe (5′-HS-(CH2)6-TAAGTTCATCTCCCCGGTTGGTGTGGTTGGT-(CH2)2-MB-3′) with 3’ C6-linked thiol and 3’-linked methylene blue label was synthesized by Biosearch Technologies (Petaluma, CA). The FAM modified aptamer, (5′-FAM-TAAGTTCATCTCCCCGGTTGGTGTGGTTGGT) was produced by Integrated DNA Technologies (Coralville, IA). Tris-(2-carboxyethyl) phosphine hydrochloride (TCEP) was obtained from Invitrogen (Carlsbad, CA). 6-mercaptohexanol was purchased via Sigma-Aldrich (St. Louis, MO). Purified human α-thrombin, prothrombin, antithrombin III, and recombinant tissue factor used for this study were produced by Haematologic Technologies Inc (Essex Junction, VT). Fibrinogen-negative and pooled normal plasma was obtained from

BioreclamationIVT (Baltimore, MD). Argatroban, Streptokinase C, EDTA as well as reagents for making reaction buffers were all purchased from Sigma-Aldrich (St. Louis, MO). Magnetic carboxylic acid Dynabeads were purchased from ThermoFisher Scientific. Tygon tubing was obtained from Sigma-Aldrich. HEPES buffered saline was obtained from Sigma-Aldrich. The pretreatment cocktail was prepared in DI as follows: 150 uM Argatroban, 1.5 mg/ml EDTA, 100 IU/ml Streptokinase. The high salt phosphate buffer (HSPB) used for functionalizing devices with probes comprised: 100 mM sodium phosphate, 1 M NaCl, 1 mM MgCl2, pH 7.4.

4.4.2 PMEDIC Sensor Preparation

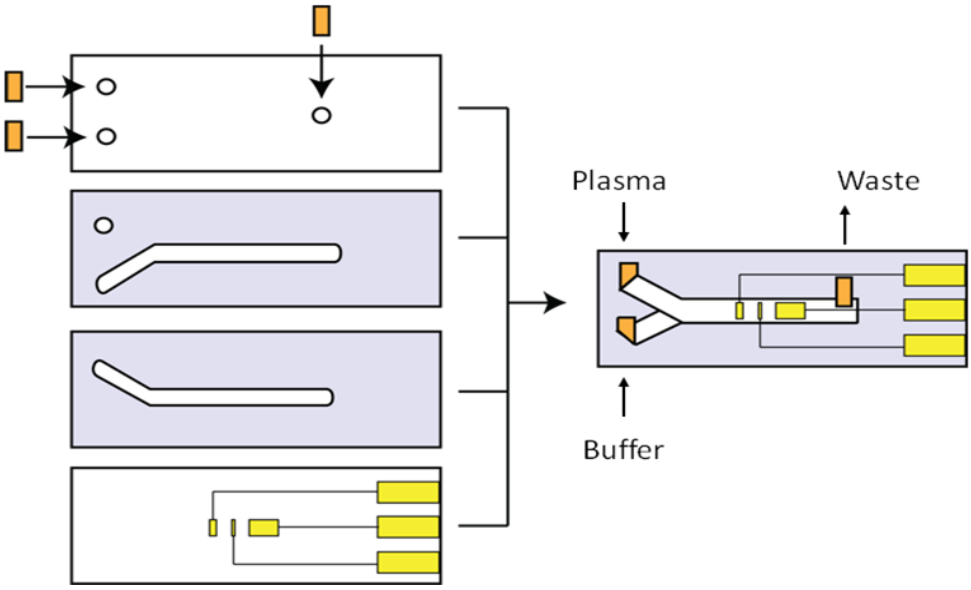

Scheme 4.2. Device architecture and fabrication.

PMEDIC chips were assembled from four separately fabricated modules consisting of the electrode substrate, the sample chamber layer, the buffer sheath chamber layer, and the fluidic via substrate. The electrode substrate was patterned with gold reference, counter, and working electrodes onto 4-inch-diameter 750-um-thick Borofloat glass wafers (University Wafer, Boston, MA) using standard photolithography and lift-off processes. A transparency mask (Grayphics, Santa Barbara, CA) was used for contact photolithography and e-beam evaporation deposition in a VES 2250 evaporation chamber (Temescal, Livermore, CA) deposited 20 nm titanium for adhesion and 180 nm of gold onto the wafers. Afterwards, the wafers were immersed in acetone for 1 hour for lift-off, followed by isopropyl alcohol and deionized water washes. Samples were dried with nitrogen. The two chamber layers were each constructed from 50-um-thick double sided tape (3M) with the channel design cut with a sign-cutting tool (CE5000-60, Graphtec, Santa Ana, CA). The fluidic via substrate was prepared by drilling eyelet holes into a second glass wafer with a 1.1-mm-diameter diamond drill bit (Tripple Ripple, Abrasive Technology, Lewis Center, Oh) using a CNC mill (Flashcut CNC, San Carlos, CA). The electrode substrate and fluidic via substrate were diced into individual chips (ADT 7100 Dicing Saw) and washed with ACE/ISO/DI procedures. The four device layers were manually assembled under an optical microscope in order to precisely align the sample chamber layer and the buffer sheath chamber layer before adhesion. Fluidic ports were epoxied over the vias to provide one buffer sheath inlet, one sample inlet, and one outlet. The finished chip measured 30 mm X 7.5 mm, with a sample chamber volume of ~20 uL.

4.4.3 PMEDIC Electrode Cleaning and Functionalization

After device assembly, the gold working electrodes in each chip was electrochemically cleaned via cyclic voltammetry performed on a Emstat3 mini-potientostat (Palmsens, Germany) using 50 mM H_2SO_4, with 12 potential sweeps ranging from -0.8V to 1.0V applied at 0.1 Vs-1 with a sample interval of 0.001V and 10 uA sensitivity. Afterwards, cleaned chips were rinsed with DI water. At this time, the chips were electrochemically clean and ready for modification with DNA probes.

To activate the thiolated DNA probes, we incubated them in 100 mM TCEP at room temperature for 1 h to reduce disulfide bonds, then diluted to 1 uM in HSPB. The activated probe solution was loaded into the electrochemically cleaned chips and was incubated for 1 h in the dark at room temperature to allow the probes to form covalent Au-thiol bonds and self-assemble on the electrode surface. Thereafter, the functionalized electrode surfaces were rinsed in DI and then passivated with 3 mM 6-mercaptohexanol in DI for 1 h in the dark at room temperature. After these processes, the chips were rinsed for a final time in DI, and will hereafter be referred to as sensors. The sensors can be stored indefinitely in HBS buffer at 4°C.

4.4.4 Time-Course Response Experiments

We used square wave voltammetry (SWV) for monitoring the MB redox current during thrombin measurements. The following SWV parameters were used (values relative to Au reference electrode): 0.08 V initial voltage, -0.2 V final voltage, 0.001 V increment, 0.03 V amplitude, 100 Hz frequency, 0.11 s sample time and autosensitivity. Under continuous microfluidic flow, we would measure the MB redox current in response to challenges with thrombin dissolved in HBS buffer or in plasma. To switch to a different concentration challenge or sample, we simply transferred the tubing connected to the sample inlet into a new test tube. All plasma samples were subjected to the pretreatment cocktail before being input into the chip for testing.

Device flow was controlled via syringe pump (PHD 2000, Harvard Apparatus, MA). We optimized the CDF barrier parameters to permit thrombin to cross the buffer sheath. To do this, we maintained a 1:1 flow ratio for the buffer stream and the sample stream. One syringe pump was connected to the output port, withdrawing at a rate of 40 ul/mn. A second syringe pump containing HBS was connected to the buffer port and pushed HBS into the chip at 20 ul/mn. The sample port was connected to open-ended Tygon tubing which could be switched between different sample test tubes.

4.4.5 Fluorescence bead-based assay of K_d

We measured the solution Kd of the thrombin aptasensor by incubating a range of concentrations of FAM-labeled thrombin aptasensor ssDNA with thrombin-coated beads for 1 hour at room temperature with gentle rotation. These samples

were then washed 4X using a magnetic particle concentrator (Invitrogen), and the remaining bound DNA was eluted from the beads by thermal melting at 95C in a heat block for 10 m. The amount of fluorescence in the elutiosn were measured with a microplate reader (TECAN 1000) and the values were fit to a saturation binding curving using nolinear regression, assuming 1:1 binding kinetics, with Origin software (OriginLab).

Chapter 5. Thermal regeneration of electrochemical aptasensors for rapid thrombin detection

5.1 Introduction

In Chapter 4, we described a platform for continuous *in situ* monitoring of α-thrombin protein in human pooled normal plasma. We had previously discussed the importance of continuous biomarker monitoring, as it gives clinicians the ability to rapidly observe changes in a patient's disease state and provide medical intervention. In particular, we have identified that the treatment of trauma-induced coagulopathy which often arises in the emergency room can greatly benefit from continuous monitoring of serum levels of α-thrombin protein as a marker for a hypercoagulatory state. In consultation with a medical expert on coagulopathy, Dr. Mitch Cohen (UCSF), we have identified that a sensor measuring updated concentrations of thrombin every 5-15 minutes would offer the most benefit to clinicians. Moreover, it is also of great importance to develop thrombin sensors with greater sensitivity, so that we can approach our ultimate goal of measuring *in vivo* concentrations (fM – pM)[105] of thrombin directly in whole blood.

The method of detection we employed in the PMDEDIC platform method was an electrochemical aptasensor for thrombin. Aptasensors are an equilibrium detection method: the target and the sensor reach a binding equilibrium over a period of time, at which point the electrochemical readout reflects the target concentration in solution[47].

At the date of compiling this thesis, June 2017, this work is still in progress. The contents are thus presented as preliminary results.

The time to equilibration represents the limit for how quickly changes in target concentration can be reported. Empirically, we observed that our thrombin aptasensor devices require ~2-5 minutes to equilibrate to increased concentration of thrombin, whereas decreases in concentration require at least 2-fold more time to fully equilibrate (see Figure 4.1). In our aptasensor devices, possibly due to a multivalent surface effect[113-115], we have observed that up to 50% of thrombin effectively stays permanently bound to the device surface (>50 m for clearance) (Figure 5.1). Although a reduced dissociation rate is advantageous for sensitivity[116], this effect is problematic because future measurements are obfuscated by still-bound thrombin.

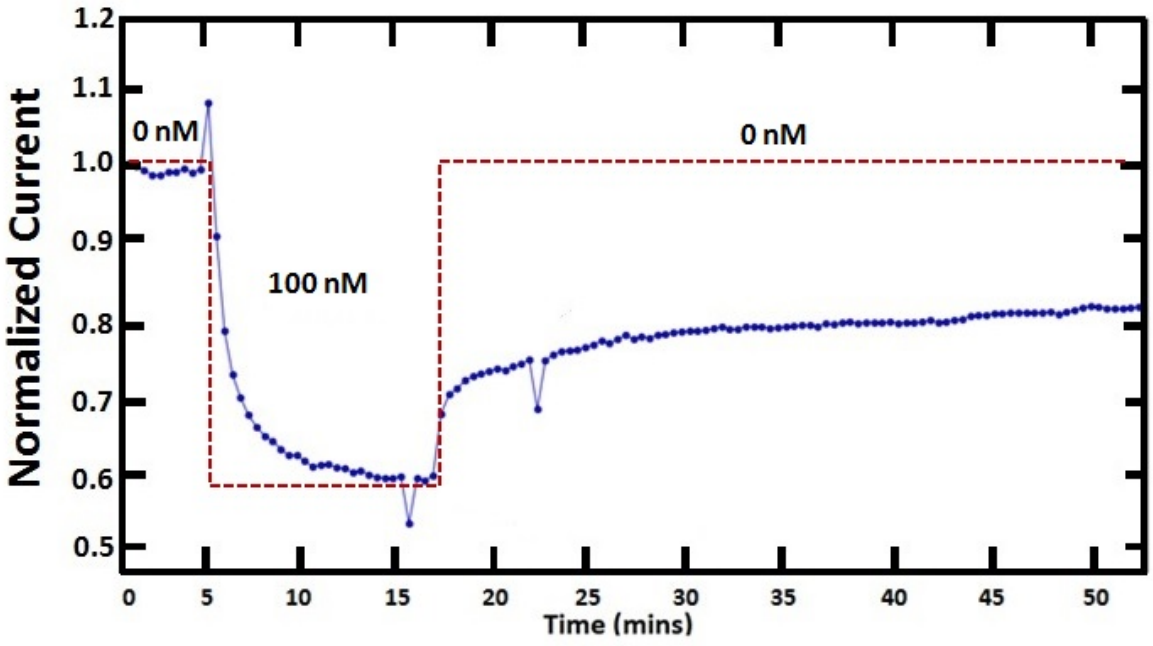

Figure 5.1. A typical thrombin pulse association and dissociation test on an aptasensor chip. After equilibration for 5 minutes in buffer (flowrate 10 ml/hr), we challenged the chip with 100 nM of purified thrombin and observed ~40% decrease in electrochemical current after equilibration for 8 minutes. Next, we flowed plain buffer through the chip once again to measure thrombin dissociation and found that the signal was restored to only half of the initial current after more than 30 minutes of

observation, indicating ~50% of thrombin is still bound to the aptasensor chip. These behaviors are typical of many chips we produced where thrombin association is reasonably rapid, but dissociation is so slow that future measurements are obfuscated by still-bound thrombin.

We have developed a simple but powerful strategy to improve accuracy and speed of thrombin aptasensor measurement through thermal regeneration of the sensor chip (Scheme 5.1). In our scheme, the aptasensor starts out in its native, unbound state (Scheme 5.1A) and then is challenged by an infusion of new sample. The aptasensor probes bind to thrombin in the sample and equilibrate to report the concentration (Scheme 5.1B). Next, an attached mini-thermoelectric cooler (TEC) element raises the temperature of the chip to 70°C, melting the aptamer and releasing thrombin, which is washed away by the continuous microfluidic flow (Scheme 5.1C). Previously, some studies have found that the melting temperature of thrombin aptamer is as high as 51°C in the presence of buffers with monovalent ions, so we tested a range of temperatures between 51-95°C to determine the minimum melting temperature required for our system, which we thereafter determined to be 70°C[117]. Then, the mini-TEC element cools the system to 25°C, re-folding the aptasensor, where it is unbound and ready to measure again. As such, we are able to update the thrombin concentration more frequently by leveraging only the more rapid association mode. Moreover, thermal regeneration of the system completely removes any bound thrombin, allowing for an accurate measurement of concentration each time.

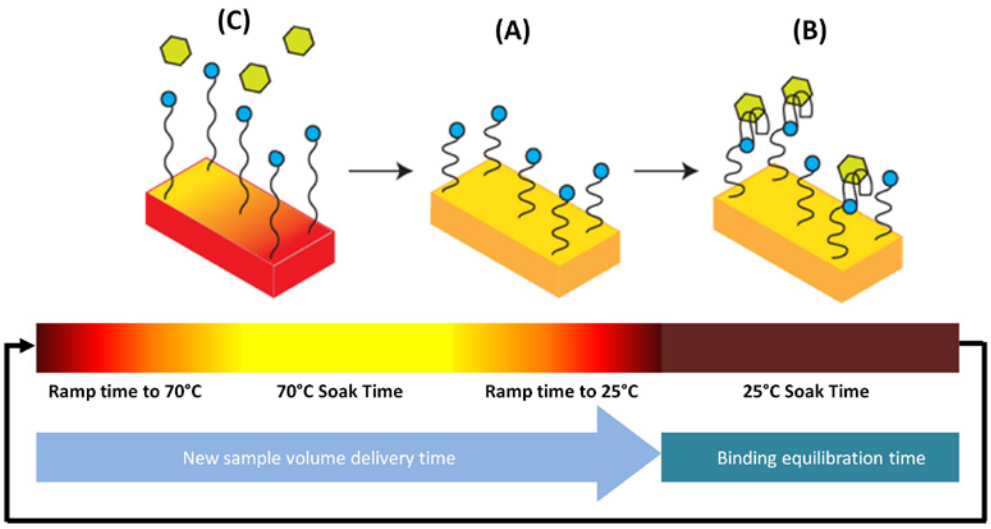

Scheme 5.1. Continuous thermal regeneration and measurement of a thrombin aptasensor. (A) The sensor chip in its native unbound state. (B) When challenged by a new sample volume, the probes bind to thrombin, undergoing a conformation change that reduces the electrochemical current and reports the thrombin concentration. (C) The sensor chip undergoes thermal regeneration at 70°C where the aptasensor DNA is melted and loses its affinity for thrombin, thus regenerating the initial state (A). This scheme also illustrates the time constraints on how quickly the system can be cycled. There are well-defined minimum times for the system to ramp to 70°C, soak at 70°C to fully thermalize the probes, ramp down to 25°C, and soak at 25°C during binding equilibration and measurement.

Previously in the literature, there have been other approaches to regenerate aptasensor chips for multiple measurements including washes with denaturating salts[118], detergents[118] and chelating agents to remove supportive ions[119] and these approaches are effective for the regeneration of single use chips. Whereas, our system is specifically optimized for rapid, continuous measurements because regeneration is performed by an external mini-TEC element which cycles the temperature in the chip automatically, without disrupting continuous microfluidic delivery of new sample volume. In this work, we showed that we are able to update the concentration of thrombin in a continuous aptasensor within ~5 minutes and

that the device has been completely regenerated to its unbound state for each new measurement.

5.2 Results and Discussion

5.2.1 Design of the thermal regeneration system

The assembly of our apparatus was a straightforward modification of the thrombin aptasensor device where we mounted the microfluidic chip containing the aptasensor-functionalized probes on top of a thermoelectric cooler linked to a 100 Ω platinum resistive temperature detector, a DC power supply, and a PID temperature controller (Figure 5.2). Thermal contact was maintained between the chip and the TEC by thermal paste. The aptasensor chip was connected via a modified PCBI connector to a potentiostat which provided the electrochemical readout.

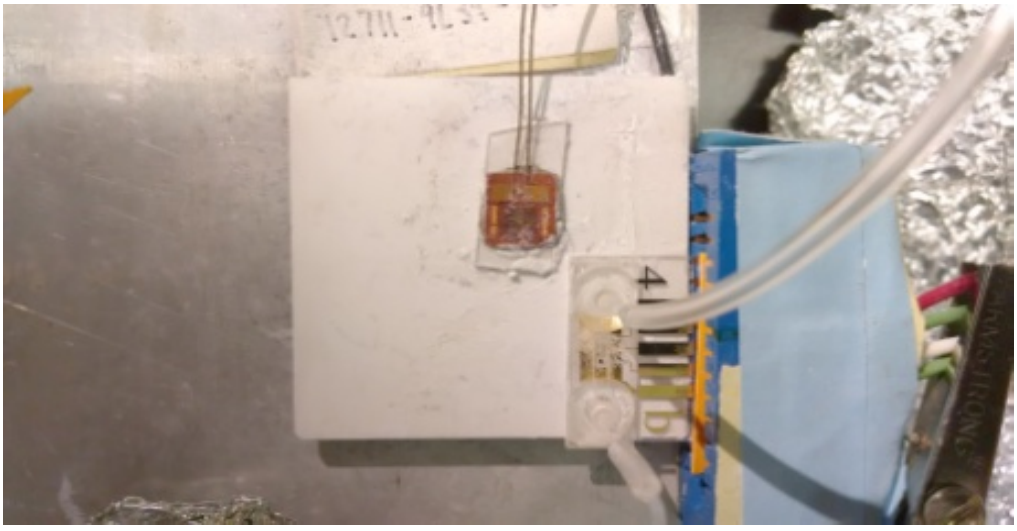

Figure 5.2. Photograph of the thermal regeneration apparatus mounted with an electrochemical thrombin aptasensor.

5.2.2 Optimization of thermal regeneration and measurement cycle time

As noted in Scheme 5.1, our goal was to minimize the time for a complete cycle of thrombin measurement and thermal regeneration. From previous measurements for PMEDIC, we determined that 2.5 minutes was a suitable amount of time for the probes to come to ~90% signal equilibrium for a 50 nM pulse of thrombin (see Figure 4.1). Since physiological concentrations of thrombin are lower than 50 nM[105] and would require less time to equilibrate, we set the "binding equilibration time" for our system to 2.5 minutes.

For thermal regeneration, we needed to minimize the ramp times to 70°C and 25°C, respectively. We tuned the PID parameters of the controller to balance speed with stability of temperature ramping. Although we wanted to achieve target temperature as quickly as possible, we were concerned that temperature overshoot past 70°C might damage the probes. We used the PID "autotune" function and found that reasonable parameters for P = 43, I = 14 s, D = 19 s. Under these settings, ramp-up time to 70°C was ~30 s and ramp-down time to 25°C was ~60 s.

To determine the soak time necessary to melt the probes, we performed an experiment where we continuously measured the electrochemical current of the device in plain buffer while ramping the temperature between 25°C and various melting temperatures between 74°C – 82°C (Figure 5.3). We found that at 25°C, the baseline measured current was ~0.05 uA, but when the chips were fully thermalized at high temperature, the probes read ~0.22 uA due to the added thermal energy (Figure 5.3). The probes achieved maximum signal due to thermal

energy within ~60s (including the time needed for the TEC to ramp up), therefore we determined that the necessary soak time at 70°C was ~30s (Figure 5.3).

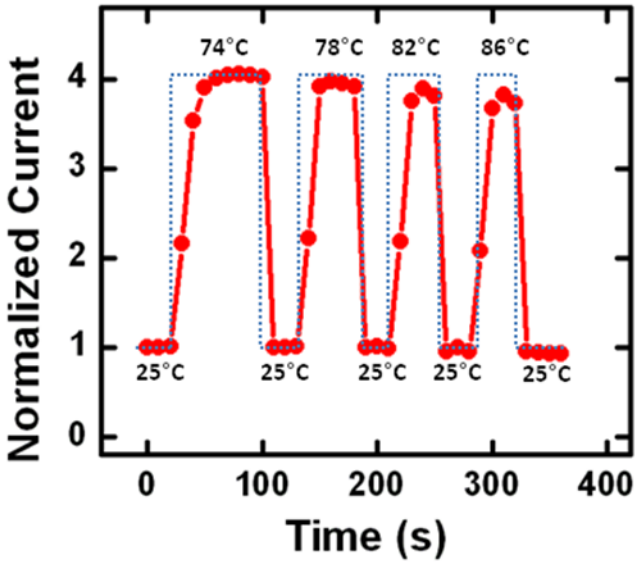

Figure 5.3. Determination of soak time needed for complete chip thermalization to target temperature. For all tested temperatures, the chip thermalized within ~60s to the target temperature when starting from 25°C.

We performed three cycles of time-optimized thrombin measurement and thermal regeneration and found that the device was thermally robust and accurately reported the thrombin concentration (Figure 5.4). First, we equilibrated the system to plain buffer (0 nM thrombin) for 60s, then we challenged the system with 50 nM thrombin and equilibrated for 140s and observed a ~32% signal decrease (Figure 5.4). Next, we performed the thermal regeneration cycle which took 100 s total including temperature ramp times and soak time. Afterwards, we re-measured the current readout corresponding to plain buffer and found it to be equivalent to our initial signal. We repeated this cycle one more time to show reproducibility and indeed, we found that the second pulse of 50 nM thrombin showed similar

equilibration times and change in current (Figure 5.4). Under these conditions, the concentration of thrombin can be accurately and rapidly updated every ~5 minutes. Given that *in vivo* serum concentrations of thrombin are typically in the fM- pM range[105], our setup will be able to respond even faster to lower concentrations of thrombin, making the temporal resolution of our system well-suited for future clinical applications.

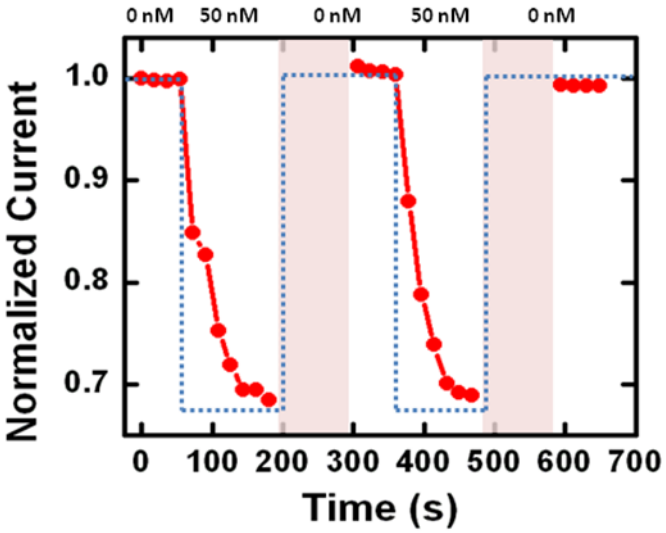

Figure 5.4. Time-optimized continuous measurement and regeneration of the aptasensor device. With our optimized system, the thrombin concentration can be accurately and reproducibly measured every ~5 minutes.

5.2.3 Batch-to-batch variation in device performance

Although our initial devices proved to be robust for multiple cycles of measurement and thermal regeneration, in later experiments, we encountered significant challenges producing devices with reproducible behaviors. A significant number of devices tested showed drift in the baseline signal (0 nM thrombin in plain buffer) after a single thermal regeneration cycle. For example, we typically found that while the signal change in response to a pulse of 100 nM thrombin caused a ~22% decrease in current, the buffer baseline current could drift up to 10% after a regeneration cycle (Figure 5.5A). The signal drift was large enough to make multiple consecutive thrombin measurements difficult to interpret, and as such, would make continuous clinical monitoring of thrombin very challenging.

In order to confirm that the shift in baseline signal was from thermal cycling, and not due to insufficient removal of bound thrombin, we flowed plain buffer through the chip, subjected the device to 12 cycles of thermal regeneration, and then applied a 100 nM pulse of thrombin to assay the performance (Figure 5.5B). We observed that each cycle of thermal regeneration decreased the baseline signal a small amount, which suggests that the decreasing baseline signal is caused by deterioration of the chip from heating. The 100 nM thrombin pulse at the end of the experiment was a control to show that the device was typical and indeed, it produced expected behaviors: a ~40% decrease in current and slow dissociation from the probes after being washed with plain buffer.

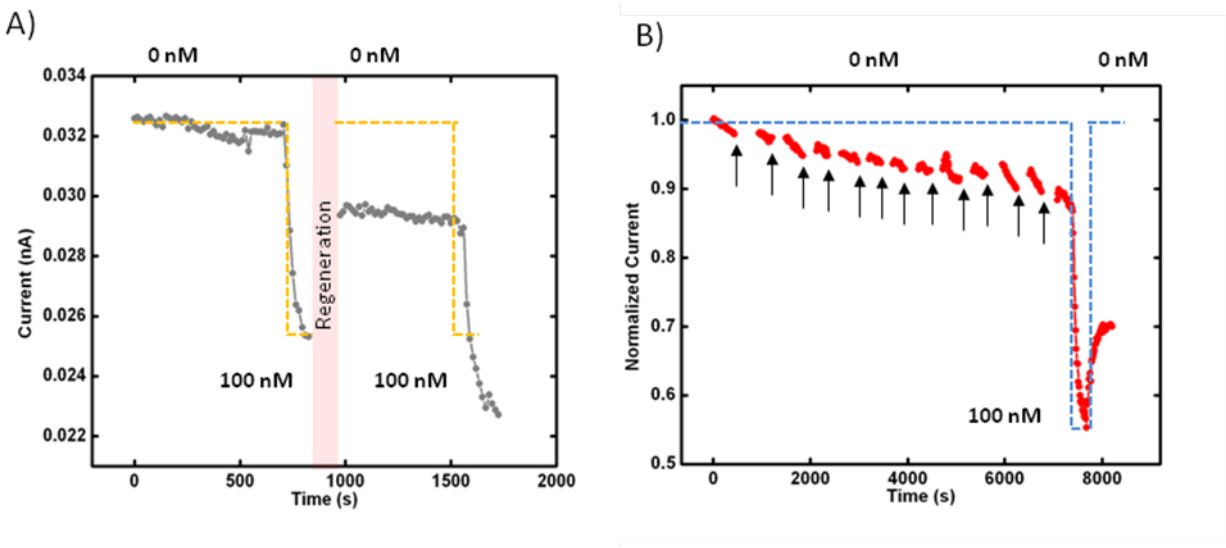

Figure 5.5. A) A thrombin aptasensor device showing ~10% baseline signal drift after 1 cycle of thermal regeneration. Although the device still produces a similar current change in response to a 100 nM pulse of thrombin, the shift in absolute currents would make continuous *in vivo* monitoring difficult to interpret. B) We found that 12 cycles of thermal regeneration in plain buffer could cause ~10% baseline signal drift, which suggests that the decreased baseline signal arises from thermal damage, not from still-bound thrombin on the sensor surface. Interestingly, a 100 nM thrombin pulse at the end of this experiment still showed reasonable current change (~40% decrease), which indicates that the chip still functions well as a sensor, relative to the new baseline current.

Nominally, all devices were produced using the same protocol: thin film Au deposition onto glass wafers, followed by self-assembly of thiol-modified aptasensor probes and a C6 alkanethiol passivation monolayer onto the Au electrode surface (see section 5.4.3). We decided to try to track down the source of inconsistent device performance.

We theorized that the E-beam evaporator we used to deposit thin film gold for our electrodes could have a contaminated Au source, so we used X-ray photoelectron spectroscopy (XPS) to determine if there were unexpected contaminants. However, XPS results showed that there was not a significant presence of unexpected elements (Figure 5.6). The only elements detected in

significant quantities were Au from our thin film deposition; Si, O, and B from the borosilicate glass wafer; and Sn which is used in float glass production[120].

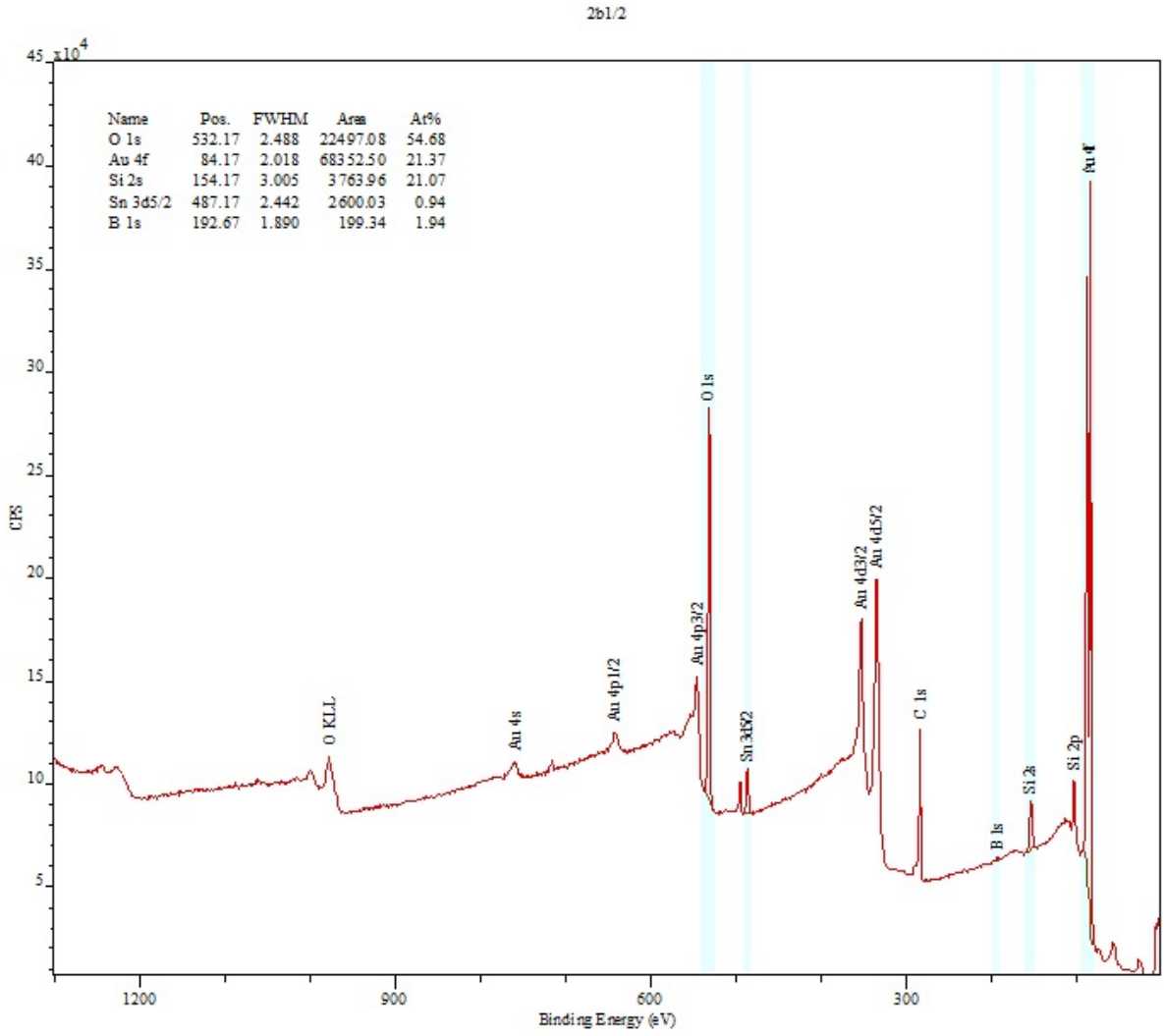

Figure 5.6. XPS of aptasensor device electrode shows that there are no significant unexpected contaminants. The main components detected are Au from our deposition process, Si and O (from the glass wafer), and Sn and B which are typical trace elements in glass wafers[120].

Having ruled out effects due to a contaminated Au source, we theorized that variation in the quality of the C6 passivation layer could affect the thermal robustness of devices. In aptasensor devices, it is thought that C6 chains help to space out individual thrombin probes to prevent entanglement, and that they also play a role in supporting proper folding of the aptamer[121][122]. Moreover, it is also thought that interchain interactions between alkanethiols raises the melting temperature of functionalized surfaces[123]. We theorized that there could be variation in C6 self-assembly due to day-to-day variation of environmental conditions. As such, we increased the reaction time for C6 functionalization from 1 hour to overnight so that the system would have longer to come to equilibrium. We did not observe significant improvement in the device tolerance for thermal regeneration (Figure 5.7). We believe that thermal regeneration of heat-intolerant batches of aptasensors results in probe and/or alkanethiol loss[123]. In contrast, a denaturing salt wash (guanidine hydrochloride, GHCl) regenerated the aptasensors with no apparent changes to baseline signal and showed a normal response to a 100 nM thrombin pulse.

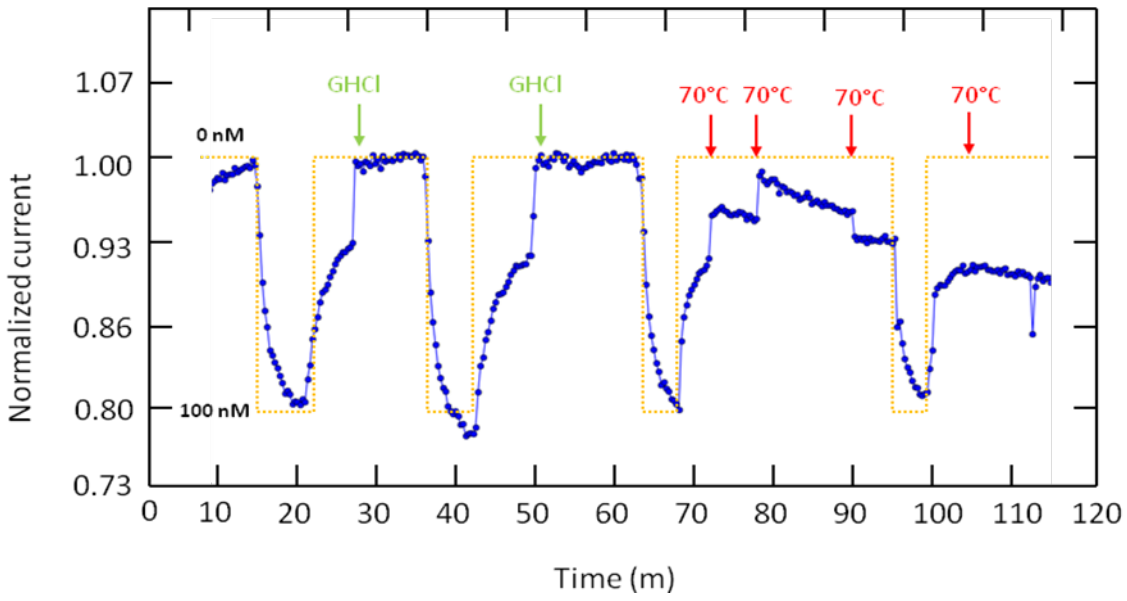

Figure 5.7. After overnight C6 treatment, thermal cycling still appears to be fundamentally destructive to heat-intolerant batches of aptasensors. The drift in absolute current suggests loss of thrombin probes and/or C6 passivation molecules. Whereas washing with GHCl appears to have a non-destructive regenerative effect.

We explored several other avenues to standardize the thermal tolerance of our aptasensor devices including slowing down the rate of Au thin film deposition and using excess thrombin probes for functionalization. However, these efforts did not appear to improve thermal tolerance of the devices either. We were not able to definitively isolate the cause of variation in aptasensor thermal tolerance, so we decided to move on to other projects.

5.3 Conclusions

In summary, we have developed a new strategy to improve the speed and accuracy of continuous thrombin monitoring. In this work, we show that it is possible to thermally regenerate an aptasensor chip via a programmed mini-TEC element, enabling us to measure the concentration of thrombin every ~5 minutes.

Our system is advantageous for continuous monitoring applications because it requires no externally applied reagents or discretized wash steps and the measurement/regeneration cycle is programmed to act automatically.

Although the principle idea of this project holds merit, we encountered significant challenges in producing consistently thermally robust devices. We found that although the sensitivity and dynamic range of thrombin aptasensors was preserved, thermal cycling could shift the baseline signal significantly, which would obfuscate continuous monitoring *in vivo*. We determined that there were no unexpected contaminants in the Au electrodes, and that differences in C6 self-assembly were unlikely to affect thermal tolerance. Since the DNA component of aptasensors is known to be thermally stable at far higher temperatures (in PCR, oligos are repeatedly heated to 95C without damage), we think that the most likely cause of probe and/or C6 loss is thermal damage to the Au-thiol bonds which anchor these components to the electrode[123]. Going forward, we believe that exploring alternative chemistries to link the probes and C6 molecules to the electrodes which are more thermally robust may be the key to making this platform work consistently.

5.4 Experimental section

5.4.1 Reagents

Since the devices produced for this project were identical those produced for the PMEDIC project, the reagents used were identical. Please see section 4.3.1.

5.4.2 Chip fabrication

Please see 4.3.2.

5.4.3 Electrode cleaning and sensor preparation

Please see 4.3.3.

5.4.4 Microfluidic sample delivery

Device flow was controlled via syringe pump (PHD 2000, Harvard Apparatus, MA). Since the experiments for thermal regeneration were only performed in buffer, we did not need to set up a CDF. As such, the chip was prepared with 1 input and 1 output port, where the buffer sheath port was plugged shut. The syringe pump was connected to the output port and operated by withdrawing 10 ml/hr of sample volume. The input port was connected to open-ended Tygon tubing which could be switched between different test tubes containing various concentrations of purified thrombin dissolved in buffer (0-100 nM).

5.4.5 Voltammetry and thermal regeneration experiment

We measured the MB peak currents of the aptasensors in the presence of either plain buffer (HBS, 0 nM thrombin) or pulses of 50 or 100 nM purified α-thrombin dissolved in HBS (Haematologic Tech, Essex, VT) under continuous microfluidic flow.

Thermal regeneration was perfomed by mounting the aptasensor chip onto a thermoelectric cooler (TEC, Custom Thermoelectric, MD) connected to a 100 Ω platinum resistive temperature detector (RTD, Minco, MN), a DC power supply, and a PID temperature controller (Omega Engineering, CT). The chip was subjected to temperature cycling between 25C and 70C, with a 2.5 m soak time at 25C and a 30s soak time at 70C. The rate of temperature ramping between these two target temperatures was maximized to optimize for the fastest rate of thermal regeneration and measurement cycling. We used the autotune function on the PID controller to balance speed of temperature ramping with temperature stability and minimal temperature overshoot (P = 43, I = 60 s, D = 19 s) . Good thermal contact was maintained between aptasensor chips and the TEC via thermal compound (Arctic Alumina, Arctic Silver, CA). Time-course continuous electrochemical measurements were taken only during the 25C sensor equilibration time, alternating with a no-read period during thermal regeneration. A single optimized measurement-and-thermal-regeneration cycle was completed in ~5 minutes.

Electrochemical measurements were performed on a Emstat3 mini-potentiostat (Palmsens, Germany). Square-wave voltammetry (SWV) was used for monitoring the changes in MB redox current during thrombin measurement experiments. Typical SWV parameters used are as follows: 0.08V initial voltage, -

0.20 V final voltage, 0.001 V increment, 0.03 V amplitude, 100 Hz freqeuncy, 0.11 s sample period, and auto sensitivity. A custom Python script was written to synchronize the PID temperature controller and the potentiostat in order to alternate between electrochemical measurements and thermal regeneration (no-read period).

5.4.6 X-ray photoelectron spectroscopy

X-ray photoelectron spectroscopy was performed on unassembled, un-functionalized Au electrode substrates using a Kratos Ultra XPS (Kratos Analytical Limited, Kyoto, Japan).

5.4.7 Denaturing salt wash regeneration of chips

6.0 M guanidine hydrochloride was manually injected into the input port of chips with a 1 mL syringe several times to displace previous sample volumes. The chip was incubated with GHCl for 5 m, rinsed with DI, and then reattached to the syringe pump to restart continuous measurement.

Chapter 6. Conclusion

The field of precision medicine encompasses myriad exciting research movements across multiple disciplines and in this thesis, we have presented several projects addressing the need for controlled drug delivery and real-time molecular diagnostics. Controlled release technologies provide for more sophisticated manipulation of the timing and targeting of an active drug payload, thereby reducing side effects and concentrating the efficacy of dosage at the site of illness. In parallel, the development of real-time diagnostics can give quantitative feedback about not only the instantaneous blood concentration of a drug but also potentially, the physiological response of the patient. As such, real-time diagnostics provide real-time insight into the efficacy of treament. These technologies, therefore, are partners in making precision medicine the new standard of healthcare.

6.1 Final comments on PADNA and PGSA

PADNA and PGSA were projects with the shared objective of controlling the bioavailability of a drug payload. We designed the PADNA system to sequester the antisense DNA drug Mipomersen[60] while circulating in the bloodstream, but to become activated after endosomal internalization. We created new, highly selective pH-switching DNA motifs to act as the gating system for Mipomersen release. Afterwards, we developed PGSA by modifying a previously published aptamer for Streptavidin with new pH-sensitive domains, where we can directly control the affinity of the aptamer for its target through modulation of the pH. In the future, PGSA may be used to achieve pH-controlled activation of therapeutic aptamers at

specific stages of the endocytosis pathway, thereby acting as a next generation prodrug.

The further development of PADNA and PGSA will involve modifications to allow these technologies to function *in vivo* as well as they have been demonstrated to work *in vitro*. First, the most imminent need is to test how resistant PADNA and PGSA are to degradation by nucleases in blood and to add chemical modifications to the DNA that lengthen circulation time[124]. Second, PADNA and PGSA must be incorporated with a targeting moiety in order to deliver the drug payload to a specific tissue or cell type. Although optimization will be needed, in principle, targeting of the drug delivery vehicle can be achieved by conjugation with cell-surface targeting aptamers, peptides, and antibodies[125], [126]. Third, PADNA and PGSA must also be combined with a module to achieve endosomal escape. While PADNA and PGSA provide for pH-specific release inside the endosome, the payload may need transport to the cytosol to act upon a specific protein or organelle. Currently, there are several well-established mechanisms to achieve endosomal escape including the proton sponge (inflow of water into the endosome causing rupture) and fusogenic peptides (fusion with endosomal membrane and lysis). We can envision concatenation of PADNA and PGSA with one of these modules to provide transport into the cytoplasm.

6.2 Final comments on PMEDIC and Thermal Regeneration

PMEDIC and the Thermal Regeneration Module were projects with the shared objective of creating an assay for endogenously secreted proteins in order to monitor the physiological status of a patient in real-time. A device which provides continuous protein monitoring that is automated, requires no additional reagents and can be self-corrected for signal drift is highly advantageous. Our contribution in PMEDIC and the Thermal Regeneration Module was to extend the useful lifetime of a single device. We addressed the challenge of biofouling over time, ensured continuous microfluidic flow despite the formation of fibrin clots, and also developed a method to quickly regenerate the sensor for faster and more accurate measurements.

While we have developed innovative supportive technologies which enable continuous operation of a single device (CDF, pretreatment cocktail, thermal regeneration), for our future work, we are considering alternative designs to achieve real-time monitoring.The biofouling phenomenon is a problem that scales with time and its degradative effects are not significant if sample incubation is less than 20 minutes[48]. The need for continuous and smooth microfluidic flow presents an especially great challenge for monitoring coagulopathic blood, as its tendency to produce spontaneous clots in the sample line is unpredictable. And perhaps most importantly, the continuous operation of the electrochemical sensor does not allow for a signal amplification step, limiting the sensitivity of our devices. If we hope to someday achieve *in vivo* sensing of endogenously secreted proteins, we must develop a platform that can detect protein in the pM or lower range of concentration[105].

Going forward, we envision that continuous protein monitoring may be better achieved via an automated grid of single-use sensors. Each miniature sensor would be programmed to automatically draw a microliter volume of blood, perform an amplification/sandwich-based assay, and then report the concentration. After a specified period of time, the next sensor is activated to perform the same operations and the next data point is recorded. Since each sensor is used only once and under static conditions, the requirements to protect the electrodes from biofouling and to ensure smooth microfluidic flow are obviated. It also follows that sensor regeneration would not be needed. Since it is relatively simple to fabricate small mini-sensors (~1 mm x 1 mm), we could easily package up to 100 tests into a single grid device employed at the bedside or perhaps even as a wearable device. An important consideration for our proposed design would be how to optimize the aptasensor self-assembly reaction to be uniform across all mini-sensors. We would also plan to include a standard curve normalization step for all the mini-sensors in the array so that the data points produced by each sensor can be directly quantitatively compared.

To conclude, whichever platform is eventually found to be most suitable for clinical implementation, there is no doubt that the future practice of medicine will rely on real-time diagnostics for better care.

6.3 Coda

As medicine advances, controlled drug delivery will play an important role in increasing the efficacy of currently approved medications. As the technology to control drug release increases in sophistication, it may be possible to revive previously unapproved drug candidates whose therapeutic window was too narrow for systemic administration, as currently evaluated by the FDA. In the future, it is possible to envision that precisely targeted drug delivery combined with real-time diagnostics could allow for the safe application of drugs with narrow therapeutic windows, thus enabling patients to receive the benefit of a greater ensemble of pharmaceuticals[127]. Looking forward, advanced drug delivery vehicles will no doubt also be a significant aspect of developing next generation therapeutics which do not fit the classical pharmaceutical profile (small molecule, highly water soluble, permeable to the cell membrane)[22], [128]. High molecular weight biologicals, negatively charged gene therapies, and nanoparticle assemblies, for example, will require innovations in packaging to increase circulation time, target specific tissues, and increase cell uptake efficiency[128].

Real-time diagnostics are likely to be a crucial tool in the future hospital environment, be it at the operating table or the bedside. Being able to monitor the blood concentration during drug administration as well as the actual physiological response of the patient will enable a new practice of medicine that is more quantitative and data-rich. Clinicians will be able to more accurately assess patient prognosis as well as react more quickly to adjust treatment. Each patient may thus experience a better clinical outcome. However, the significance of real-time molecular diagnostics extends beyond, to the patient population as a whole.

Importantly, the data gathered from real-time quantitative diagnostics will be more easily compiled and compared than phenomenonological observations, thus allowing for improved bioinformatics and statistical analysis. As such, these data may be invaluable for future study into improving treatment for specific patient and disease populations.

Bibliography

[1] Hershey A.D.; Chase M. *J. Gen. Physiol.* **1952**, *36*, 39.

[2] Voet D.; Voet J. *Biochemistry* **2011**, *4*, 85.

[3] Watson J.D.; Crick F.H.C. *Nature* **1953**, *171*, 737.

[4] Bikard D.; Loot C.; Baharoglu Z.; Mazel D. *Microbiol. Mol. Biol. Rev.* **2010**, *74*, 570.

[5] Strobel S. A.; Cochrane, J. C. *Curr. Opin. Chem. Biol.* **2007**, *11*, 636.

[6] Wang P.; Meyer T. A.; Pan V.; Dutta P. K.; Ke Y. *Chemistry* **2017***, 2*, 359.

[7] Kallenbach N. R.; Ma R. I.; Seeman, N.C. *Nature* **1983**, *305*, 829.

[8] Hong F.; Zhang F.; Liu Y.; Yan H. *Chem. Rev.* **2017**.
DOI: 10.1021/acs.chemrev.6b00825 (online only).

[9] Song K.M.; Lee S.H.; Ban C. G.; *Sensors* **2012**, *12*, 612.

[10] Bock L.C.; Griffin L.C.; Latham J.A.; Vermaas E.H.; Toole J.J. *Nature* **1992**, *355*, 564.

[11] Tasset D.M.; Kubik M.F.; Steiner W. *J. Mol. Biol.* **1997**, *272*, 688.

[12] Green S. J.; Bath J.; Turberfield A. J. *Phys. Rev. Lett.* **2008**, *101*, 238101.

[13] Yuan Q.; Zhang Y. F.; Chen T.; Lu D. Q.; Zhao Z.L.; Zhang X. B.; Li Z. X.; Yan C. H.; Tan W. H. *ACS Nano.* **2012**, *6*, 6637.

[14] Yang H.; Liu H.; Kang H.; Tan W. *JACS*. **2008**, *130*, 6320.

[15] Fang X. H.; Liu X. J.; Schuster S.; Tan W. H. *JACS* **1999**, *121*, 2921.

[16] Breaker R. R.; Joyce G. F.; *Chem. Biol.* **1994**, *1*, 223.

[17] Collins F. S.; Varmus H. *N. Engl. J. Med.* **2015**, *372*, 793.

[18] Doghramji P. P. *MedGenmed.* **2007**, *9*, 11.

[19] Spencer T. J.; Abikoff H. B.; Connor D. F.; Biederman J.; Pliszka S. R.; Boellner S.; Read S. C.; Pratt R. *Clin Therapeutics.* **2006**, *28*, 402.

[20] Pazdur R.; Hoff P.M.; Medgyesy D.; Royce M.; Brito R. A. *Oncology*. **1998**, *12*, 48.

[21] Park K. *J. Controlled Release* **2014**, *190*, 3.

[22] Kalepu S.; Nekkanti V. *Acta Pharmaceutica Sinica B* **2015**, *5*, 442.

[23] Phillips A. J. *J.P.P.* **2001**, *53,* 1169.

[24] Besterman J. M.; Low R. B.; *Biochem. J.* **1983**, *210*, 1.

[25] Bareford L. M.; Swaan P. W. *Adv. Drug Delivery Rev.* **2007**, *59*, 748.

[26] Duncan R.; Richardson S. C. W. *Mol. Pharm*. **2012**, *9,* 2380.

[27] Dautry-Varsat A.; Ciechanover A.; Lodish H. F.; *PNAS* **1983**, *80*, 2258.

[28] Schmaljohann D. *Adv. Drug Delivery Rev.* **2006**, *58*, 1655.

[29] Bae Y.S.; Jang W. D.; Nishiyama N.; Fukushima S.; Kataoka K.; *Mol. Biosyst.* **2005**, *1*, 242.

[30] Liu S. Y.; Weaver J. V. M.; Tang Y. Q.; Billingham N. C.; Armes S. P.; Tribe K. *Macromol*. **2002**, *35*, 6121.

[31] Teller C.; Willner I. *Curr. Op. Biotech.* **2010**, *21*, 376.

[32] Nesterova I. V.; Nesterov E. E. *JACS* **2014**, *136*, 8843.

[33] Phan A. T.; Mergny J. L. *Nuc. Acids Res.* **2002**, *30*, 4618.

[34] Kim J.; Lee Y. M.; Kang Y.; Kim W. J. *ACS Nano.* **2014**, 8, 9358.

[35] Chen C.; Pu F.; Huang Z. Z.; Liu Z.; Ren J. S.; Qu X. G.; *Nuc. Acids Res.* **2011**, *39*, 1638.

[36] Idili A.; Vallée-Bélisle A.; Ricci F. *JACS* **2014**, *136*, 5836.

[37] Lee J. A.; DeRosa M. C. *Chem. Comm.* **2010**, *46*, 418.

[38] Stoltenburg R.; Reinemann C.; Strehlitz B. *Anal. Bioanal. Chem.* **2005**, *383*, 83.

[39] Oh S. S.; Plakos K.; Xiano Y.; Eisenstein M.; Soh H.T. *ACS Nano.* **2013**, *7*, 9675.

[40] Gross T. M.; Bode B. W.; Einhorn D.; Kayne D. M.; Reed J. H.; White N. H.; Mastrototaro J. J. *Diabetes Tech. Therapeutics* **2004**, *2*, 49.

[41] Kost G. J.; Tran N. K.; Louie R. F. *Enc. Anal. Chem.* **2008**. DOI: 10.1002/9780470027318.a0540.pub2 (online only).

[42] Hess J. R.; Rohi K.; Dutton R. P.; Hauser C. J.; Holcomb J. B.; Kluger Y.; Mackway-Jones K.; Parr M. J.; Rizoli S. B.; Yukioka T.; Hoyt D. B.; Bouillon B. *J. Trauma* **2008**, *65*, 748.

[43] Park M. S.; Martini W. J. Z.; Dubick M. A.; Salinas J.; Butenas S.; Kheirabadi B. J. S.; Pusateri, A. E.; Wang J. J.; Vos J. A.; Guymon C. H.; Wolf S. E.; Mann K. G.; Holcomb J. B. *J. Trauma* **2009**, *67*, 266.

[44] Katona E.; Haramura G.; Karpati L.; Fachet J.; Muszbek L.; *Thromb. Haemost*. **2000**, *83*, 268.

[45] Meijers J. C.; Davie E. W.; Chung D. W. *Blood*. **1992**, *79,* 1435.

[46] Fan C. H.; Plaxco K. W.; Heeger A. J. *PNAS* **2003**, *100*, 9134.

[47] Xiao Y.; Lubin A. A.; Heeger A. J.; Plaxco K. W. *Ange. Chem. Int. Ed.* **2005**, *117*, 5592.

[48] Ferguson B. S.; Hoggarth D. A.; Maliniak D.; Ploense K.; White R. J.; Woodward N.; Hsieh K.; Bonham A. J.; Eisenstein M.; Kippin T.; Plaxco K. W.; Soh H. T. *Science Translational Medicine* **2013**, *5*, 213ra165.

[49] Ganta S.; Devalapally H.; Shahiwala A.; Amiji M. *J. Cont. Rel.* **2008**, *126*, 187.

[50] Charoenphol P.; Bermudez H. *Acta. Biomat.* **2014**, *10*, 1683.

[51] Modi S.; Swetha M. G.; Goswami D.; Gupta G.D.; Mayor S.; Krishnan Y. A. *Nat. Nano*. **2009**, *4*, 325.

[52] Son S.; Nam J.; Kim J.; Kim W.J. *ACS Nano*. **2014**, *8*, 5574.

[53] Keum J. W.; Bermudez H. *Chem. Comm.* **2012**, *48*, 12118.

[54] Kim J.; Lee Y. M.; Kang Y.;Kim W. J. *ACS Nano* **2014**, 8, 9358.

[55] Liu D. S.; Balasubramanian S. *Angew. Chem. Int. Ed.* **2003,** *42*, 5734.

[56] Liu D. S.; Bruckbauer A.; Abell C.; Balasubramanian S.; Kang D. J.; Klenerman D.; Zhou D. *JACS*. **2006**, *128*, 2067.

[57] Porchetta A.; Idili A.; Vallee-Belisle A.; Ricci F. *Nano Lett.* **2015**, *15*, 4467.

[58] Nesterova I. V.; Briscoe J. R.; Nesterov E. E. *JACS* **2015**, *137*, 11234.

[59] Nesterova I. V.; Elsiddieg S. O.; Nesterov E. E. *J. Phys. Chem. B* **2013**, *117*, 10115.

[60] Raal F. J.; Santos R. D.; Blom D. J.; Marais A. D.; Charng M. J.; Cromwell W. C.; Lachmann R. H.; Gaudet D.; Tan J. L.; Chasan-Taber S.; Tribble D. L. *Lancet* **2010**, *375*, 998.

[61] Chakraborty S.; Sharma S.; Maiti P. K.; Krishnan Y. *Nuc. Acids Res.* **2009**, *37*, 2810.

[62] Frank-Kamenetskii M. D.; Mirkin S. M. *Ann. Rev. Biochem.* **1995**, 64, 65.

[63] Li T.; Famulok M. *JACS* **2013**, *135*, 1593.

[64] Moreira B. G.; You Y.; Behlke M. A.; Owczarzy R. *Biochem. Biophys. Res. Comm.* **2005**, *327*, 473.

[65] Zuker M. *Nuc. Acids Res.* **2003**, *31*, 3406.

[66] Siegfried N.A.; O'Hare B.; Bevilacqua P.C. *Biochem.* **2010**, *49*, 3225.

[67] Boulard Y.; Cognet J.A.H.; Gabarro-Arpa J.; Le Bret M.; Sowers L.C.; Fazakerley G.V. *Nuc. Acids Res.***1992,** *20*, 1933.

[68] Wang C.; Gao H.T.; Gaffney B.L.; Jones R. A. *JACS*. **1991**. *113*, 5486.

[69] Legault P.; Pardi A. *JACS*. **1997**. *119*, 6621.

[70] Ellington A. D.; Szostak J. W. *Nature* **1990**, *346*, 183.

[71] Stojanovic M.N.; dePrada P.; Landry D.W.; *JACS* **2001**, *123*, 4928.

[72] Fang X.H.; Tan W.H. *Acc Chem Res* **2010**, *43*, 48.

[73] Jayasena S.D. *Clin. Chem* **1999**, *45*, 1628.

[74] Ng E. W. M.; Shima D. T.; Calias P.; Cunningham, Jr. E.T.; Guyer D. R.; Adamis A. P. *Nat. Rev. Drug Disc.* **2006**, *5*, 123.

[75] McConnell E. M.; Bolzon R.; Mezin P.; Frahm G.; Johnston M.; DeRosa M. C. *Bioconj. Chem.* **2016*,*** *27*, 1493.

[76] Yan L.; Shui H.; He D. G.; He X. X.; Wang K. M.; Xu F. Z.; *Sci. China Chem.* **2016,** *59*, 802.

[77] Shastri A.; McGregor L. M.; Liu Y.; Harris V.; Nan H. Q.; Mujica M.; Vasquez Y.; Bhattacharya A.; Ma Y. T.; Aizenberg M.; Kuksenok O.; Balazs A. C.; Aizenberg J.; He X. M. *Nat. Chem.* **2015**, *7*, 447.

[78] Fong F. Y.; Oh S. S.; Hawker C. J.; Soh H. T. *Ange. Chem. Int. Ed.* **2016**, *128*, 15484.

[79] Bing T.; Yang X. J.; Mei H. C.; Cao Z. H.; Shangguan D. H. *Bioorg. Med. Chem.* **2010**, *18*, 1798.

[80] Ouellet E.; Lagally E. T.; Cheung K. C.; Haynes C. A. *Biotech. Bioeng.* **2014**, *111*, 2265-2279.

[81] Jorgensen A. S.; Hansen L. H.; Vester B.; Wengel J. *Bioorg. Med. Chem. Lett.* **2014**, *24*, 2273-2277.

[82] Ruigrok V. J. B.; Duijn E. V.; Barendregt A.; Dyer K.; Tainer J. A.; Stoltenburg R.; Strehlitz B.; Levisson M.; Smidt H.; der Oost J. V. *ChemBioChem* **2012**, *13*, 829.

[83] Hasegawa H.; Sode K.; Ikebukuro K. *Biotech. Lett.* **2008**, *30*, 829.

[84] Mendonsa S.D.; Bowser M.T. *Anal. Chem.* **2004**, *76*, 5387.

[85] Wang J. P. Gong Q.; Maheshwari N.; Eisenstein M.; Arcila M. L.; Kosik K. S.; Soh H. T. *Ange. Chem.* **2014**, *53*, 4796.

[86] *Carbodiimide Crosslinker Chemistry*. Retrieved from https://www.thermofisher.com/us/en/home/life-science/protein-biology/protein-biology-learning-center/protein-biology-resource-library/pierce-protein-methods/carbodiimide-crosslinker-chemistry.html

[87] Wiegand T. W.; Williams P. B.; Dreskin S. C.; Jouvin M. H.; Kinet J. P.; Tasset D. *J. Immunol.* **1996**, *157*, 221.

[88] Kaur H.; Yung L. L. *Plos One* **2012**, *7*, e31196.

[89] Mei H. C.; Bing T.; Qi C.; Zhang N.; Liu X. J.; Chang T. J.; Yan J. L.; Shangguan D. H., *Chem. Commun.* **2013**, *49*, 164.

[90] *Primer Design Tips & Tools.* Retrieved from https://www.thermofisher.com/us/en/home/products-and-services/product-types/primers-oligos-nucleotides/invitrogen-custom-dna-oligos/primer-design-tools.html

[91] Oh S. S.; Plakos K.; Lou X. H.; Xiao Y.; Soh H. T. *PNAS* **2010**, *107*, 14053.

[92] Brohi K.; Singh J.; Heron M.; Coats T. *J. Trauma.* **2013**, *54*, 1127.

[93] In consultation with Mitch Cohen, MD (UCSF), December **2012**.

[94] Davie E. W.; Fujikawa K. Z.; Kisiel W. *Biochem.* **1991**, *30*, 10363.

[95] Uzawa T.; Cheng R. R.; White R. J.; Makarov D. E.; Plaxco K. W. *JACS* **2010**, *132*, 16120.

[96] Marciniak E.; Gockerman J.P. *Lancet* **1977**, *310*, 581.

[97] Abildgaard U. *Scandinavian J. Clin. Lab. Investigation*. **1969**, *24*, 23.

[98] Wisniewski N.; Moussy F.; Reichert W. M. *Fresenius' J. Anal. Chem.* **2000**, *366*, 611.

[99] Tarvers R. C.; Church F. C. *Int. J. Peptide Protein Res.* **1985**, *26*, 539.

[100] Goldstein B.; Wolfsy C. *Immunology Today*. **1996**, *17***,** 77.

[101] Ahmad K. M.; Oh S. S.; Kim S.; McClellen F. M.; Xiao Y.; Soh H.T. *PlosOne*, **2011**, *6*, e27051.

[102] Owen W. G.; Esmon C. T.; Jackson C. M. *J. Biol. Chem.* **1974**, *249*, 594.

[103] Krishnaswamy S. *J. Thromb. Haemost.* **2013**, *11*, 265.

[104] Smirnov M. D.; Safa O.; Esmon N. L.; Esmon C. T. *Blood*. **1999**, *94*, 3839.

[105] Muller J.; Becher T.; Braunstein J.; Berdel P.; Gravius S.; Rohrbach F.; Oldenburg J.; Mayer G.; Potszch B. *Ange. Chem. Int. Ed.* **2011**, *50*, 6075.

[106] Gosselin R. C.; Dager W. E.; King J. H.; Janatpour K.; Mahackian K.; Larkin E. C.; Owings J. T. *Amer. J. Clin. Pathology* **2004**, *121*, 593.

[107] Duchemin J.; Pan-Petesch B.; Arnaud B.; Blouch M. T.; Abgrall J. F. *Thromb. Haemost.* **2008**, *99*, 767.

[108] Hemker H. C.; Dieri R. A.; Smedt E. D.; Beguin S. *Thromb. Haemost.* **2006**, *96*, 553.

[109] Tirumalai R. S.; Chan K. C.; Prieto D. R. A.; Issaq H. J.; Conrads T. P.; Veenstra T. D. *Mol. Cell. Proteomics.* **2003**, *2*, 1096.

[110] Janeway C. A.; Travers P.; Walport M.; et al. *Immunobiology: The Immune System in Health and Disease*. **2001**, *5*. Retrieved from https://www.ncbi.nlm.nih.gov/books/NBK27144/

[111] Carter D. C.; He X. M.; Munson S. H.; Twigg P. D.; Gernert K. M.; Broom M. B.; Miller T. Y. *Science* **1989**, *244*, 1195.

[112] Banerjee A.; Chisti Y.; Banerjee U. C. *Biotech. Adv.* **2004**, *22*, 287.

[113] Muller J.; Wulffen B.; Potzsch B.; Mayer G. *ChemBioChem* **2007**, *8*, 2223.

[114] Di Giusto D. A.; King G. C. *J. Biol. Chem*. **2004**, *279*, 46483.

[115] Collins B. E.; Paulson J. C. *Current Opinion Chem. Biol.* **2004**, *8*, 617.

[116] Gold L.; Ayers D.; Bertino J.; Bock C.; Bock A.; et al. *Plos One* **2010**, *5*, e15004.

[117] Macaya R. F.; Schultze P.; Smith F. W.; Roe J. A.; Feigon J. *PNAS* **1993**, *90*, 3745.

[118] Lee J. O.; So H. M.; Jeon E. K.; Chang H. J.; Won K. H.; Kim Y. H. *Anal. Bioanal. Chem.* **2008**, *390*, 1023.

[119] Liss M.; Petersen B.; Wolf H.; Prohaska E. *Anal. Chem.* **2002**, *74*, 4488.

[120] *Do you know how to manufacture float glass?* **2011**, Retrieved from http://www.novalglass.com/glass/do-you-konw-how-to-manufacture-float-glass/

[121] Ricci F.; Zari N.; Caprio F.; Recine S.; Amine A.; Moscone D.; Palleschi G.; Plaxco K. W. *Bioelectrochem*. **2009***, 76*, 208.

[122] Lao R. J.; Song S.P.; Wu H. P.; Wang L. H.; Zhang Z. Z.; He L.; Fan C. H. *Anal. Chem.* **2005**, *77*, 6475.

[123] Cometto F. P.; Calderon C. A.; Berdakin M.; Paredes-Olivera P.; Macagno V. A.; Patrito E. M. *Electrochimica Acta* **2012**, *61*, 132.

[124] Pestourie C.; Tavitian B.; Duconge F. *Biochimie.* **2005**, *87*, 921.

[125] Cao Z. H.; Tong R.; Mishra A.; Xu W. C.; Wong G. C. L.; Cheng J. J.; Lu Y. *Ange. Chem. Int. Ed.* **2009**, *48*, 6494.

[126] Cho K. J.; Wang X.; Nie S. M.; Chen Z.; Shin D. M. *Clin. Cancer Res.* **2008**, *14*, 1310.

[127] Burns M. *J. Thrombosis and Thrombolysis* **1999**, *7*, 137.

[128] Gibson S. *Bioengineering of Innovative Biologic Therapies and Devices* **2016**, Presented at UCSB.